ENGINEERING ON ENERGY MATERIALS

EDITED BY: Dr. Defne AKAY

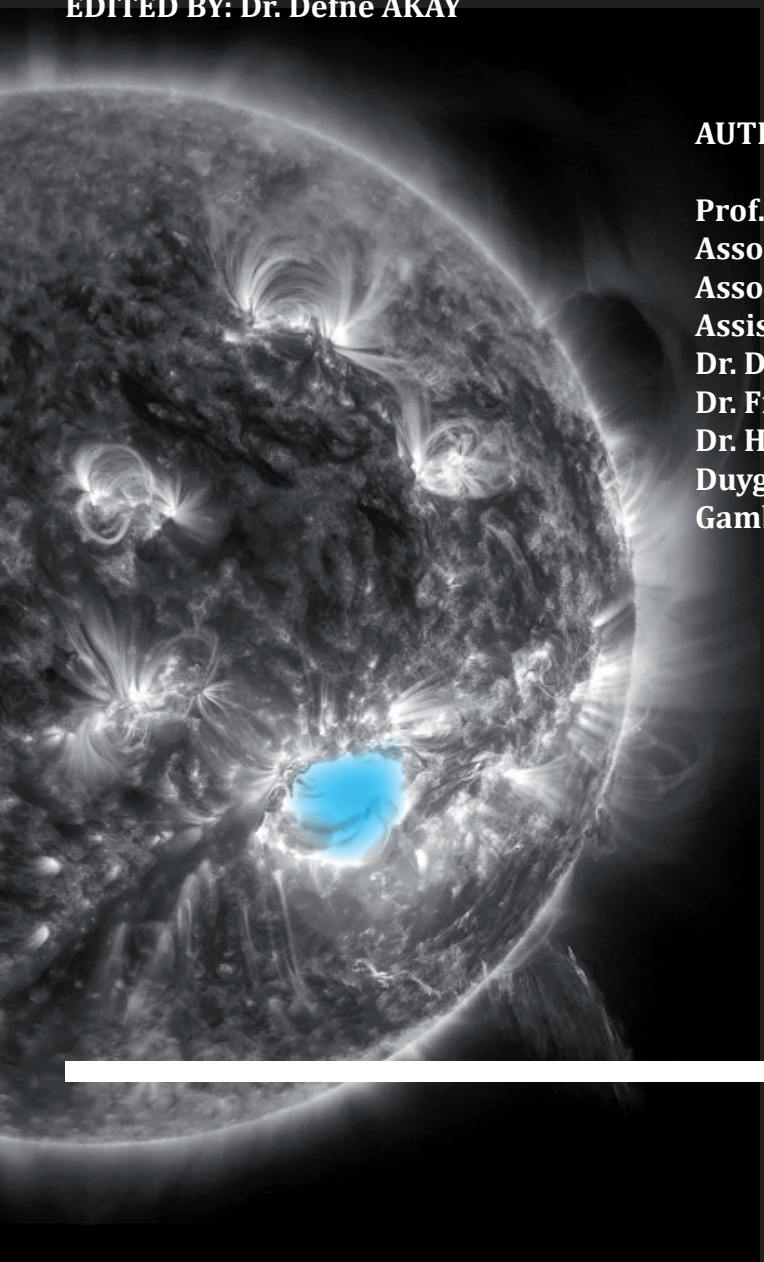

AUTHORS

Prof. Dr. Sema Bilge OCAK
Assoc. Prof. Dr. Özgür DEMIRCAN
Assoc. Prof. Dr. Uğur GÖKMEN
Assist. Prof. Dr. Ebru ALAKAVUK
Dr. Defne AKAY
Dr. Filiz SARI
Dr. Hasan DEMİR
Duygu ÇINAR UMDU
Gambo WURMA BARA'U

İKSAD
Publishing House

ENGINEERING ON ENERGY MATERIALS

EDITED BY

Dr. Defne AKAY

AUTHORS

Prof. Dr. Sema Bilge OCAK
Assoc. Prof. Dr. Özgür DEMIRCAN
Assoc. Prof. Dr. Uğur GÖKMEN
Assist. Prof. Dr. Ebru ALAKAVUK
Dr. Defne AKAY
Dr. Filiz SARI
Dr. Hasan DEMİR
Duygu ÇINAR UMDU
Gambo WURMA BARA'U

İKSAD
Publishing House

(The Licence Number of Publicator: 2014/31220)
TURKEY TR: +90 342 606 06 75
USA: +1 631 685 0 853
E mail: iksadyayinevi@gmail.com
www.iksadyayinevi.com

ISBN: 978-625-7139-55-7
Cover Design: İbrahim KAYA
October / 2020
Ankara / Turkey
Size = 16 x 24 cm

CONTENTS

PREFACE

The book **"**Engineering on Energy Materials**"** is devoted review papers and original papers on the two main topic which are energy saving materials and industrial robotic materials. Original papers are printed for appreciate of their authors for the critical eyes of readers but review articles are provide basic guides and rough draft plans in the energy material literature for their readers.

Credible solutions for some of the energy saving materials including controlled daylighting during the solar receiving hours and learning how to manage electronic and structural properties of semiconductor heterostructures and also composites, need a considerable effort in novel technology. Additionally, industrial robotic materials have become employees of intelligent factories which have played an important role in bypassing a new era in the industry. Their important properties, which are very different from those of more common known systems, can give rise to a rich variety of unusual physical phenomena.

Our aim in writing this book is to provide a pedagogical introduction to the essential concepts for newcomers, while also endeavouring to provide a comprehensive- though not exhaustive-reference text for the specialist in electronic and energy saving material fields. Thus, we hope to cater for both with an introduction to the pedagogical essential from which researcher in enginneering and guide for experts in the predominat field.

Dr. Defne AKAY

CHAPTER 1

COMPARISON OF ELECTRONIC PROPERTIES OF POLY (METHYL METHACRYLATE) WITH THE DOUBLE HETEROSTRUCTURE (PMMA/ LEAD OXIDES)

Dr. Defne AKAY[1]

Assoc. Prof. Dr. Uğur GÖKMEN[2]

Prof. Dr. Sema Bilge OCAK[3]

[1] Department of Physics, Faculty of Science, Ankara University, 06100 Ankara, Turkey. E-mail: dakay@science.ankara.edu.tr. ORCID: 0000-0001-8990-007X

[2] Graduate School of Natural and Applied Sciences, Department of Advanced Technologies, Gazi University, 06500 Ankara, Turkey. ORCID: 0000-0002-6903-0297

[3] Graduate School of Natural and Applied Sciences, Department of Advanced Technologies, Gazi University, 06500 Ankara, Turkey. sbocak@gazi.edu.tr. ORCID: 0000-0002-0590-7555

1. INTRODUCTION

Since the semiconductor hetero-structures appeared in the novel technology, to discuss the importance, improvement, and advancement of the structures has been seen as a common interest of many researchers of the century. That's why heterostructures have the great attention of many researchers in the field of material scientist and condensed matter physicist. The earliest electronic devices are based on the contact between a metal and a vacuum. But the new generation industry is based on junctions between semiconductors as well as insulators and junctions between different many kinds of semiconductor alloys.

Scientists are seeking to establish better material with desired properties and are wanting its manipulation with different dopings as a tool mechanism. The advantage of these is that a heterostructure can be constructed by modifying semiconductors of different types with different band gaps and different electron varieties that to create an alternating variation of the potential seen by electrons in the conduction band and holes in the valence band. The possibility of the control of semiconductor material by doping with various impurities, e.g., mobilities, electronic energy spectrum, effective masses of the charge carriers namely controlling the fundamental parameters inside the semiconductor crystals and device, seems to be more possible in double heterostructures. The double heterostructures including quantum-dots (QDs), quantum-wires (QWis), and quantum-well (QW), are the subject of interesting physics of the semiconductor

physics community. If a semiconductor is sufficiently small to give overlap of adjacent electron (hole)s and periodically perfect repeated in space can become a superlattice when the thicknesses of the heterostructure fulfill the required conditions. PMMA, i.e., Poly (Methyl Methacrylate) is a polymer class that has two structure names Poly[1-(methoxycarbonyl)-1-methylethylene] and Poly(methyl 2-methylpropenoate), but its common name is Methyl methacrylate. The poly structure is produced from monomer methyl methacrylate and its chemical structure of polymethyl methacrylate (PMMA) can be seen from Fig.1.

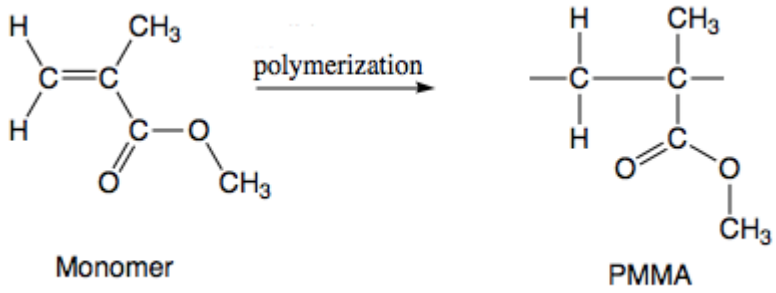

(a) (b)

Fig.1 (a) Structure of methyl methacrylate (b) basic unit of the monomer that makes up PMMA.

Poly-methacrylates are amorphous raw material thermoplastics of high transparency that can be used as an alternative to glass. The material is easily processed and converted into films, rods, tubes, and sheets. The semi-finished products commercially considerable important and it shows numerous sound mechanical properties. The

structure is generally known as an acrylate, plexiglass, lucite, altuglass and is often used as an alternative to glass. Moreover. PMMA has a higher impact strength than glass and is softer than glass so will not shatter like a glass. PMMA transmits more light than a glass and PMMA does not filter ultraviolet (UV) light. Because of its high transparency (up to 90% transmission of visible light), toughened acrylics are often used as a shatter-resistant replacement for regular glass and used in the lenses of exterior lights of automobiles. The amorphous thermoplastic material is superior weather ability that has better properties when exposed to moisture but is not resistant to many (polar) solvents such as alcohols, organic acids and ketones. PMMA has a good degree of compatibility with human tissue so it can be used as medical technologies and implants. Hard contact lenses are frequently made of this material. Dentures are often made of PMMA. In cosmetic surgery and has also been linked to cardiopulmonary events. The other side we have approached the structure as a nanomaterial. It is an invaluable tool in nanotechnology. In the semiconductor industry, the material supports as a resist in the electron beam lithography process. In the process, the polymer in a solvent is used to spin coat silicon wafers with a thin film. Any patterns on this stage are made by exposure to an electron microscope, deep UV or X-rays, and perform chain scission in the PMMA. This permits to leave of selective area on the material. In the stage, the advantage of the PMMA is to let there be no trouble on the material and permits for exceedingly high-resolution patterns to be realized.

Despite the many advantage, the material has also some disadvantages low chemical resistance, low impact resistance and possible stress problems. Many proposals have been made to improve matters efficiency but to do best of our knowledge, there has been no study to compare the efficiency of the PMMA with powered by lead oxides (PMMA/PbO) heterosructures. In this study we will extend the material by constructing a heterostructure with lead oxides. Lead oxide (PbO)s can be found in many forms despite that two crystalline modifications which are (red-tetragonal (litharge) α-PbO and yellow-orthorhombic (massicot) β-PbO) the two most used forms. Orthorhombic crystal phases come into being at higher temperatures than 486°C whereas litharge which have orthorhombic structures obtained at lower temperatures and is stable at low pressure. The exists two polymorphs have the low electrical conductivity and also have remarkable semiconducting properties. Therefore, PbO possess important potential implementations of industrial area including; laser technology, electroradiography, electrophotography, and for imaging devices. In particular, thin films of lead oxide(PbO) have received much attention in the fabrication of detectors and production of semiconductor gas sensors. Lead oxides is also interest as optical gratings and IR transmitting devices. Because of the optical properties like extension of transmission in the UV (ultraviolet) region can be varying amounts altered by incorporating suitable additives, is possible. It is well known that PbO exhibits excellent structural, mechnical and morphological properties and also chemical stability. Above all, in the battery industry has been used as a lead powder for

different applications. It is produced by two methods which are Barton pot (Pavlov. 2017) and Ball mill (Pavlov. 2017) methods. In the Barton pot method oxidized molten lead pulverized by humidified air flow whereas in latter method the lead balls get oxidized under the strike and rub so the action of cause heat generation. Oxides particles are carried by air flow and cyclone separators save the lead oxide grains of the desired size. The latter method only can be used for yellow-orthorhombic forms whereas the first method can be used for both phase forms. Lead oxide thin films can be achieved by a variety of techniques like thermal evaporation (Koskinen. 2014), atomic layer epitaxy (Leskela. 2014), laser-assisted deposition (Matias and Hammond. 2011), metal-organic CVD, ALD, and exposing films to RF oxygen plasma. It is well known that PbO exhibits excellent chemical stability. So, the commercial a lead oxide (PbO) if contains some PMMA or supported with PMMA as a heterostructure how it will react its magnificent properties on the electronic materials which it is a big curiosity for material scienciest. To understand the influence of the chemical reaction on the area, PMMA on PbO have been performed as a heterostructure and realized with a demanding experimental process that requires labor. In this study, thermal evaporation method has been used. First designed of the $Al/PMMA/p-Si$ thin film, detailed description has been made in the experimental part of the (Akay et al. 2019). Than characterization measurements of capacitance and conductance –voltage has been realized by operate an Agilent (4294A) impedance analyzer. But it should be take into account that capacitance-voltage ($C-V$) and

conductance-voltage ($G-V$) evaluations have been actualized a high-frequency regime (1 MHz). Following all measurements completed, coated wafers has been covered PbO with a pressure of $2\times 10^{-6}\,Torr$ and used as a substrate for Poly (Methyl Methacrylate). To construct the two structure to produce uniform heterostructure polymer, spin coating technique has been employed which technique is extensively used in to perform poly-structure. After performed Poly (Methyl Methacrylate)/Lead Oxide heterostructure again all measurements has been realized and by a microcomputer through measurements formed to evaluate the values.

2. RESULTS AND DISCUSSION

2.1 Current-Voltage (I-V) Contribution of Poly (Methyl Methacrylate) and Poly (Methyl Methacrylate)/Lead Oxide

Material science provides an outstandingly successful account of the dielectric and electronic properties of solids. In the part reverse and forward bias measurements of the PMMA /p-Si and PMMA/PbO /p-Si were implemented at room temperature and its form is given of $I-V$ characteristic in the Fig. 2 and its semi-logaritmic $ln(I)-V$ characterisic of the structure given in the Fig.3 . The two figures show a good agreement, i.e., behave in harmony with each other. As can be seen from the Fig. 3, the reverse current demonstrate weak voltage dependency, the forward current has increment an exponentially with the voltage. The forward bias semi-logaritmic $\ln(I)-V$ plots have a linear region in the voltage range of $0.5-1\,V$. Because of the interfacial polymer layer, its leave from the linearity of

the plot. The deviate is markedly seen from the $I-V$ plot of PMMA/PbO structure whereas I-V characteristic of the plastic based acrylate, i.e., PMMA (Poly (Methyl Methacrylate)) shows a linearity. It shows that series resistance (R_s) has effects the linearity because interfacial layers interact with each other. It can be evaluated doping of the polymers. As known that dopants are strong oxidizing or reducing agents, on doping, positive or negative charge carriers are developed in the polymers. Furthermore, slightly non-saturation movement has been noticed as a function of applied bias voltage in the reverse bias area that can be expressed by the image force lowering of barrier height(BH). To evaluate the series resistance and an interfacial layer of the heterostructure Current-voltage ($I-V$) relations can be written as [6],

$$I = I_0\, Exp\left[\frac{q(V - IR_s)}{nkT}\right] \qquad (1)$$

Here, n is the ideality factor which is important both linear and non-linear regions of the $I-V$ plots, R_s is series resistance of the diode. I_0 is the reverse bias saturation current that can be extracted from the straight line intercept of $ln\, I-V$ characteristic at zero bias and can be evaluated as,

$$I_0 = AA^*T^2 Exp\left[-\frac{q\Phi_{Bzero}}{kT}\right]. \qquad (2)$$

To evaluate the reverse bias saturation current I_0, rectifier contact area A and Richardson constant A^* should be calculated for the material. Richardson constant is 32 $A/cm^2\,K^2$ for p-type Si. Φ_{BH} is the

effective barrier heigh in the polymers and T is the absolute temperature as a Kelvin. Boltzmann constant is k. n is the ideality factor which can be supplied by taking the deviation of the $I-V$ experimental data. The experimental process is compatible with the thermionic emission theory (TE), and the results also comply with the slope of linear region of the forward bias. Our calculations have been realized with $lnI-V$ characteristics and was represented as,

$$n=\frac{q}{kT}\frac{d(V-IR_s)}{d(\ln\ I)}. \qquad (3)$$

The values of Φ_{BH} can be achieved by reverse bias saturation current I_0. So, the $Eq.2$ is useful tool for the zero bias values. The experimental values of I_0, n, and Φ_{BH} have been obtained for the $PMMA/p-Si$ and $PMMA/PbO/p-Si$ at room temperature. For the $PMMA/p-Si$ the barrier height is $0{,}77\ eV$, the ideality factor is $5{,}04$ and the reverse bias saturation current is $4{,}02\times10^{-9}A$, whereas for the $PMMA/PbO/p-Si$ the reverse bias saturation is $0{,}81\ eV$, the ideality factor is $7{,}11$ and the reverse bias saturation current is $7{,}52\times10^{-10}A$. The high value of ideality factor can be attributed to the effect of inhomogeneties and high density of interface states (D_{it}). Therefore, from the evaluation of thermionic emission theory can be seen that two fold heterostructure ($PMMA/PbO$) has higher ideality factor so has high barrier height The calculations made with Cheung method (Cheung and Cheung. 1986) can also be seen from the from the Table 1. What is done with thermionic emission theory supports

Cheung method. According to the Cheung method the evaluated functions can be expressed as:

$$\frac{dV}{d(ln\, I)} = n\frac{kT}{q} + IR_s \tag{4}$$

$$H(I) = V - \left(\frac{nkT}{q}\right) ln\left(\frac{I}{AA^*T^2}\right) = R_s I + n\Phi_B \tag{5}$$

For the $PMMA/p-Si$ the barrier height is 0,79 eV, the ideality factor is 1,84 and the reverse bias saturation current is $1{,}68 \times 10^{-9} A$, whereas for the $PMMA/PbO/p-Si$ the reverse bias saturation is 0,81 eV, the ideality factor is 3,34 and the reverse bias saturation current is $7{,}07 \times 10^{-10} A$. The series resistance (R_s) of the materials are also prominent parameters that impact on the performance of the structures. The values of R_s was obtained by using Cheung method. For the ideal situation, R_s series resistance of any materials must be zero, but in the application as in our study the conditions are different from the ideal case. Thus, the values of R_s were obtained from the structures. To obtained these, $I-V$ characteristics have been used. Experimental $dV/d(lnI) - I$ characteristics of the $PMMA/p-Si$ and $PMMA/PbO/p-Si$ are presented in Fig.4 at room temperature. Intercept of $dV/d(lnI) - I$ plots will give series resistance R_s. The values of R_s for $PMMA/p-Si$ and $PMMA/PbO/p-Si$ were found as 32Ω and 660 Ω, respectively. It is clearly seen from the values $PMMA/p-Si$ has low series resistance than the $PMMA/PbO/p-Si$ heterostructure. Previously expressed (Cheung method) n ideality factor values were found from the slope of the $dV/d(lnI) - I$

characteristics that was given to be nkT/q. Then by using the ideality factor values of structures which determined from Eq.4 and the datum of downward curvature region in forward bias region $I-V$ plots in Eq.5 will lead to a straight line with y-axis intercept which corresponds to $n\Phi_{BH}$. In this way $h(I)\ vs.I$ will deliver Φ_{BH} and R_s values were found to be all values as in the Table 1. In Cheung functions high-voltage section of the forward bias $lnI\ vs.V$ plots are convenient to the nonlinear region. Series resistance values may be great for the higher ideality factor values. The values of R_s are high for the $PMMA/PbO/p-Si$ heterostructure device due to the low homogeneity which has two fold structure. Therefore, it causes low electrical conductivity and mobility. The result of series resistance values are generally ascribed to series combination of resistance and demonstrate that the structure feels a current limiting factor on the movement of its current.

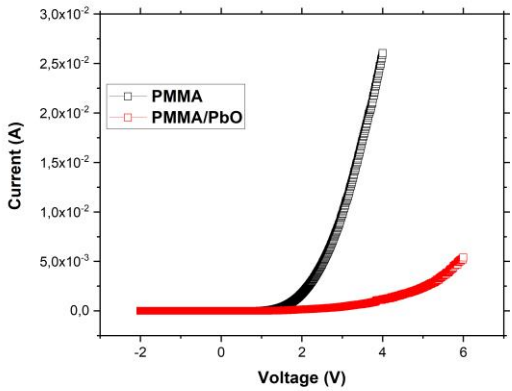

Fig. 2 Experimental Current-Voltage ($I-V$) characteristics of the Al/PMMA/p-Si Schottky barrier diode and Al/PMMA/PbO/p-Si heterostructure at room temperature.

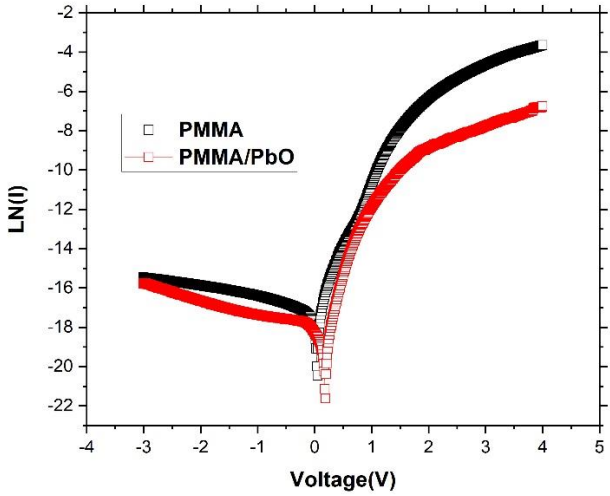

Fig. 3 Experimental forward and reverse bias semi-logarithmic ln I–V characteristics of Al/PMMA/p-Si, Al/ZnO/p-Si and Al/PMMA/ZnO/p-Si devices at room temperature.

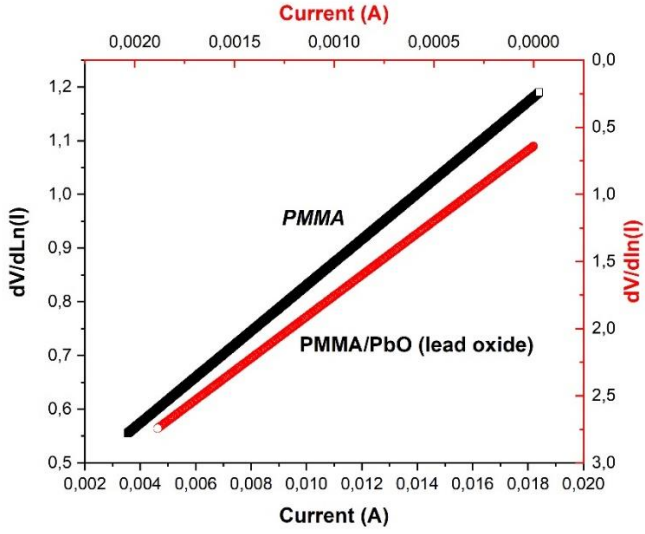

Fig. 4 Experimental $dV/d(lnI) - I$ characteristics characteristics of the Al/PMMA/p-Si Schottky barrier diode (black color) and Al/PMMA/PbO/p-Si heterostructure (red color) at room temperature.

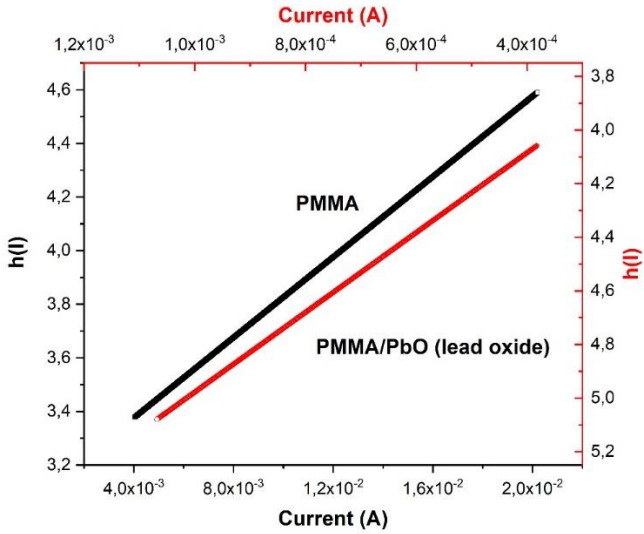

Fig.5 $h(I)\ vs.\ I$ characteristics of the Al/PMMA/p-Si Schottky barrier diode (black color) and Al/PMMA/PbO/p-Si heterostructure (red color) at room temperature.

	I-V Parameters							
	Thermionic Emission Theory				*Cheung Method*			
	$\Phi_b(eV)$	n	$R_s(\Omega)$	$I_0(A)$	$\Phi_b(eV)$	n	$R_s(\Omega)$	$I_0(A)$
PMMA	0,77	5,04	- -	$4{,}02 \times 10^{-9}$	0,79	1,84	32	$1{,}68 \times 10^{-9}$
PMMA/PbO	0,81	7,11	---	$7{,}52 \times 10^{-10}$	0,81	3,34	660	$7{,}07 \times 10^{-10}$

Table1. I-V parameters of materials

2.2 Capacitance-Voltage (C-V) and Conductance-Voltage (G-V) Contribution of Poly (Methyl Methacrylate) and Poly (Methyl Methacrylate)/Lead Oxide

Capacitance-Voltage $(C-V)$ and Conductance-Voltage $(G-V)$ works are most popular electrical meaurement evaluation techniques used generally to desribe a Schottky device. In the part of the study, the reverse and forward bias of the $C-V$ and $G-V$ measurements has been realized at room temperature in the frequency of $1MHz$. The analysis has been performed by the impedance analyzer and the measurements strongly depend on the bias voltage because junction capacitance distinction mechanism for the reverse biased structures. In the study bias voltage has been altered between -3V and +3V direct – current and measured capacitance and conductance has been evaluated. The C–V graphs exhibit a typical p-type organic metal-insulator-semiconductor (MIS) and metal-semiconductor (MS) motion described that can be seen from the Fig. 6. It shows the typical MIS and MS structure characters and have not surprised us. These has two regimes which by depletion at less negative bias, a deep depletion, and an accumulation at negative bias regions. The results of dielectric constant values in this beneficial method strong depend strongly on the frequency. Lower frequency can be causes dipolar and ionic surface charge polarizations at the boundary interfaces. To avoid such situations high frequency regime (1MHz) is the best. Additionally, the practical method is from time to time influence from some structurel defects. Maykusiak and Jakubowski (Maykusiak and Jakubowski.)

have showed that because of the work function, some values of the $C-V$ curves can be replace. And Akay et al. (Akay et al. 2019) have showed that irradiation can cause a shift of the real $C-V$ curve with respect to the ideal one. In this study, they also test that increament of the radiation doses which does not big changes on the material. Furthermore, on the some other MIS structures (HfTiSiO and HfTiO) have been analyzed. Their results supports the parallel shift on the $C-V$ curves. As can be seen in the $C-V$ curves of $PMMA/p-Si$ (black color) and $PMMA/PbO/p-Si$ (red color), the accumulation worth of $PMMA/p-Si$ is $3{,}5\times10^{-9}\,F$ whereas the values of $PMMA/PbO/p-Si$ is $2{,}25\times10^{-9}\,F$. In Fig. 7, the $G-V$ curve is similar the C-V curve and its characterisric behavior is indeed severely based on the frequency regime. So that, it has been analyzed in the high frequency regime and it has accumulation, depletion and deep depletion regions at the regime.

In order to analyze better with the our datum, we have also study on the series resistance of the MIS and MS materials. This depends on the measurent capacitance and conductance values of the structure. In this study we also prefered to study on the series resistance (R_s) rather than R_i which depend on the voltage dependence of the resistance. The well-known method attributed to Nicollian and Brews (Nicollian and Brews. 1982). But we think that the knowledge of the regimes of structures is more suitable for the study. The series resistance of the diode supplied by

$$R_s = \frac{G_c}{(G_c)^2 + (\omega C_c)^2} \tag{6}$$

here the elements G_c and C_c are measured conductance and capacitance values in the accumulation region, respectively. The values has been evaluated at high frequency regime (1MHz). The measured parameters can be expressed as,

$$C_c = \left(\frac{(G_m^2 + \omega^2 C_m^2)C_m}{(a^2 + \omega^2 C_m^2)}\right), \qquad G_c = \left(\frac{(G_m^2 + \omega^2 C_m^2)a}{(a^2 + \omega^2 C_m^2)}\right) \tag{7}$$

together with

$$a = G_m - (G_m^2 + \omega^2 C_m^2)R_s. \tag{8}$$

The R_s values in Eq.6 can also be based upon the interfacial polymer layer. The particular distribution of localized density of the interface states metal, insulator and inorganic semiconductor interface and also, metal insulator inteface. In high frequency regime the contribution of the interface states on the conduction and capacitance values can be disregard its contribution. Because interface state density can not follow the signals, thus the D_{it} can formulated as,

$$D_{it} = \frac{2}{qA}\frac{G_{cmax}/\omega}{\left(\frac{G_{cmax}}{\omega C_i}\right)^2 + \left(1 - \frac{C_c}{C_i}\right)^2} \tag{9}$$

where açısal frequency is $\omega = 2\pi f$. The interface states density was ensured by Hill-Coleman method and C_i corressponds to capaitance of interfacial layer and is written as,

$$C_i = C_c\left[1 + \frac{G_c^2}{(\omega C_c)^2}\right] = \frac{\varepsilon_i \varepsilon_0 A}{d}. \quad (10)$$

In Fig.8 the $R - V$ plot gives the recognizable peak for the PMMA/p-Si structure at $350\ \Omega$ whereas, PMMA/PbO/p-Si has approximately $75\ \Omega$ of resistance value. The value really so small when compared with the PMMA/p-Si under voltage effect. The corresponding interfacel states density is also affected from the series resistance-voltage relation. As can be seen from the Table 2, small D_{it} value means that small resistance for the structure. In Fig. 9, $C^{-2} - V$ characterization is ploted. As seen from the figure that the plot yield straight line in the range of performed bias voltage. The C^{-2} values increase with the applied bias voltage both for PMMA/p-Si (MS) and PMMA/PbO/p-Si (MIS) heterostructure. Bhajantri et al. (Bhajantri et al. 2007) has studied on $BaCl_2$ doped polyvinyl alcohol polymer films. In this study, the researchers exhibited that $C^{-2} - V$ characterization represents the interfacial state density, i.e., $C^{-2} - V$ scheme is a function interfacial density states (D_{it}). The expression of C^{-2} can be given by,

$$\frac{1}{C^2} = \frac{2(V_0 + V)}{q\varepsilon_s \varepsilon_0 A^2 N}\ . \quad (11)$$

$$\frac{d(C^{-2})}{dV} = \frac{2}{q\varepsilon_s \varepsilon_0 A^2 N} \quad (12)$$

Here, V is described as a gate voltage which decided from the interpretation and extrapolation of straight lines of bias voltage axis and diffusion potential at zero bias represented by V_0. The important

characteristic plot is also very advantageous to find the other electrical parameters of the materials. Fermi energy, barrier height, doping concentration and depletion layer can also be estimated from the Fig. 9 and Eq. 11 and Eq. 12.

Barrier height values of the PMMA/p-Si (MS) and PMMA/PbO/p-Si (MIS) are found from the relation,

$$\Phi_b(C-V) = V_b + E_F - \Delta\Phi_b \tag{13}$$

together with,

$$\Delta\Phi_b = \left(\frac{qE_{max}}{4\pi\varepsilon_s\varepsilon_0}\right)^{1/2} \quad ; \quad E_{max} = \sqrt{2qN_AV_b/\varepsilon_s\varepsilon_0}\,. \tag{14}$$

The electrical parameter of $\Delta\Phi_b$ is the energy gap between the conduction band edge and bulk Fermi level and maximum electric field (E_{max}) can be represented in the Eq.(14). ε_s is the dielectric constant of p-type Si. It is value of the ε_0 is $8{,}85 \times 10^{-14} F/cm$ that is permittivity of free space.

By using the expressions, Table 2 has been completed. Fermi energy levels of PMMA/p-Si and PMMA/PbO/p-Si evaluated by the using of Eq.(15),

$$E_F = \frac{kT}{q}\ln\left(\frac{N_v}{N_A}\right). \tag{15}$$

N_A is the carrier concentration of the materials. It can be determined by the experimental measurements. With the help of effective density of states, as seen in Eq. (16),

$$N_v = 4.82 \times 10^{15} T^{3/2} \left(\frac{m_h^*}{m_0}\right)^{3/2} \quad (16)$$

The expression is evaluated in valance band for p-Si. m_h^* is the effective mass of holes and m_0 is the rest mass of electron. The two masses have the a special relation each other $m_h^* = 0.16\, m_0$. The width of space charge layer can written as,

$$W_d = \sqrt{\frac{2\varepsilon_s V_b}{qN_A}}\,. \quad (17)$$

All the analytical parameters, which are arranged in categories according to shared characteristics in Table 2. The tabulated values strongly based on the carrier concentration of the PMMA/p-Si (MS) and PMMA/PbO/p-Si (MIS) structures.

Table2. C-V parameters of materials

	C-V Parameters					
	$\Phi_b(eV)$	$D_{it}(eV^{-1}cm^{-2})$	$R_s(\Omega)$	$E_F(eV)$	$\Phi - \Delta\Phi$	$V_d(V)$
$PMMA$	1,066	$7{,}83 \times 10^{12}$	233	0,141	1,031	0,92
$PMMA/PbO$	0,374	$5{,}19 \times 10^{12}$	45	0,138	0,348	0,23

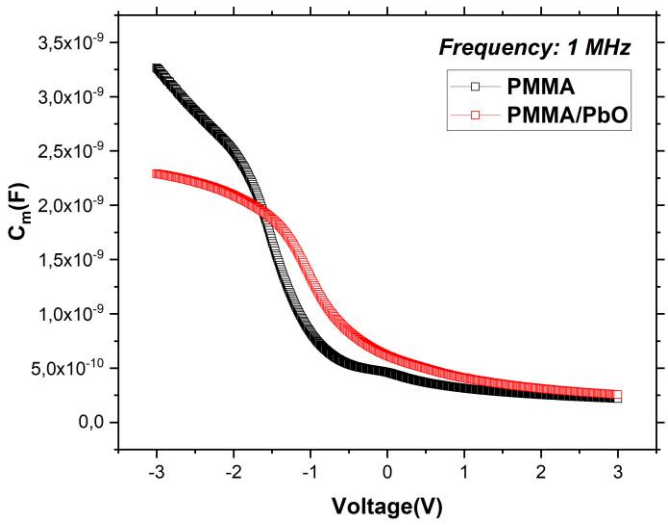

Fig.6 $C-V$ characterization of $PMMA/p-Si$ (MS) and $PMMA/PbO/p-Si$ (MIS) in 1MHz

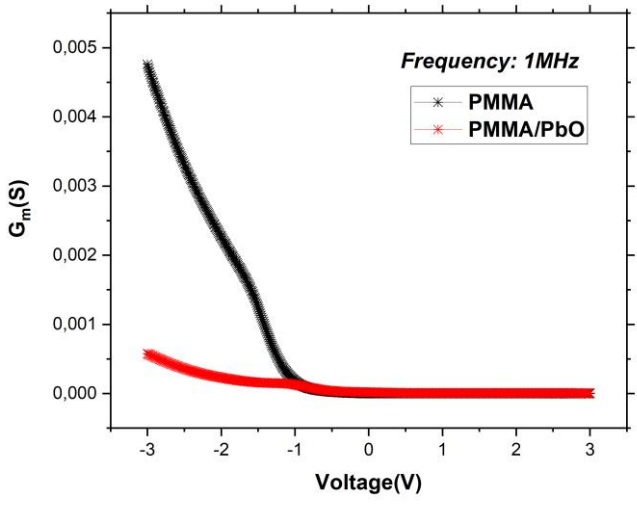

Fig.7 $G-V$ characterization of $PMMA/p-Si$ (MS) and $PMMA/PbO/p-Si$ (MIS) in 1MHz

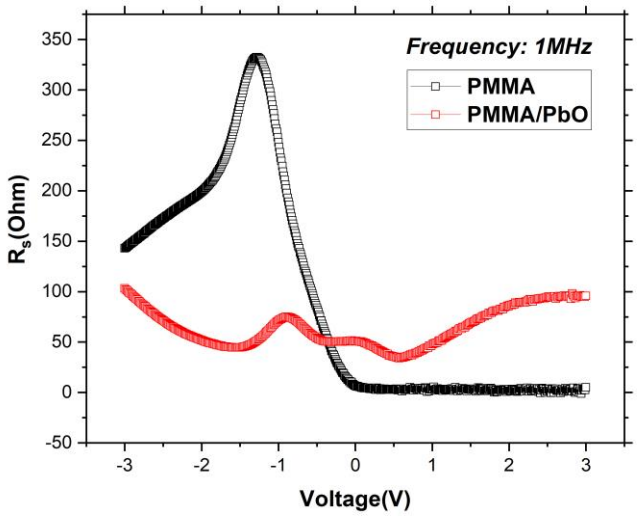

Fig.8 $R_s - V$ characterization of $PMMA/p - Si$ (MS) and $PMMA/PbO/p - Si$ (MIS) in 1MHz

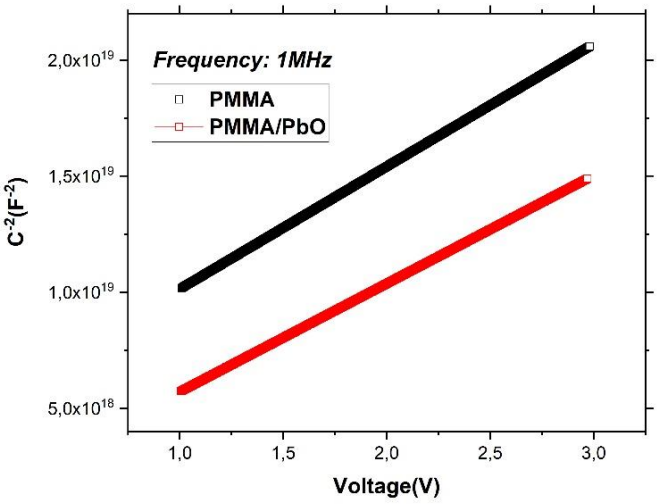

Fig.9 $C^{-2} - V$ characterization of $PMMA/p - Si$ (MS) and $PMMA/PbO/p - Si$ (MIS) in 1MHz

CONCLUSION

With the advent of the semiconductor hetero-structures in the novel technology, considerable effort has been expanded in learning how to manage electrical and electronic properties of the material, or more precisely to measure the parameters in the materials. It is well known that the computations are based conceptually upon the experimental procedure of starting in a reverse and forward bias of the characteristics of the produced PMMA/p-Si (MS) and PMMA/PbO/p-Si (MIS) Schottky barrier diodes have been examined at room temperature. It is well known that PMMA is a great and magnificent properties on its own. In this study the need to know the how PMMA, i.e., Poly (Methyl Methacrylate) polymer will react by creating a hetero-structure with PbO (Lead oxide) structure. Thus, to determine the effect of series resistance (R_s), saturation current, ideallity factor, Fermi level, maximum electrical field, energy gap ($\Delta\Phi_b$) between the conduction band edge and bulk Fermi level, etc. we evaluated $I-V$ (current-voltage), $C-V$ (capacitance-voltage) and $G-V$ (conductance-voltage) measurements of the structures. I-V method is based upon Ohm's law with thermionic emmission theory. The parts of the study show that the values $PMMA/p-Si$ has low series resistance than the $PMMA/PbO/p-Si$ heterostructure. Low series resistance corresponds to small ideallity factor fort he both method which are standart method and Cheung method. The saturation current, i.e., scale currents are fragment of the reverse currents in PMMA, i.e., Poly (Methyl Methacrylate) polymer and PMMA/PbO/p-

Si heterostructure. Saturation current which is nearly independent of the reverse voltage. The current completely caused by diffusion of minority carriers from the neutral regions to the depletion region. Its values $4{,}02 \times 10^{-9}\,A$ for $PMMA/p-Si$ and $7{,}52 \times 10^{-10}A$ for $PMMA/PbO/p-Si$, when evaluated with Thermionic emmission theory whereas its values $1{,}68 \times 10^{-9}A$ for $PMMA/p-Si$ and $7{,}07 \times 10^{-10}A$ for $PMMA/PbO/p-Si$, when evaluated with Cheung method. The results of these two methods are compatible with each other.

C-V and G-V methods are based upon Nicollian method. Depending on the method, two material evaluated. These has two regimes and three regions which are a depletion at less negative bias, a deep depletion and an accumulation for the C-V and G-V characteristics in high frequency regime (1MHz). The C-V studies use a DC (direct-current) whereas I-V measurements use AC (alternative-current). Because of the this, some difference can be seen in the evaluated parameters especially of the R_s. Additionally, energy density distribution side of the materials has been examined by the corrected values of experiment. To evalute the interfacial states density (D_{it}), series resistance-voltage relation is important factor. The high value of interfacial density D_{it} was attributed to the existence of high values R_s. But it is clear that interfacial layer is lead to significant errors on the evaluation of the results and two fold interlayer can also increased the errors so it should be take into account when evaluated the parameters of the materials. As a result, the material can be

manipuleted by the doped layer. Not ignoring the factors, we use extend our studies with different layers. The decisive experiment in bring about acceptance of the Ohm's law for I-V measuremets and Nicollian method for C-V and G-V measurements. Because of great importance of the electrical and dielectrical properties in polmers (MIS and MS), almost all words and technique are in order on how it is measured, calculated, and all detailed. Neither experimental measuremet nor theoretical calculation is straightforward. The most percise experimental technique has been used. The actual story of what happens in such experiments is sufficiently explained. Thus, our study will be guide for future research in material science.

REFERENCES

Akay, D., Gokmen U., Ocak, S. B. (2019). Radiation-induced changes on poly(methyl methacrylate) (PMMA)/lead oxide (PbO) composite nanostructure. Phys. Scr. 94 (2019) 115302 (8pp).

Bhajantri, R.F., Ravindrachary, V., Harisha, A., Ranganathaiah, C., Kumaraswamy, G.N. (2007). Effect of barium chloride doping on PVA microstructure: positron annihilation study, Appl. Phys. A: Mater. Sci. Process. 87, 797.

Cheung S. K., Cheung N. W. (1986). Extraction of Schottky diode parameters from forward current-voltage characteristics. Appl. Phys. Lett. 49 (1986) 85.

Koskinen, J. (2014). Cathodic-Arc and Thermal-Evaporation Deposition. Reference Module in Materials Science and Materials Engineering, Comprehensive Materials Processing, Volume 4, 2014, Pages 3-55.

Leskela, M., Niinistö, J., Ritala, M. (2014). Atomic Layer Deposition. Reference Module in Materials Science and Materials Engineering. Comprehensive Materials Processing Volume 4, Pages 101-123.

Matias, V., Hammond, R. H. (2011). In-situ deposition vapor monitoring. In Situ Characterization of Thin Film Growth, Woodhead Publishing Series in Electronic and Optical Materials Pages 212-238.

Maykusiak, B, and Jakubowski, A. (1988). A new method for the simultaneous determination of the surface-carrier mobility and the metal-semiconductor work-function difference in MOS transistors. IEEE Trans. Electron Devices 35, 439–43.

Nicollian, E. H., Brews, J. R. (1982). MOS Physics and Technology. John Wiley & Sons, New York.

Pavlov, D. (2017). A Handbook of Lead-Acid Battery Technology and Its Influence on the Product, Lead-Acid Batteries: Science and Technology (Second Edition).

Sze, S. M. (1981) Physics of Semiconductor Devices, second ed.. Willey & Sons, New York, 1981.

CHAPTER 2

EFFECT OF PROCESSING CONDITIONS ON THE MECHANICAL PROPERTIES OF GLASS FIBER-PP REINFORCED THERMOPLASTIC COMPOSITES

Assoc. Prof. Dr. Özgür DEMIRCAN[1]

[1] Metallurgical and Materials Engineering Department, Ondokuz Mayis University, Kurupelit 55139, Samsun/TURKEY.ozgur.demircan@omu.edu.tr, ORCID ID: 0000-0001-8235-3966

INTRODUCTION

Thermoplastics are widely used in aeronautic and automobile industries, sport, and many other sectors due to specifications of lightweight and recyclability (Florea et al., 2012, Awaja et al., 2005). Therefore, it is important to study glass fiber reinforced thermoplastic composite materials.

The commingled yarn technique, which was a mixing of reinforcing and matrix fibers, was developed to fabricate thermoplastic composites. Brown et al., 2010 reported the properties of a commingled E-glass/polypropylene composite. Knitted multi-layer textile preform reinforced thermoplastic composite was studied by Abunaim et al., 2011. Aslan, 2013 reported the damage mechanism of flax fibre LPET commingled composites. Mäder et al., 2017 reported commingled yarn spinning for composites. They obtained important enhancements in the fiber/matrix bonding due to developed sizing chemistry in fibers.

Some of the researchers studied the effect of processing conditions on the mechanical properties of composite materials. Takagi et al., 2008 studied the flexural properties of cellulose nanofiber reinforced composites. The impact properties of glass/polyamide-6 composite were investigated by Balakrishnan et al., 2019. They reported that the specimen of GPA-6_01 (1.11 bar, 245 °C) had the highest mechanical properties compared to the specimens prepared in other processing conditions (2.77 bar, 235, 245, and 255 °C).

The properties of hot compacted self-reinforced polypropylene composites was reported by Swolfs et al., 2014.

There are some studies on the mechanical properties of composites with various processing parameters. It was found little work on the mechanical properties of the thermoplastic composites with commingled yarns of glass and polypropylene fibers in the literature. Mechanical tests were carried out during this study.

1. EXPERIMENTAL PROCEDURES

1.1. Composite constituents

The glass fibers (GF) and polypropylene fibers (PP) were used in the non-crimp fabrics (NCFs). The density and lengths of binding yarns were 5/inch and 3 mm.

1.2. Fabrication method

The composites with two and eight layers were fabricated on hot-press machine (Table 1). Two and eight layers of the composites had non-symetric stacking sequences, such as $[0_{wa}/90_{we}]_{2T}$ and $[0_{wa}/90_{we}]_{8T}$. The molding pressures and temperature were 1.0, 1.7, 2.5 MPa and 155 °C.

Table 1. Fiber Volume fraction (Vf) and thickness of composites

Composites	Weft Vf (%), GF/PP commingled yarns (500 tex)	Warp Vf (%), GF/PP commingled yarns (500 tex)	Binding Vf (%), Polyester fibers (76 tex)	Total (warp, weft and binding) Vf (%)	Thickness (mm)
GF-PP, 1 MPa, two layers	21.0	21.0	1.40	43.4	0.70
GF-PP, 1.7 MPa, two layers	18.7	18.7	1.30	38.7	0.72
GF-PP, 2.5 MPa, two layers	19.8	19.8	1.30	40.9	0.72
GF-PP, 1 MPa, eight layers	19.0	19.0	1.40	39.4	2.90
GF-PP, 1.7 MPa, eight layers	19.5	19.5	1.30	40.3	2.52
GF-PP, 2.5 MPa, eight layers	23.9	23.9	1.80	49.6	2.01

1.3. Characterization

Two mechanical characterization tests (tensile and three-point bending tests) were conducted on the specimens using INSTRON 5982 100KN testing machine with 1 mm/min linear displacement speed. The dimension of composite coupons had 20 x 160 mm^2 for tensile tests and that was 15 x 90 mm^2 for three-point bending tests.

2. RESULTS AND DISCUSSION

2.1. Tensile properties

Figure 1a and b demonstrates the results of the tensile properties of the glass-PP composites with various molding pressures and with two (Figure 1a) and eight layers (Figure 1b). The results in 90^{o} direction were higher than the results in +45^{o} and -45^{o} directions in both two and eight layers of composites. The specimens with 1.0 MPa molding pressure had the highest values of the tensile modulus (9.3 GPa) and strength (319 MPa) compared to the specimens with 1.7 MPa and 2.5 MPa molding pressures in 90 ^{o} direction in two layers. The specimens with 1.0 MPa molding pressure had the highest values of the tensile modulus (5.5 GPa) and strength (339 MPa) compared to the specimens with 1.7 MPa and 2.5 MPa molding pressures in 90^{o} direction in eight layers. The tensile modulus and strength were enhanced 22% and 14% with 1.0 MPa compared to 2.5 MPa in eight layers.

Comparing these results with others found in the literature, 5% increase in tensile strength for the glass-polyamide 6 composites in 1.11 bar compared to the glass-polyamide 6 composites in 2.77 bar was reported by Balakrishnan et al., 2019.

a)

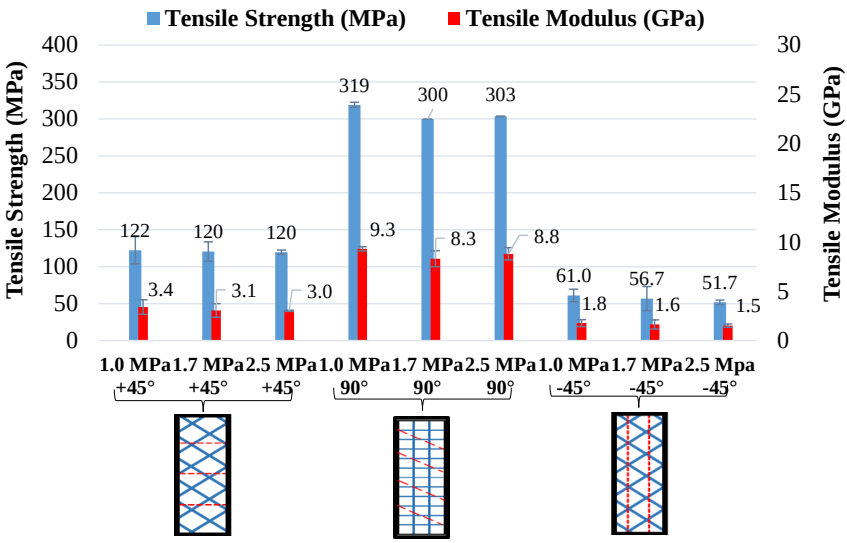

b)

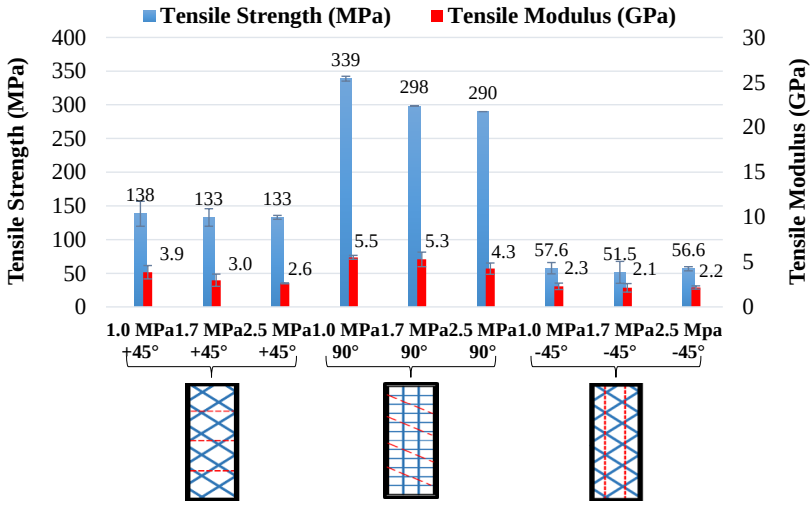

Figure 1. a) Tensile test results of two layers of the composites with various molding pressures, b) Tensile test results of eight layers of the composites with various molding pressures

2.2. Three-point bending properties

The results in 90^{o} direction were higher than the results in +45^{o} and -45^{o} directions in eight layers of composites (Figure 2). The specimens with 2.5 MPa molding pressure had the highest value of the flexural strength (293 MPa) and the second highest value of the flexural modulus (9.5 GPa) compared to the specimens with 1.0 MPa and 1.7 MPa molding pressures in 90 ^{o} direction.

The higher fiber volume fractions of the composites with 2.5 MPa molding pressure (23.9%) compared to the composites with 1.0 MPa (19.0%) in the 90° direction would be the reason for the better bending properties of the PP specimens with 2.5 MPa compared to the PP specimens with 1.0 MPa.

Comparing these results with others found in the literature (Takagi et al., 2008), 25% increase in flexural modulus and strength for the composites in 25 MPa molding pressure compared to the composites in 10 MPa molding pressure.

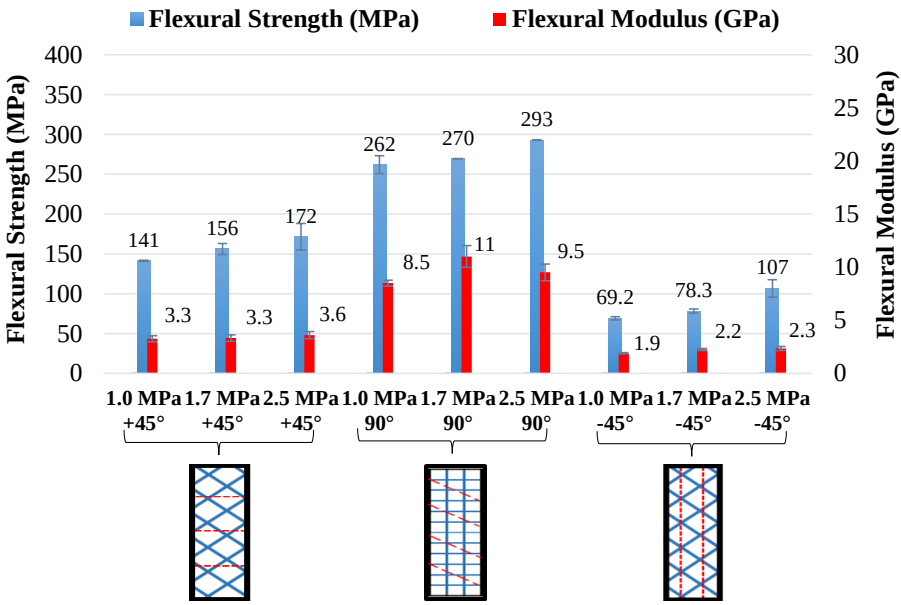

Figure 2. Flexural test results of eight layers of the composites with various molding pressures

CONCLUSION

Our study demonstrated that the mechanical properties of the thermoplastic composites can be controlled by changing the molding pressure. The specimens with 2.5 MPa molding pressure showed the highest values of bending properties compared to 1.0 MPa in 90° direction. Furthermore, the best tensile and bending properties were obtained from the specimens in the 90° direction.

REFERENCES

Abounaim, M. D., Diestel, O., Hoffmann, G., Cherif, C. 2011. High performance thermoplastic composite from flat knitted multi-layer textile preform using hybrid yarn, Composites Science and Technology, Vol: 71, pp: 511–519.

Aslan, M. 2013. Investigation of damage mechanism of flax fibre LPET commingled composites by acoustic emission", Composites: Part B, Vol: 54, pp: 289–297.

Awaja, F., Pavel, D. 2005. Recycling of PET. European Polymer Journal, Vol: 41, pp: 1453-1477.

Balakrishnan, V. S., Wartig, K., Tsombanis, N., Seidlitz, H. 2019. Influence of processing parameters on the impact behaviour of glass/polyamide-6 composite, Composites Part B, Vol: 159, pp: 292–299.

Brown, K. A., Brooks, R., Warrior N. A. 2010. The static and high strain rate behaviour of a commingled E-glass/polypropylene woven fabric composite, Composites Science and Technology, Vol: 70, pp: 272–283.

Florea, R. M., Carcea, I. 2012. Polymer matrix composites – routes and properties, International Journal of Modern Manufacturing Technologies, Vol: IV, pp: 59-64.

Swolfs, Y., Zhang, Q., Baets, J., Verpoest, I. 2014. The influence of process parameters on the properties of hot compacted self-reinforced polypropylene composites, Composites: Part A, Vol: 65, pp: 38–46.

Takagi, H., Asano, A. 2008. Effects of processing conditions on flexural properties of cellulose, nanofiber reinforced ''green'' composites, Composites: Part A, Vol: 39, pp: 685–689.

Wiegand, N., Mäder, E. 2017. Commingled yarn spinning for thermoplastic/glass fiber composites, Fibers, Vol: 26, pp: 1–15.

CHAPTER 3

INVESTIGATION OF THE MECHANICAL PROPERTIES OF BASALT FIBER-PA 6.6 REINFORCED THERMOPLASTIC COMPOSITES

Assoc. Prof. Dr. Özgür DEMIRCAN[1]

[1] Metallurgical and Materials Engineering Department, Ondokuz Mayis University Kurupelit 55139, Samsun/TURKEY.ozgur.demircan@omu.edu.tr, ORCID ID: 0000-0001-8235-3966

INTRODUCTION

To fabricate environmentally friendly materials, using of natural fibers reinforced polymer composites is increasing in recent years. Basalt is one of the most common rocks in the world. Basalt fibers are made from basalt rock (Asadi et al., 2017). One of the studies reported that basalt fiber showed high performance compared to glass fiber (GF) (Lopresto et al., 2011).

The advantages of the thermoplastics are lightweight, highly recyclable, high-impact resistance, and reshaping capabilities (3).

The mechanical properties of basalt fiber reinforced composites were studied by several researchers in the literature (Asadi et al., 2017, Lopresto et al., 2011, Fragassa et al., 2018, Aslan et al., 2018, Wittek et al., 2008, Deák et al., 2010, Arslan et al., 2018, Dhand et al., 2014, Vikas et al., 2017). Flax and basalt fiber vinyl ester composites and their hybrids were studied by Fragassa et al., 2018. Asadi et al., 2017 reported that BF reinforced composites had a more cost-saving alternative to GF reinforced polymer composites. Basalt fiber reinforced plastic was studied by Lopresto et al., 2011. Effect of the fiber content of polylactic acid (PLA)-basalt fiber composites were reported by Aslan et al., 2018.

Some of the researchers studied interfacial properties of basalt fiber-reinforced composites (Wittek et al., 2008, Deák et al., 2010, Arslan et al., 2018). Biodegradable starch resin and basalt fibers were investigated by Wittek et al., 2008. Deák et al., 2010 reported

interfacial properties of basalt fiber reinforced composites. The effects of silane coupling agents of basalt fiber-poly(butylene terephthalate) composites was reported by Arslan et al., 2018.

Some researchers have done studies to review the mechanical properties of basalt fiber-reinforced composite materials (Dhand et al., 2014, Vikas et al., 2017, Singha et al., 2012, Fiore, et al., 2015).

Some of the researchers used nanomaterials to improve the properties of basalt fiber reinforced composite materials (Szakacs et al., 2018, Wang et al., 2018, Bulut et al., 2017). Szakacs et al., 2018 found a remarkable improvement in tensile properties thanks to the proper dispersion of carbon nanotubes. Wang et al., 2018 studied the interfacial properties of basalt fiber-graphene oxide-polydopamine composites. Basalt/epoxy/graphene nano-pellets (GnPs) composite laminates were investigated by Bulut et al., 2017.

This work aims to study whether it is possible to replace the GF with BF in thermoplastic composites. Tensile, bending, and impact tests were carried out during this study. Overall better behavior of basalt compared to glass were evidenced by comparing the performance of the two composites.

1. EXPERIMENTAL PROCEDURES

1.1. Composite constituents

The chopped basalt and glass fibers were obtained from Dost Kimya Hammaddeler Sanayi ve Tic. Ltd. Sti, Istanbul/Turkey. Polyamide 6.6 (PA 6.6) polymer was obtained from Hazar Plastik Sanayi ve Tic. Ltd. Sti, Istanbul/Turkey.

1.2. Fabrication method

The chopped basalt and glass fibers were placed inside a mold of the hot-press machine. The processing conditions of composites were 24.5 bar molding pressure and 240 °C molding temperature.

The average fiber volume fraction and thickness of the specimens with basalt fibers were about 50% and 2.7 mm. These were 50% and 4.0 mm for glass fibers.

1.3. Characterization

The tensile, three-point flexural (by The INSTRON 5982 100KN) and charpy impact tests were conducted on the specimens. The dimensions of the samples were 20 x 190 x 2.7-4.0 mm^3 in the tensile tests. For three-point flexural tests, the dimensions of the specimens were 15 x 90 x 2.7-4.0 mm^3. The span length was ranged between the 44 mm and 64 mm. Three samples were tested for each type of the tests.

In the charpy impact tests (ISO 179 standards), three specimens with sample dimension of 15 x 90 x 2.7-4.0 mm^3 were tested.

2. RESULTS AND DISCUSSION

2.1. Tensile properties

Figure 1 shows the results of the tensile modulus and strength of the glass-PA 6.6 and basalt-PA 6.6 composites. The specimens with BF had the higher values of the tensile modulus (7.3 GPa) and strength (110.3 MPa) compared to the specimens with GF (4.7 GPa and 47.5 MPa). The tensile modulus and strength were improved 36% and 57% with BF compared to GF. The tensile strength of glass fiber is 3450 MPa, tensile strength of basalt fiber is 4840 MPa (Liu vd., 2006). Due to higher mechanical properties of the BF compared to the GF, the composites reinforced with BF showed higher tensile properties than GF in the same volume fraction.

35-42% increase in tensile modulus for BF-epoxy reinforced composites compared to the GF was reported by Lopresto et al (2). 13% increase in tensile modulus for BF reinforced composites compared to GF was reported by Kalaitzidou et al (1).

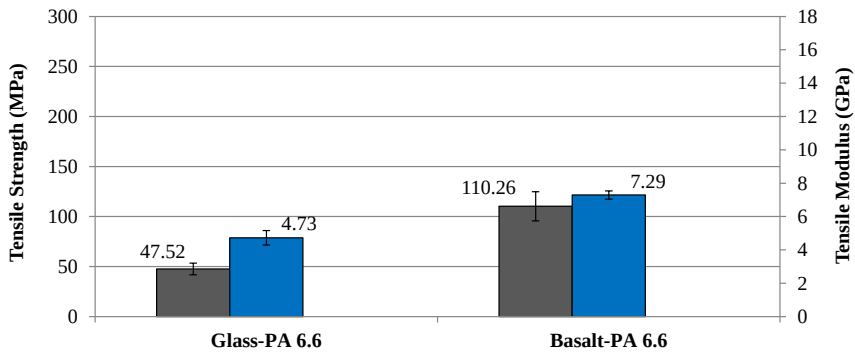

Figure 1. The tensile properties of the glass-PA 6.6 and basalt-PA 6.6 composites

2.2. Three-point flexural properties

Figure 2 shows the results of the bending tests of the glass-PA 6.6 and basalt-PA 6.6 composites. The specimens with BF had the higher values of the bending modulus and strength (13.7 GPa and 228.6 MPa) compared to the GF (10.8 GPa and 165.7 MPa). The specimens with BF showed 21% and 28% higher flexural modulus and strength comparing to the specimen with GF. As mentioned earlier, due to higher mechanical properties of the BF compared to the GF, the composites reinforced with BF showed higher bending properties than GF in the same volume fraction.

The good agreements from our results and from the results of Lopresto et al. (2) and Kalaitzidou et al (1) were obtained. 55% increase in flexural strength for BF-epoxy reinforced composites compared to the GF was reported by Lopresto et al (2). 15% increase in flexural modulus for BF reinforced composites compared to GF reinforced composites was reported by Kalaitzidou et al (1).

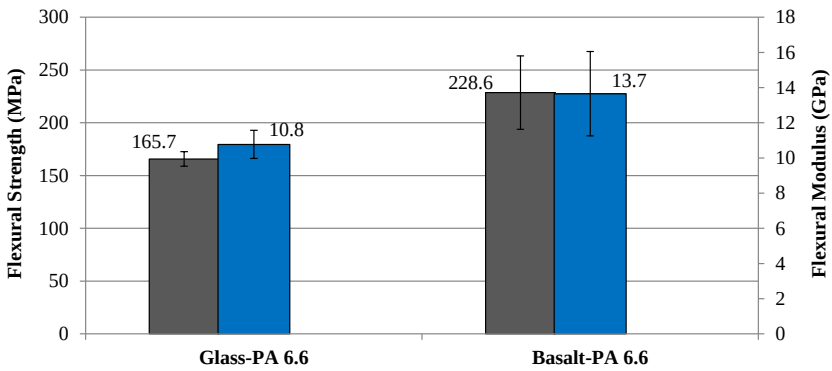

Figure 2. Results of the flexural properties of the glass-PA 6.6 and basalt-PA 6.6 composites

3.3. Charpy impact properties

The results of the Charpy impact strength properties of the glass-PA 6.6 and basalt-PA 6.6 composites were shown in Figure 3. The specimens with BF had higher values of the impact strength (51,2 kj/m^2) compared to the specimens with GF (44.7 kj/m^2). When we further divide the results of impact strength of the specimens to the thickness of them, we can obtain the energy results per thickness. The energy results per thickness of the specimens with BF was 18.4 kj/m^2, that was for the GF 11.2 kj/m^2. The specimens with BF showed 39% higher energy results comparing to the specimen with GF. 11% increase in charpy impact strength for BF-epoxy reinforced composites compared to the GF was reported by Lopresto et al (2).

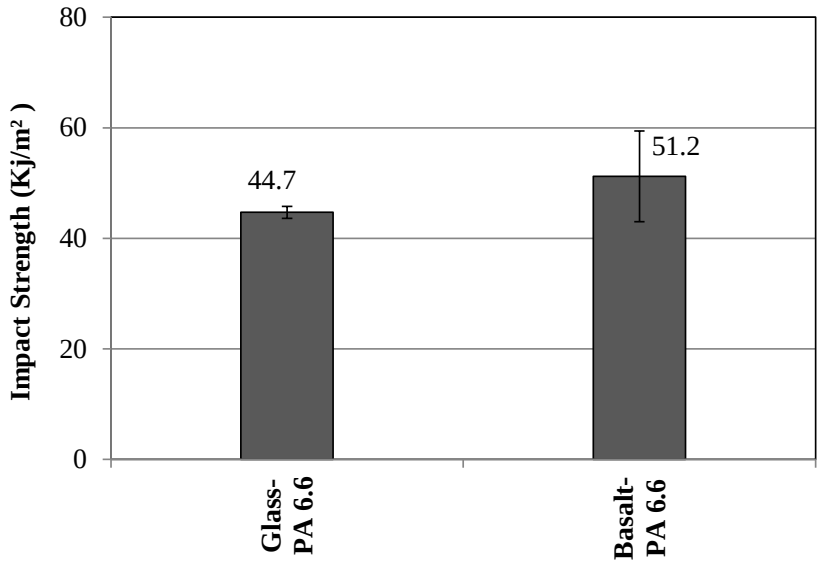

Figure 3. The Charpy impact strength properties of the glass-PA 6.6 and basalt-PA 6.6 composites

Table 1 shows the results of the energies from three-point bending tests of basalt-PA 6.6 and glass-PA 6.6 composites. The obtained maximum load with BF was 490 N, that was with GF 450 N. The total absorbed energies of the specimens with BF and GF from the three-point bending test were almost same. The total energy per thickness with BF was 0.52 J/mm, that was with GF 0.40 J/mm. The specimens with BF showed 23% higher energy results comparing to the specimen with GF.

Table 1. Results of the energies from three-point bending tests of basalt-PA 6.6 and glass-PA 6.6 composites

Samples	Maximum load (N)	Energy until max load (J)	Energy after max load (J)	Total absorbed energy (J)	Thickness (mm)	Total absorbed energy/mm (J)
Basalt-PA 6.6	490	0.90±0.02	0.62±0.04	1.52±0.90	2.7	0.52±0.06
Glass-PA 6.6	450	1.14±0.06	0.44±0.14	1.58±1.15	4.0	0.40±0.08

CONCLUSION

Our study showed that mechanical properties of BF reinforced composites were higher than GF. It was shown that BF could be used in place of GF without any modification.

The specimens with BF showed the best results in terms of the tensile, flexural, and Charpy impact properties compared to the GF. Composites with BF had 36% and 21% higher results in tensile and flexural modulus and 57% and 28% higher results in tensile and flexural strength and 39% higher results in Charpy strength compared to GF.

REFERENCES

Arslan, C., Dogan, M. 2018. The effects of silane coupling agents on the mechanical properties of basalt fiber reinforced poly(butylene terephthalate) composites, Composites Part B, Vol: 146, pp: 145-154.

Asadi, A., Baaij, F., Mainka, H., Rademacher, M., Thompson, J., Kalaitzidou, K. 2017. Basalt fibers as a sustainable and cost-effective alternative to glass fibers in sheet molding compound (SMC), Composites Part B, Vol: 123, pp: 210-218.

Aslan, M., Kata, M., Güler, O., Alver, Ü. 2018. Effect of fibre content on the mechanical properties of basalt fibre reinforced polylactic acid (pla) composites, Tekstil ve Konfeksiyon, Vol: 28(1), pp: 66-71.

Bulut, M., 2017. Mechanical characterization of Basalt/epoxy composite laminates containing graphene nanopellets, Composites Part B, Vol: 122, pp: 71-78.

Deák, T., Czigány, T., Tamás, P., Németh, C. 2010. Enhancement of interfacial properties of basalt fiber reinforced nylon 6 matrix composites with silane coupling agents, eXPRESS Polymer Letters, Vol: 4, No.10, pp: 590-598.

Dhand, V., Mittal, G., Yop, R. K., Jin, P. S., Hui, D. 2014. A short review on basalt fiber reinforced polymer composites, Composites: Part B, Vol: 73, pp: 166-180.

Fiore, V., Scalici, T., Di, B. G., Valenza, A., 2015. A review on basalt fibre and its composites, Composites Part B, Vol: 74, pp: 74-94.

Fragassa, C., Pavlovic, A., Santulli, C. 2018. Mechanical and impact characterisation of flax and basalt fibre vinylester composites and their hybrids, Composites Part B, Vol: 137, pp: 247-259.

https://www.online-sciences.com/industries/thermoplastics-properties-types-uses-advantages-and-disadvantages/.

Liu, Q., Shaw, T. M., Parnas, S. R., McDonnell, A. M. 2006, Investigation of basalt fiber composite mechanical properties for applications in transportation, Polymer Composites, DOI 10.1002/pc.20162, pp: 1-8.

Lopresto, V., Leone, C., De, Iorio I. 2011. Mechanical characterization of basalt fibre reinforced plastic, Composites: Part B, Vol: 42, pp: 717-723.

Singha, K. 2012. A Short Review on Basalt Fiber, International Journal of Textile Science, Vol: 1(4), pp: 19-28.

Szakacs, J., Meszaros, L., 2018. Synergistic effects of carbon nanotubes on the mechanical properties of basalt and carbon fiber-reinforced polyamide 6 hybrid composites, Journal of Thermoplastic Composite Materials, Vol: 31(4), pp: 553–571.

Vikas, G., Sudheer, M. 2017. A Review on Properties of Basalt Fiber Reinforced Polymer Composites, American Journal of Materials Science, Vol: 7(5), pp: 156-165.

Wang, J., Zhou, S., Huang, J., Zhao, G., Liu, Y. 2018. Interfacial modification of basalt fiber filling composites with graphene oxide and polydopamine for enhanced mechanical and tribological properties, The Royal Society of Chemistry, pp: 12222–12231.

Wittek, T., Tanimoto, T. 2008. Mechanical properties and fire retardancy of bidirectional reinforced composite based on biodegradable starch resin and basalt fibres, eXPRESS Polymer Letters, Vol: 2, No.11, pp: 810-822.

CHAPTER 4

THE EFFECT OF ARTIFICIAL INTELLIGENCE AND INDUSTRY 4.0 ON ROBOTIC SYSTEMS

Dr. Hasan DEMİR[1]
Dr. Filiz SARI[2]

[1] Corresponding Author, Aksaray University, Ortaköy Vocational School, Mechatronic, Aksaray, Turkey. hasandemir@aksaray.edu.tr. ORCID ID : 0000-0001-5424-7242
[2] Aksaray University, The Faculty of Engineering, Electrical-Electronic Engineering Department, Aksaray, Turkey. filizsari@aksaray.edu.tr. ORCID ID :0000-0001-8462-175X

INTRODUCTION

Robotic systems, also known as mechatronics systems, diversify the requirement of areas, for example, precise robots for medical systems, mobile robots, industrial robot arm for the industry, etc. Examples of mechatronic systems in the industry are industrial robot arms. Robotic arms are indispensable elements of automation systems. Industrial robotic arms have increased production in the industry and increased product quality. Robots increase the efficiency of the systems, so this field has attracted researchers' attention to this topic.

I4.0 is the latest the industrial revolution. As in previous industrial revolutions, it reveals many innovations in industry. Innovations such as digitalization, internet of things, human-robot interaction, sensors, communication protocols, intelligent industrial robots that can work together and make decisions, cybersecurity are realized with industry 4.0. Automated processes, intelligent machines concepts are components of I4.0. Industrial robot arms are the leading intelligent machines. With I4.0, industrial robotic arms have become employees of smart factories and have played an important role in bypassing a new era in the industry. Sensors and control theories are used for the design robotic system and their efficiency can be increased by the use of AI (Savage et al., 2019). The requirement of robotic power increases day by day so advanced mechatronic systems with AI are raising (Kanoh, 2017; Rajan & Saffiotti, 2017).

AI is software that simulates the human brain that has been developing since 1956. AI applications have started to increase in the last decade. AI is used in many fields such as medicine, smart clothes, finance, and engineering. Industrial applications of AI have increased production speed and quality and improved manufacturing systems. The most striking application of AI in the industry is realized with industrial robot arms. I4.0 enables the creation of intelligent factories of industrial robots controlled by AI. It foresees that robots make their own lower-level management decisions with AI. On the other hand, robotics with AI works on robots in human form. Humanoid robots that help people are developed with the studies.

In this study, the relationship between robotic systems and AI and I4.0 is discussed. I4.0 is described in the second section. The concepts of I 4.0 have been explained and the changes have been mentioned. Besides, how robotic systems are used in I4.0 is presented. In the third section, AI is explained and application areas are shown. The common working areas of AI and robotic systems are presented. In the fourth section, robotic systems with AI and I4.0 are evaluated. It is stated that robotic systems form independent systems with AI and these systems are integrated into production systems with industry 4.0. Robots equipped with AI have become part of a new industrial revolution. In fifth section, the final remarks are introduces the summary and gives future outlooks.

1. INDUSTRY 4.0

At the end of the 18th century, machines was used in production. The manual production is developed with steam powered motors. These developments are called the first industrial revolution. In the early 19th century, the mass production conception initiated the second industrial revolution. In this revolution, railways and telegraph technology developed. The third industrial revolution took place in the middle of the 19th century. Production systems started to be digitalized. There have been great developments in communication, computer and information technologies. The automation of production systems through computers has come to a new level (Javaid & Haleem, 2019).

I4.0 is a new industrial revolution. I4.0 was introduced in 2011 by the German government. The German manufacturing strategy played a major role in the transition to I4.0. It has led to developments digital transformation in the production (Alcácer & Cruz-Machado, 2019). It is possible to define products as a new organization and control level in chain of the life cycle of product. I4.0 highlights are the Internet of Things, Industrial Internet and Cloud based Manufacturing (Vaidya et al., 2018). Figure 1 is a schematic representation of I4.0.

The goal of I4.0 is to increase productivity and operational efficiency (Thames & Schaefer, 2016). Developing the automation systems, providing digitalization, optimization, automation and adaptation, data exchange are the striking features of I4.0. These features indicate that

I4.0 is a concept that raises knowledge management and process (Posada et al., 2015; Roblek et al., 2016).

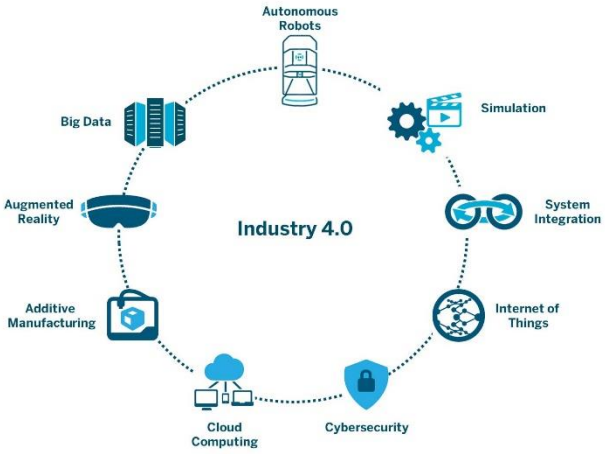

Figure 1: The Schematic Representation of I4.0 (Melanson, n.d.)

In I4.0, physical systems are thought to be monitored, controlled and managed using the Internet of Things (IoT). Processes such as product development, management of resources, service provision will interact with the internet of objects. These developments will result in shortening of the product cycle and autonomous maintenance (Gilchrist, 2016; Jeschke et al., 2016).

1.1. Rise of the Robotics with Industry 4.0

The production concept requires fast production as well as mass production. Mass and rapid production has increased the need for robots. Today, as a result of the digitalization of the industry, robots have gained importance (Vaidya et al., 2018). Robots have given

flexibility to their production systems and nowadays robots have become a necessary part of production systems (Pedersen et al., 2016).

The adaptive robots in production processes such as product development, production and assembly are very useful. Robots that make their own decisions and interact with their environment are defined as full autonomous industrial robots (AIR) (Ben-Ari & Mondada, 2017). In I4.0, production lines were developed by using AIR. Figure 2 is shown a production line consisting of an AIR interacting with each other and environment.

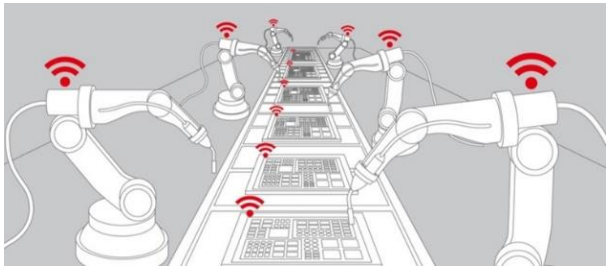

Figure 2: A Production Line Consisting of an AIR Which is Interacting with Each Other and Environment

Industrial robots are used to fulfill a task in production. A robot performs a task in a working cell. I4.0 predicts that AIRs can operate in multiple co-operation. These robots that work in multiple collaboration are called cobot. Cobots increase the performance of AIRs in a task. In Figure 3, cobots which give spray painting process are given (Hassan & Liu, 2017).

In I4.0 applications, multi-robots are used to increase efficiency. AIRs that work together are called multi-robots. Multi-robots can be used in the assembly of complex structures. Multi robots that work as teams can perform high accuracy and speed operations (Dogar et al., 2019). Multi-robots work with a cloud instance to avoid waste of resources and increase the efficiency of resource management. Figure 4 is shown multi-robots that work with cloud-based (Afrin et al., 2019).

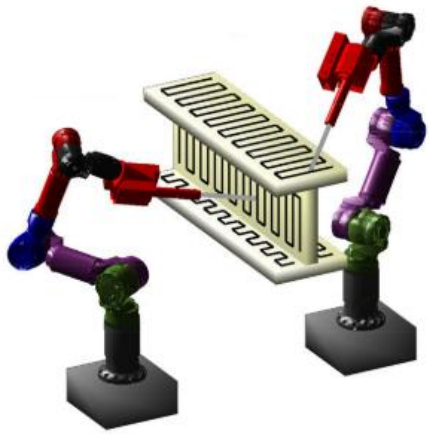

Figure 3: The Cobots Which Give Spray Painting Process

Another important component of I4.0 is human-robot interaction (Koch et al., 2017). By combining the high accuracy of the robots with the capabilities of people, it improve product quality and the working conditions of workers (El Makrini et al., 2018). The work of humans and robots closely together forms the concept of smart factories that are a form of production foreseen by the concept of I4.0. Human-robot cooperation has led to the creation of dynamic factories and has created a flexible production model (Gambao et al., 2012;

Weiss & Huber, 2016). Figure 5 shows the human-robot cooperation. The robot that shows the red block put the different colored blocks in the boxes.

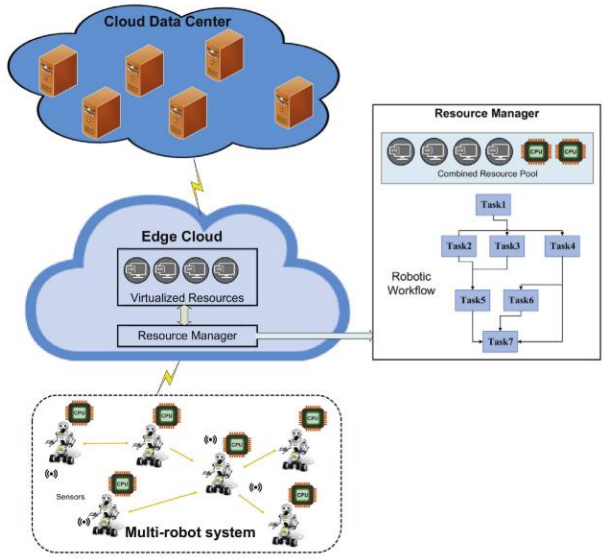

Figure 4: The Cloud-Based Multi-Robots (Afrin et al., 2019)

Figure 5: Human-Robot Cooperation

With I4.0, industrial robots have been updated to become AIRs. The smart factories was established with I4.0. In the smart factories, systems that can make production in the dark and maximize

production are developed. AIRs are tireless workers of intelligent factories. Multi-robot have been developed and dynamic production systems have been created by providing human robot interaction. AIRs have communicated of the environment with IoT and increased the effectiveness of resource management with cloud systems. With cloud-based production, factories can be controlled and monitored from headquarters. Industrial robots undertake important roles for I4.0. I4.0 will build the full-fledged factories of the future by using AIRs.

I4.0 will lead to improvements in the field of production and innovation by increasing the effectiveness of robotic systems. The factories of the future will provide raw materials and production line communication with the I4.0. In the future, smart factories with I4.0 and AIRs will be established and productivity will increase (Otles & Sakalli, 2019). In addition, artificial intelligence-equipped robots will be realized in the future. In the future I4.0 will establish intelligent production systems with AIRs (Linert & Kopacek, 2018).

2. ARTIFICIAL INTELLIGENCE

Artificial intelligence (AI) was first introduced in Dartmouth college in 1956 (Russell & Norving, 2016). AI is a calculation method that tries to simulate human cognition (Salehi & Burgueño, 2018). Learning, reasoning and self-correction, etc. are added to computers or machines by using AI methods (Durán et al., 2018). AI is an interdisciplinary science that is a combination of computer sciences,

control theory, information theory, and psychology (Wei, 2018). There are some terms referring to AI in the literature. One of them is machine intelligence (MI). AI and MI are used interchangeably. While MI expresses machines with intelligent behaviours, AI expresses the cognition of a machine (Fadlullah et al., 2017; Fogel, 2006). Another term is cognitive computing (CC). CC is inspired by human intelligence and allows machines to solve problems using learned experiences (Demirkan et al., 2017; Noor, 2015).

AI is divided into sub-headings as machine learning and deep learning. Machine learning designs a model for learning trends and uses this model to solve new problems. Deep learning is the subset of machine learning. Learns the properties of the data to be processed and makes it ready for processing. Figure 6 shows the AI scheme.

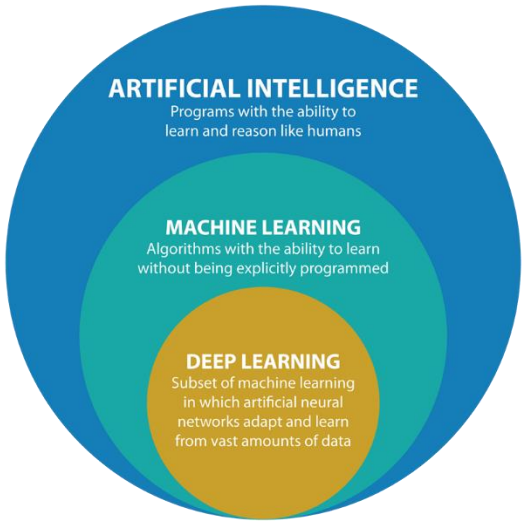

Figure 6: The AI Scheme (*Artificial Intelligence | Machine Learning | Deep Learning | Argility*, n.d.)

There is a dramatic increase in systems developed with AI today. AI has been used in many applications in different fields. AI has been used to support constructivist learning in education. The effects of developmental learning in early stage were investigated (Georgeon, 2017). The latest trend in the design of smart clothing is AI. Smart clothing, which perceive the external environment and the changes in the internal situation, can react in real time with AI. Equipped with AI, these clothes can adapt to the needs of people (Wei, 2018).

AI is gaining importance in medicine as in other fields. Deep learning based pattern recognition methods are used to diagnose diseases using clinical and radiological data. This function of AI will facilitate the pathological identification of diseases in the future. The process of evaluating clinical data will be a simple procedure (Chang et al., 2018).

AI is also used in many areas such as image processing, financial, engineering risk analysis, etc. Basic AI algorithms developed by some companies such as Microsoft are used in applications. One of the most important uses of AI is the industry. In the industry, AI algorithms have led to the development of production systems and improved product quality. AI has started to be used with robots in the industry and it has become an important topic for I4.0.

2.1. AI and Robotics

In the early 1990s, AI and robot researchers studied theoretical models. In these researches, interaction models between AI and intelligent robots were formed. Different hypotheses such as artificial vision and cognitive architecture have been used in robotic systems. But in those years, full-fledged practices could not be done and results could not be obtained (Chella et al., 1997; Stojanov et al., 2006). In the years that followed, cooperation between AI and robotic increased and found itself in different areas of application. Studies in the field of management have used the ability of AI and robotic to reproduce certain actions in typical situations. It has been targeted to improve product quality, product variants and autonomous production lines with autonomous running industrial robots has shown that it will increase production efficiency in the future (Hagemann et al., 2019; RADACEANU, 2010). It can also reduce programming time by using AI with industrial robots and no need for system integration specialist. A generic knowledge-based system architecture has been created and it can be used in industrial robotic systems (Stenmark & Malec, 2015). AI techniques are applied to industrial robots to eliminate the human factor in production. In this way, the robots are dynamically adapted to the task plans (Cesta et al., 2018). On the other hand, the effects of the spread of AI lead to a reduction in aggregate wages (DeCanio, 2016). The use of robotics with AI is one of the important issues in today's industry. The developed smart industrial robots have started to replace people with their decision-making and self-correction

capabilities. On the other hand, as a result of the cooperation of AI and robotics, it has started to be developed in human robots. As shown in Figure 7, we can divide robotic systems into two main groups: industrial robots and mobile robots. Humanoid robots are the result of the collaboration of two groups and they are autonomous robots that try to achieve human intelligence and performance. Humanoid robots are designed in the form of human form. Together with AI, humanoid robots began to think for themselves, to show their emotions and to learn about their environment (Linert & Kopacek, 2018). AI has opened a new chapter in the field of robotics. It has made robots that are self-deciding systems. It is certain that developments in the field of AI and robotic systems in the future will affect both fields.

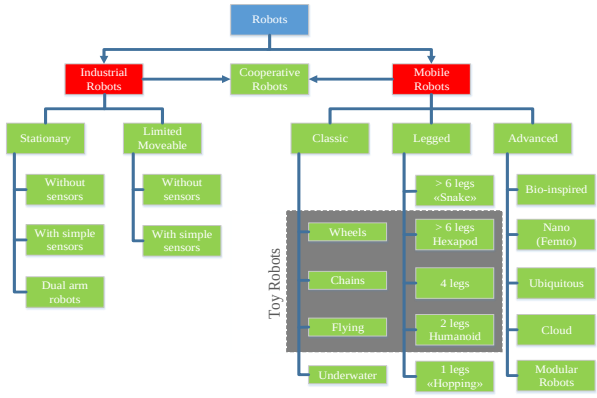

Figure 7. Classification of Robots (Linert & Kopacek, 2018)

The robots with AI in the future will cause significant improvements. Robot assistants will be present at every stage of our lives. They can code a software on their own or surgeon robots with AI will be able to perform surgeries. Even with the emergence of big data analysis in the

next 10 years, it is expected that image processing methods will be used for surgical planning and AI samples will be performed both for educational and patient care (Tarassoli, 2019).

3. ROBOTICS SYSTEMS WITH AI AND INDUSTRY 4.0

In the past, robotic systems are designed to do a certain job. Industrial robots were thought to perform operations in the industry, such as speeding up production, improving quality, lowering operating costs, and making jobs dangerous to humans. For this reason, industrial robots have been regarded as electromechanical structures that perform the programmed tasks. Traditionally, industrial robots have been used in large scale manufacturing processes for the same processes (Ghosh, 1985; Lozano-PÉrez, 1983). Nowadays, robotic systems are required to be digitalized and to increase the automation level more, instead of performing only the programmed works (Lu, 2017).

I4.0 uses AI, where machines and other technologies are programmed as human intelligence. AI is used to provide a higher level of knowledge about the concepts such as quality, raw material, waste, output and to share information digitally (Javaid & Haleem, 2019).

Most traditional industrial robots are programmed with teaching. Programming of industrial robots for complex tasks does not meet the requirements. For this reason, it is necessary to increase the capacity of the robots to make their own decisions in real time by being equipped with sensors. With the application of AI in industrial robots,

robots have gained the ability to move autonomously. Industrial robots can create their own task planning and processing sequence with AI (Elmaraghy, 1987).

I4.0 will lead to improvements in the field of production and innovation by increasing the effectiveness of robotic systems. The factories of the future will provide raw materials and production line communication with the I4.0. In the future, smart factories with I4.0 and robotics systems will be established and productivity will increase (Otles & Sakalli, 2019). Digitalization will be increased by establishing human robot interaction with I4.0. Humans and robots will share and analyse information using big data and cloud systems (McKinsey, 2015).

In addition, artificial intelligence-equipped robots will be in human form. Although humanoid robots can be used as a guide in some airports and serve as waiters in bars, they will probably come into our lives as individuals who may think and decide in the future (Linert & Kopacek, 2018).

In the future, industrial robots will be able to perform complex operations by controlling them with AI and robots will make every stage of production. The robots will decide on their own and will be involved in all areas from raw material input to product output. Robots using AI according to the data they collect with sensors will manage their own job descriptions, concepts such as processing time and sequence.

CONCLUSION

When robots were first used in industry they increased both the quantity and quality of the products. Along with advancing technology, AI technology has now been used in industrial robots and systems that can take decisions, learn and reason have been developed. AI and robots are integrated for autonomous systems. Autonomous industrial robots (AIR), multi-robots (cobots), human-robot interaction applications are the cornerstones of intelligent factories of the Industrial 4.0 revolution. Industrial robots will no longer perform their programmed tasks, but they will be able to make their own decisions due to AI, as well as the data they receive with sensors. In the future, industrial robots will be indispensable systems for I4.0 and will make all the operations which are handled by traditional machines and human beings.

Many researches on humanoid robots are done and robots even in human form are developed. Nowadays these robots are used to assist people. However, humanoid robots using AI are evolving day by day. In the future, perhaps humanoid robots will take part in our lives as individuals which can think and make intelligent decisions. Humanoid robots which use the Iot will be able to follow the developments in the world and obtain all the information, thus becoming systems that produce rather than just learn.

REFERENCES

Afrin, M., Jin, J., Rahman, A., Tian, Y. C., & Kulkarni, A. (2019). Multi-objective resource allocation for Edge Cloud based robotic workflow in smart factory. *Future Generation Computer Systems*, *97*, 119–130. https://doi.org/10.1016/j.future.2019.02.062

Alcácer, V., & Cruz-Machado, V. (2019). Scanning the Industry 4.0: A Literature Review on Technologies for Manufacturing Systems. *Engineering Science and Technology, an International Journal*. https://doi.org/10.1016/j.jestch.2019.01.006

Artificial Intelligence | Machine learning | Deep learning | Argility. (n.d.). Retrieved May 21, 2019, from https://www.argility.com/argility-ecosystem-solutions/iot/machine-learning-deep-learning/

Ben-Ari, M., & Mondada, F. (2017). Robots and Their Applications. In *Elements of Robotics*. https://doi.org/10.1007/978-3-319-62533-1

Cesta, A., Orlandini, A., & Umbrico, A. (2018). Fostering Robust Human-Robot Collaboration through AI Task Planning. *Procedia CIRP*, *72*, 1045–1050. https://doi.org/10.1016/j.procir.2018.03.022

Chang, H. Y., Jung, C. K., Woo, J. I., Lee, S., Cho, J., Kim, S. W., & Kwak, T.-Y. (2018). Artificial Intelligence in Pathology. *Journal of Pathology and Translational Medicine*, *53*(1), 1–12. https://doi.org/10.4132/jptm.2018.12.16

Chella, A., Frixione, M., & Gaglioa, S. (1997). Artificial Intelligence A cognitive architecture for artificial vision *. *Artificial Intelligence*, *89*(1–2), 73–111.

DeCanio, S. J. (2016). Robots and humans – complements or substitutes? *Journal of Macroeconomics*, *49*, 280–291. https://doi.org/10.1016/j.jmacro.2016.08.003

Demirkan, H., Earley, S., & Harmon, R. R. (2017). Cognitive Computing. *IT Professional*, *19*(4), 16–20. https://doi.org/10.1109/MITP.2017.3051332

Dogar, M., Spielberg, A., Baker, S., & Rus, D. (2019). Multi-robot grasp planning for sequential assembly operations. *Autonomous Robots*, *43*(3), 649–664. https://doi.org/10.1007/s10514-018-9748-z

Durán, R. J., Jukan, A., Singh, S. K., de Miguel, I., Mata, J., Merayo, N., &

Chamania, M. (2018). Artificial intelligence (AI) methods in optical networks: A comprehensive survey. *Optical Switching and Networking*, *28*, 43–57. https://doi.org/10.1016/j.osn.2017.12.006

El Makrini, I., Elprama, S. A., Van Den Bergh, J., Vanderborght, B., Knevels, A. J., Jewell, C. I. C., Stals, F., De Coppel, G., Ravyse, I., Potargent, J., Berte, J., Diericx, B., Waegeman, T., & Jacobs, A. (2018). Working with Walt: How a Cobot Was Developed and Inserted on an Auto Assembly Line. *IEEE Robotics and Automation Magazine*, *25*(2), 51–58. https://doi.org/10.1109/MRA.2018.2815947

Elmaraghy, H. A. (1987). *Artificial intelligence and robotic assembly*. *155*, 147–155.

Fadlullah, Z. M., Tang, F., Mao, B., Kato, N., Akashi, O., Inoue, T., & Mizutani, K. (2017). State-of-the-Art Deep Learning: Evolving Machine Intelligence Toward Tomorrow's Intelligent Network Traffic Control Systems. *IEEE Communications Surveys and Tutorials*, *19*(4), 2432–2455. https://doi.org/10.1109/COMST.2017.2707140

Fogel, D. B. (2006). *Evolutionary Computation: Toward a New Philosophy of Machine Intelligence*. Wiley-IEEE Press.

Gambao, E., Hernando, M., & Surdilovic, D. (2012). A new generation of collaborative robots for material handling. *Gerontechnology*, *11*(2). https://doi.org/10.4017/gt.2012.11.02.362.776

Georgeon, O. L. (2017). Little AI: Playing a constructivist robot. *SoftwareX*, *6*, 161–164. https://doi.org/10.1016/j.softx.2017.06.007

Ghosh, A. (1985). INDUSTRIAL ROBOTICS. *Journal of the Institution of Engineers (India), Part PR: Production Engineering Division*.

Gilchrist, A. (2016). *Industry 4.0 - The Industrial Internet of Things*. Apress. https://doi.org/https://doi.org/10.1007/978-1-4842-2047-4

Hagemann, S., Sünnetcioglu, A., & Stark, R. (2019). Hybrid Artificial Intelligence System for the Design of Highly-Automated Production Systems. *Procedia Manufacturing*, *28*, 160–166. https://doi.org/10.1016/j.promfg.2018.12.026

Hassan, M., & Liu, D. (2017). Simultaneous area partitioning and allocation for

complete coverage by multiple autonomous industrial robots. *Autonomous Robots*, *41*(8), 1609–1628. https://doi.org/10.1007/s10514-017-9631-3

Industry 4.0: from sensors to business value. (2019). https://www.delaware.pro/en-lu/solutions/industry-4-0

Javaid, M., & Haleem, A. (2019). Industry 4.0 applications in medical field: A brief review. *Current Medicine Research and Practice*. https://doi.org/10.1016/j.cmrp.2019.04.001

Jeschke, S., Brecher, C., & Song, H. (2016). *Industrial Internet of Things Cybermanufacturing Systems* (D. B. Rawat (Ed.)). https://doi.org/10.1007/978-3-319-42559-7_29

Kanoh, H. (2017). Immediate Response Syndrome and Acceptance of AI Robots - Comparison between Japan and Taiwan. *Procedia Computer Science*, *112*, 2486–2496. https://doi.org/10.1016/j.procs.2017.08.184

Koch, P. J., van Amstel, M. K., Dębska, P., Thormann, M. A., Tetzlaff, A. J., Bøgh, S., & Chrysostomou, D. (2017). A Skill-based Robot Co-worker for Industrial Maintenance Tasks. *Procedia Manufacturing*, *11*(June), 83–90. https://doi.org/10.1016/j.promfg.2017.07.141

Linert, J., & Kopacek, P. (2018). Humanoid robots Robotainment. *IFAC-PapersOnLine*, *51*(30), 220–225. https://doi.org/10.1016/j.ifacol.2018.11.290

Lozano-PÉrez, T. (1983). Robot Programming. *Proceedings of the IEEE*. https://doi.org/10.1109/PROC.1983.12681

Lu, Y. (2017). Industry 4.0: A survey on technologies, applications and open research issues. *Journal of Industrial Information Integration*, *6*, 1–10. https://doi.org/10.1016/j.jii.2017.04.005

McKinsey. (2015). Industry 4.0 - how to navigate digitization of the manufacturing sector. *McKinsey Digital*, 1–62.

Melanson, T. (n.d.). *Industry 4.0 and Mobile Robots - Connecting Islands of Automation*. Retrieved May 13, 2019, from https://aethon.com/mobile-robots-and-industry4-0/

Noor, A. K. (2015). Potential of cognitive computing and cognitive systems. *Open Engineering*, *5*(1), 75–88. https://doi.org/10.1515/eng-2015-0008

Otles, S., & Sakalli, A. (2019). Industry 4.0: The Smart Factory of the Future in Beverage Industry. In *Production and Management of Beverages* (Vol. 1, pp. 439–469).

Pedersen, M. R., Nalpantidis, L., Andersen, R. S., Schou, C., Bøgh, S., Krüger, V., & Madsen, O. (2016). Robot skills for manufacturing: From concept to industrial deployment. *Robotics and Computer-Integrated Manufacturing*, *37*, 282–291. https://doi.org/10.1016/j.rcim.2015.04.002

Posada, J., Toro, C., Barandiaran, I., Oyarzun, D., Stricker, D., De Amicis, R., Pinto, E. B., Eisert, P., Döllner, J., & Vallarino, I. (2015). Visual Computing as a Key Enabling Technology for Industrie 4.0 and Industrial Internet. *IEEE Computer Graphics and Applications*, *35*(2), 26–40. https://doi.org/10.1109/MCG.2015.45

RADACEANU, E. (2010). Artificial Intelligence & Robots for Performance Management – Some Methodic Aspects. *IFAC Proceedings Volumes*, *40*(18), 319–324. https://doi.org/10.3182/20070927-4-ro-3905.00053

Rajan, K., & Saffiotti, A. (2017). Towards a science of integrated AI and Robotics. *Artificial Intelligence*, *247*, 1–9.

Roblek, V., Meško, M., & Krapež, A. (2016). A Complex View of Industry 4.0. *SAGE Open*, *6*(2). https://doi.org/10.1177/2158244016653987

Russell, S. J., & Norving, P. (2016). *Artificial Intelligence : A modern aproach*. Pearson Education Limited.

Salehi, H., & Burgueño, R. (2018). Emerging artificial intelligence methods in structural engineering. *Engineering Structures*, *171*(May), 170–189. https://doi.org/10.1016/j.engstruct.2018.05.084

Savage, J., Rosenblueth, D. A., Matamoros, M., Negrete, M., Contreras, L., Cruz, J., Martell, R., Estrada, H., & Okada, H. (2019). Semantic reasoning in service robots using expert systems. *Robotics and Autonomous Systems*, *114*, 77–92. https://doi.org/10.1016/j.robot.2019.01.007

Stenmark, M., & Malec, J. (2015). Knowledge-based instruction of manipulation tasks for industrial robotics. *Robotics and Computer-Integrated Manufacturing*, *33*, 56–67. https://doi.org/10.1016/j.rcim.2014.07.004

Stojanov, G., Trajkovski, G., & Kulakov, A. (2006). Interactivism in artificial intelligence (AI) and intelligent robotics. *New Ideas in Psychology*, *24*(2), 163–185. https://doi.org/10.1016/j.newideapsych.2006.07.005

Tarassoli, S. P. (2019). Artificial intelligence, regenerative surgery, robotics? What is realistic for the future of surgery? *Annals of Medicine and Surgery*, *41*(April), 53–55. https://doi.org/10.1016/j.amsu.2019.04.001

Thames, L., & Schaefer, D. (2016). Software-defined Cloud Manufacturing for Industry 4.0. *Procedia CIRP*, *52*, 12–17. https://doi.org/10.1016/j.procir.2016.07.041

Vaidya, S., Ambad, P., & Bhosle, S. (2018). Industry 4.0 - A Glimpse. *Procedia Manufacturing*, *20*, 233–238. https://doi.org/10.1016/j.promfg.2018.02.034

Wei, X. (2018). The application and development of artificial intelligence in smart clothing. *IOP Conference Series: Materials Science and Engineering*, *320*(1). https://doi.org/10.1088/1757-899X/320/1/012017

Weiss, A., & Huber, A. (2016). *User Experience of a Smart Factory Robot: Assembly Line Workers Demand Adaptive Robots*. 1–3. http://arxiv.org/abs/1606.03846

CHAPTER 5

MULTI-OBJECTIVE OPTIMISATION DAYLIGHTING PERFORMANCE OF CAMPUS BUILDING FACADE

Duygu ÇINAR UMDU[1]
Assist. Prof. Dr. Ebru ALAKAVUK[2]

[1] Yaşar Üniversitesi Fen Bilimleri Enstitüsü Mimarlık Anabilim Dalı, Orcid no: 0000-0001-9186-5074 duygu.cinar.88@gmail.com
[2] Yaşar Üniversitesi Mimarlık Fakültesi Mimarlık Bölümü,
Orcid no: 0000-0001-7482-8116.ebru.alakavuk@yasar.edu.tr

INTRODUCTION

Today, while working conditions and limitless working hours forces people to stay indoor spaces, the quality and quantity of these areas have a serious impact on both labor productivity and human psychology and health. Environmental control systems should be applied indoors under maximum and most efficient conditions.

The illumination of the area should also be evaluated in this respect. Especially the use and the management of daylight are very important for the education and office spaces. Therefore, daylight is one of the main factors for the survival of every life, and at the same time, people need daylight without being different from other living things. Efficient, controlled daylight lightning during daytime hours makes work efficient and supports humans health. Good quality lighting is the basic requirement of these. Good quality lighting is the lighting that lets you see what happens you should see it efficiently and will not cause a disturbance in a visual way. It offers well-being to human (Ruffles, 2017). But, lighting is the system that uses energy the most after the HVAC system in the building, so for the energy-efficient lighting design is a crucial task for the buildings (Ruffles, 2017). Throughout the year, daylighting change due to climate conditions, geographical location, and seasonal variations. Therefore, the façade material of buildings, window openings affect the daylight in buildings. There are scientific metrics such as daylight factor, annual daylight, daylight autonomy, illuminance that need to be known to

discuss daylight's properties, and standards that have been revealed in the light of these terms and daylight analysis (Turan et al. 2019).

Hopkins (1963) defines that Daylight factor (DF) is a ratio about daylight availability metric that shows the amount of daylight available in an indoor space as a percentage of the amount of clear daylight available outside in cloudy sky conditions (Hopkins, 1963). The basic structure characteristics that determine the size and distribution of daylight factor in space are as follows (Mardaljevic et al, 2011):

- Qualitative and qualitative characteristics such as size, condition, and the material of windows, facades, and roofs
- Capacity and structure of the area
- Properties about reflection internal and external surfaces
- The effect of external structures on the angle of arrival of the sun

If an interior gets too much the daylight, it means DF is high. Indoors with an average DF between %2 and %5 are acceptable on a daily basis, but artificial lighting may still be required while performing visual tasks. If the average DF % 5 or more than the value a room is strongly visible, in which case electric lighting is probably not used during the day time (Boyce and Raynham, 2009).

People generally use daylight factor in calculations because it is easy to find according to annual daylight in simulations. However, DF doesn’t consider the absolute sky, climate conditions, direction of the

building, and seasonal changes (Mardaljevic et al, 2011). In addition, it cannot give accurate results since it can be considered valid only when working with cloudy weather conditions and does not include the existing weather conditions and clear sky calculations (Brotas and Wilson, 2008).

Daylight Autonomy (DA) is one of the daylight measurements, now commonly referred to as 'dynamic daylight metrics'. It is displayed as a percentage of the annual daylight hours in a space where a given point is above a certain lighting level. It was first expressed by the Association Suisse des Electricians in 1989 and developed by Christoph Reinhart from 2001 to 2004 (PatternGuide, 2019).

This is a great metric since it considers weather information and geographic region annually. In addition, if the threshold defined by the user is set according to the electrical lighting criteria, the electrical lighting has power in relation to energy saving. The user can set the threshold at which Daylight Autonomy is calculated. According to the Illuminating Engineering Society of North America (IESNA) and LEED standards, the sufficiency of the threshold is 50% for 300 lux for working space. In addition to this, Compared to DF, it is more functional and gives more absolute results (Reinhart et al., 2006; Turan et al., 2019).

In addition to all this, to obtain a sustainable structure and benefit from daylight in terms of both thermal comfort and visual comfort, the climate type, which are 31 sub-categories in 5 main climate types for Köppen- Geiger Climate Classification (Öztürk et al., 2017), of the

building, the prevailing wind, the shell type of the building, the façade structure and the building position in the site plan are very important. All these processes and decisions should be taken interrelated during the planning phase of the structure (Alakavuk et al., 2015; Alakavuk, 2018).

1. MATERIALS AND METHODS

In recent years, many studies have found many results-based calculation methods, algorithms and physical modelling based on simplification for daylight measurement (Ayoub, 2019). For daylight analysis, researchers generally use the programs such as Autocad, 3dsMax, Rhino, Revit, Sketch-Up to model actual building at first then they use analysis such as Diva (via Grasshopper), Daysim and Radiance and Ecotect (Panitz and Garcia-Hansen, 2013; Solmaz, 2015).

In this project, Building H of canteen part has been selected for daylight analysis in Campus of Yasar University in İzmir. Firstly, the physical measurements of the building were made and then the technical drawings and 3D model were transferred to the digital environment. The plan of the building is shown in Figure 1.

After that, using Izmir Region climate data and to obtain 300 lux illumination by the program of Diva 4 (via Grasshopper) for Rhino 6 was used for daylight analysis.

In addition to analysis of the actual façade of the building, 10 different façade solution analyzes were also calculated as alternatives. Finally, In the calculations, the samples with Daylight Factor 2% and above and Daylight Autonomy 50% and above were determined.

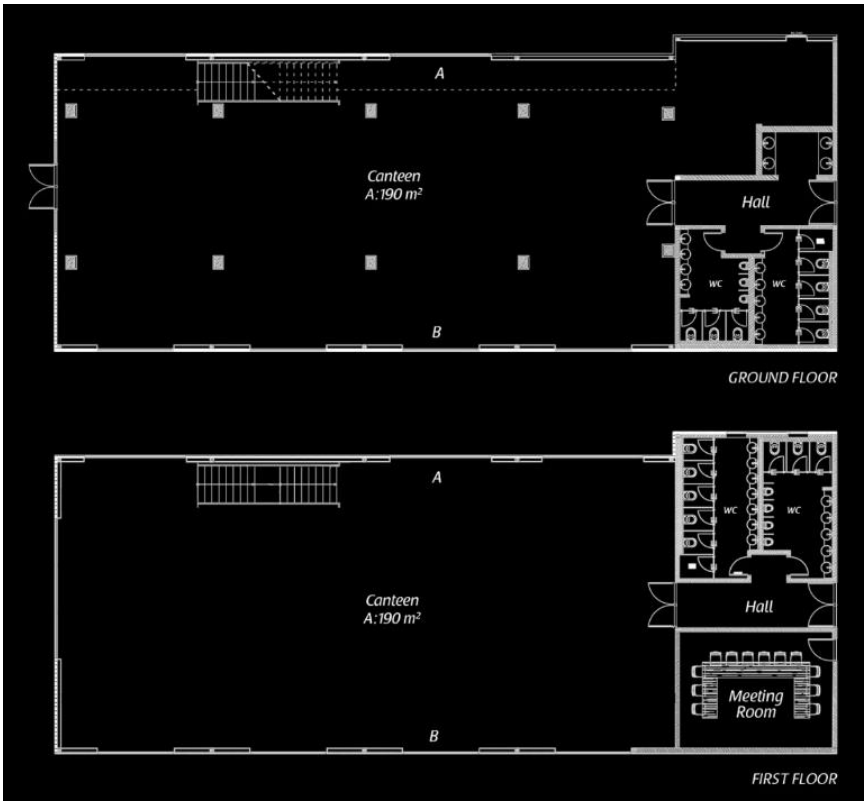

Figure 1: Plans of Building H

2. RESULTS AND DISCUSSION

The building is located on the Campus of Yasar University in İzmir. Building H of the canteen part has been selected for daylight analysis. In Figure 2, the building, sun, and prevailing wind directions and place in site plan are shown. İzmir is in Northern Hemisphere and the

climate zone is Csa which is the Meditarnian Climate Type and Prevailing wind directions are It is located in NorthWest-South East Direction (Öztürk et al., 2017). The is South East in winter and Etesian winds also become the prevailing wind in the summertime (Baş and Doğrusoy, 2019).

Building H has no sun protection for sunlight changes during the day. Its glazing is double panel LowE-65. Moreover, its ceiling, wall, and other structural features are generic. Its animation graphic is shown in Figure 3. Since it is a two-story building, daylight factor (DF) and daylight autonomy (DA) of the floors were measured separately.

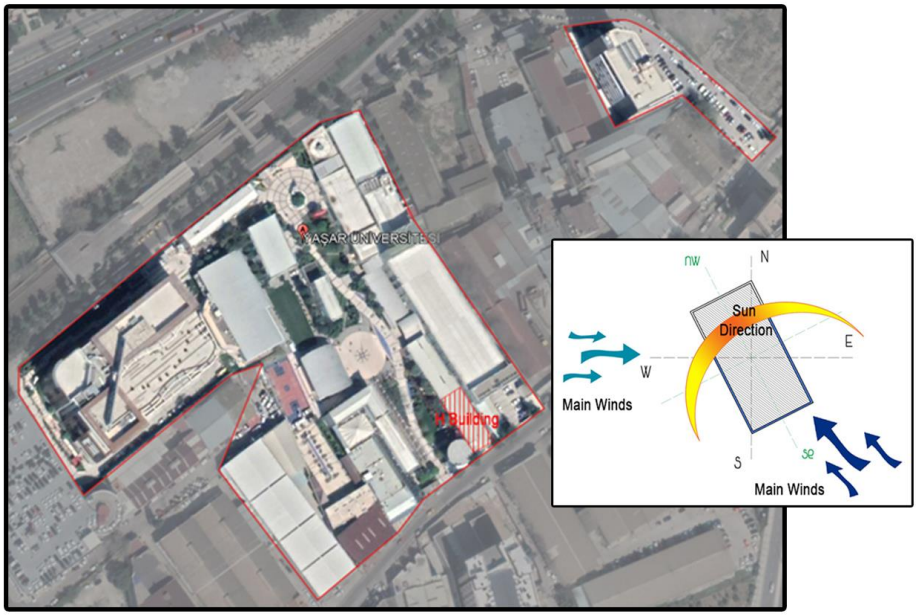

Figure 2. The place of the building in Site Plan and Sun, Prevailing Wind Directions

Window Sizes of actual buildings are 400*210 cm and 400* 120cm in the ground floor and first floor, respectively in A side of the building

and 300*210 cm and 300* 120cm is used in the ground floor and first floor, respectively in B side of the building. Moreover, after calculating actual building's metric, various possibilities of using different glazing, solar shading panels and window sizes were modified to achieve different DF and DA results.

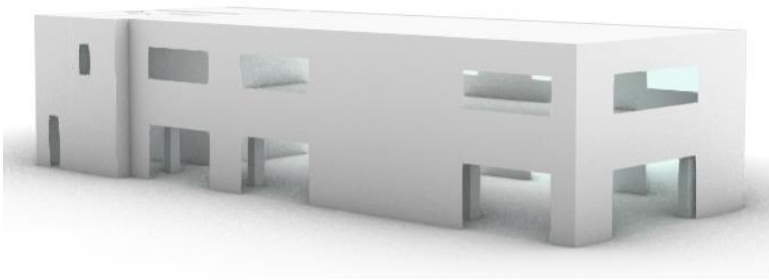

Figure 3: Graphic of Actual Building

The Ground Floor's DF and DA were calculated as 3.64%, 69%, respectively. It's Df and DA is enough for standards. The First Floor's DF was calculated as 3.01% when its DA was 61%. They are seen in Figure 4. According to standards, the adequacy of the results is the same as the ground floor.

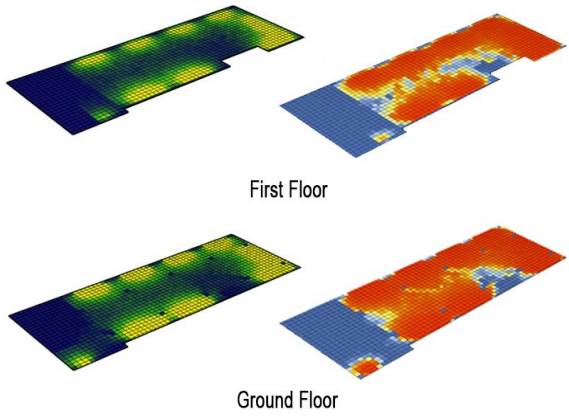

Figure 4: Graphic of DF and DA of the Actual Building

On the other hand, the lighting of the part of the building with artificial lighting and not using daylight is the reason for the lower calculation of DF and DA. Toilets are located in this part. As a matter of fact, according to standards, the results of DF and DA vary when the toilet part is removed. When the canteen section is taken, the results change as follows: DF 4.6%, DA 75% for the ground floor and DF 3.5%, DA 70% for the first floor.

Various simulations of the building were examined as possible solutions. In these variations, the glass material was changed, the window sizes were changed and sunscreens were applied. In some options, only one of them has been changed, while in others two features or all have been changed. These modifications can be listed as:

- The simulation was applied to the glazing material according to 4 options: Single Panel 88, Double Glazing Panel Clear 80, Double Glazing Panel LowE-65 and Double Glazing Panel LowE-65 Argon. However, since there was no difference in the variation of the last two materials, only the data obtained with Double Glazing Panel LowE-65 was presented in the study.
- In addition, the degree of applied sunshades 90 and 45 degrees. This is because they are perpendicular and half angles and are basically two of the four angles used. The reason for not using other angle grades is for better classification of the obtained simulations.
- In the variations made in the window dimensions, the window sizes are as follows: A side changed to 2100 * 210 cm in the lower floor and 2100 * 120cm in the upper floor when B side changed to 3000 * 210cm in the lower floor and 3000 * 120cm in the upper floor.

The percentage of the dimension of the windows which are used in the actual building and other variations according to the walls are shown in Table 1.

Table 1: The percentage of the dimension of the windows

Actual Building	Wall Dimension	Window Count		Glazing Dimension		%
A side	31 *6	3	3	4*2.1	4*1.2	21,3
Enterence	11*6	1	1	3.6*2.1	3.6*1.	18
B side	31 *6	4	4	3*2.1	3*1.2	21,3
Glazing Size Modified Variation	**Wall Dimension**	**Window Count**		**Glazing Dimension**		**%**
A side	31 *6	1	1	21*2.1	21*1.2	37,3
Enterence	11*6	1	1	3.6*2.1	3.6*1.2	18
B side	31 *6	1	1	30*2.1	30*1.2	53,2

In 1st possibility, glazing was changed and single panel 88 was used. Ground floor and first floor were calculated as DF 5.17%, DA 77% and DF 2.91, DA 54%, respectively. They are displayed in Figure 5.

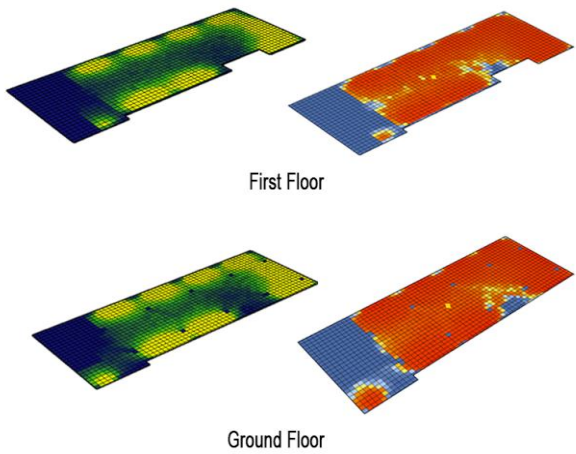

Figure 5: Graphic of DF and DA of the 1st Possibility

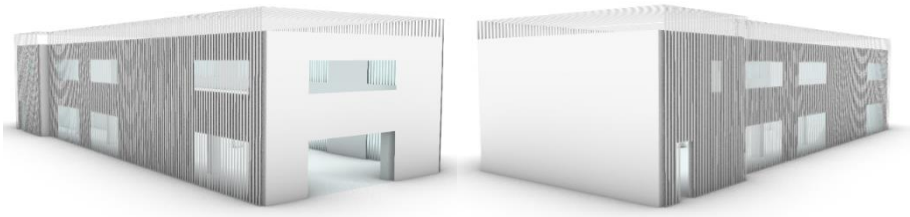

Figure 6: 2nd Possibility of Building H

In 2nd possibility is shown in Figure 6, Metal Sheet Sun Protector Facade (90° degree) and Double Panel LowE-65 glazing were used, in Figure 5 its graphic is shown. Ground floor and first floor were calculated as DF 2.16%, DA 45% and DF 1.12%, DA 31%, respectively which are shown in Figure 7. This version is not suitable because it does not fit established standards and the received sunlight is not sufficient.

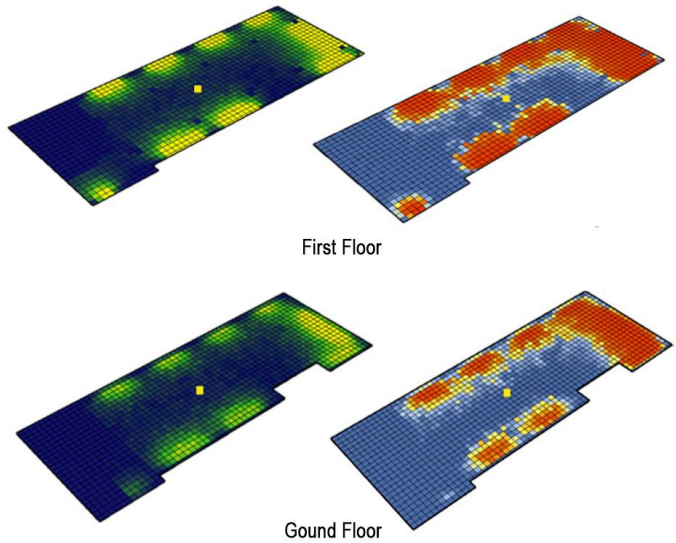

Figure 7: Graphic of DF and DA of the 2nd Possibility

In 3rd possibility which is displayed in Figure 8, metal sheet sun protector façade (90° degree) and single panel 88 glazing were used. The results are DF: 2.55%, DA: 54% for the ground floor and DF: 1.62%, DA: 41% for the first floor.

In 4th possibility, metal sheet sun protector façade (90° degree) glazing was changed and double glazing panel clear 80 was used. The graphic of the calculation is shown in Figure 9. Ground floor and first floor were calculated as DF 2.49%, DA 50% and DF 1.45, DA 38%, respectively. This two versions also are not suitable because they do not fit established standards and the received sunlight is not sufficient.

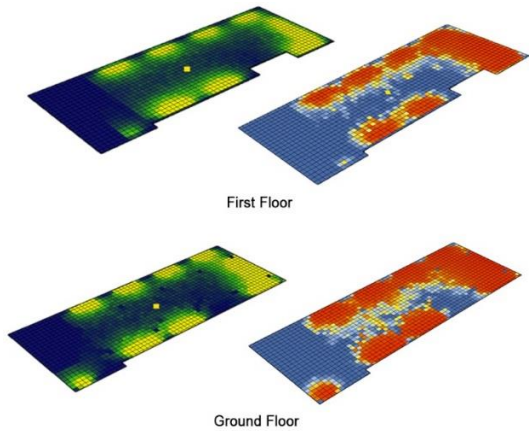

Figure 8: Graphic of DF and DA of the 3rd Possibility

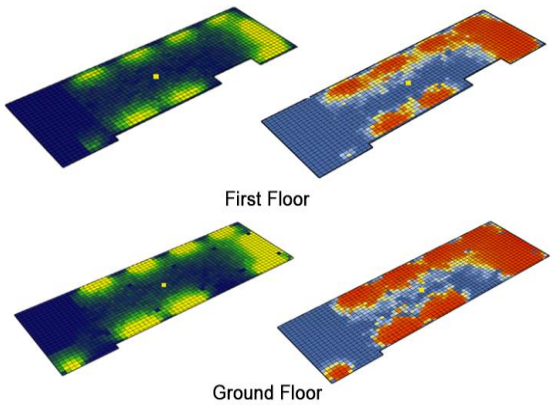

Figure 9: Graphic of DF and DA of the 4th Possibility

In 5th, 6th and 7th versions, metal sheet sun protector (45° degree) and single panel 88 glazing, double clear panel 80 glazing and double panel LowE-65 glazing were used respectively.

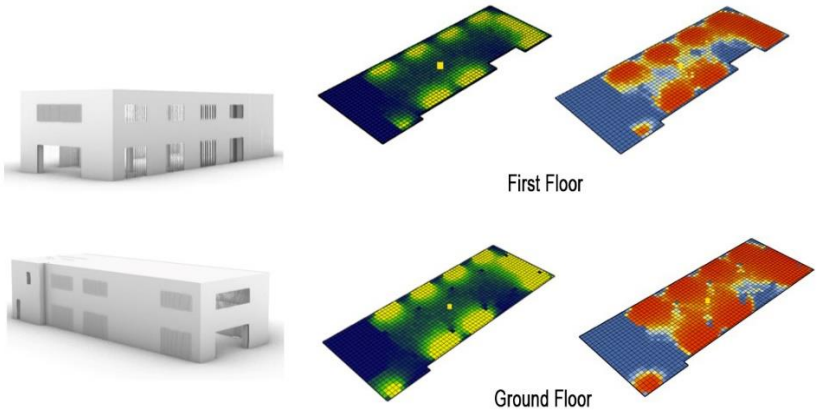

Figure 10: 5th option of Building H

Firstly, in the 5th version which is shown in Figure 10 results are DF: 2.80 %, DA 54% for first floor and DF: 3.64%, DA: 69% for the ground floor.

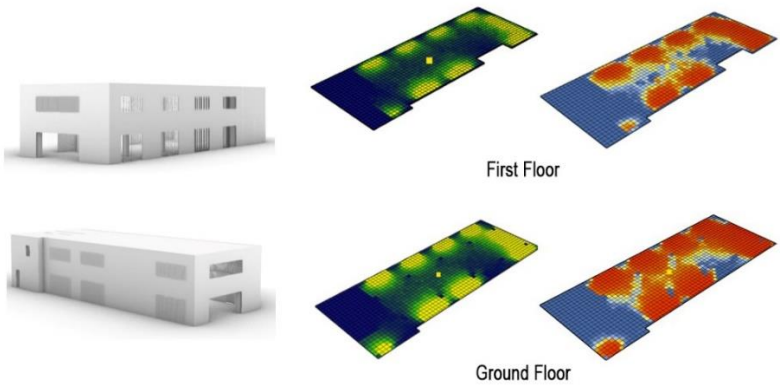

Figure 11: 6th version of Building H

In second, the results are DF: 2,49 %, DA 50% for first floor and DF: 3.23%, DA: 63% for ground floor in 6th version, its graphics are displayed in Figure 11.

At last, in 7th version results are DF: 1.40%, DA: 36% for first floor and DF: 2.55%, DA: 54% for the ground floor. It is also shown in Figure 12.

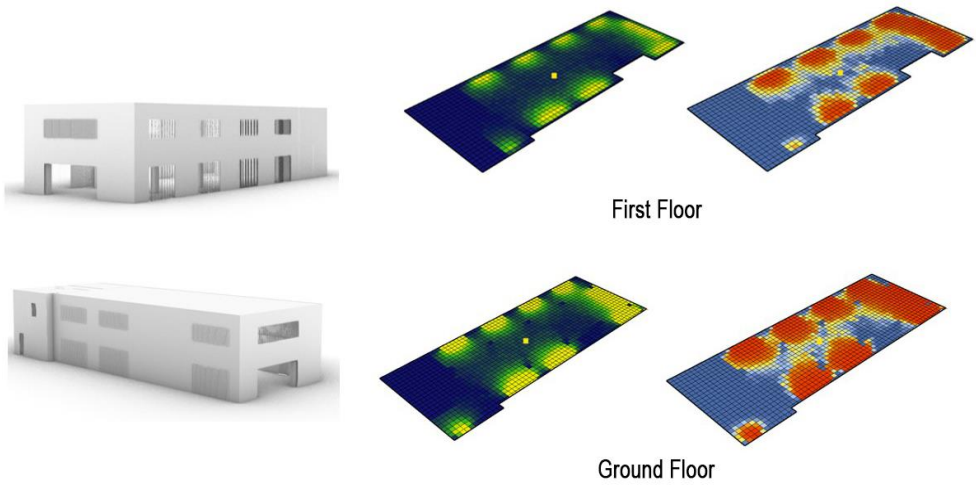

Figure 12: 7th version of Building H

In 8th, 9th and 10th versions, window sizes have been changed. The heights are the same and their lengths are enlarged as 2100*210cm and 2100*120cm in A-side and 3000*210cm and 3000*120 in B side. In all options, glazing is not changed. It is same as the actual building version (Double Glazing Panel LowE-65).

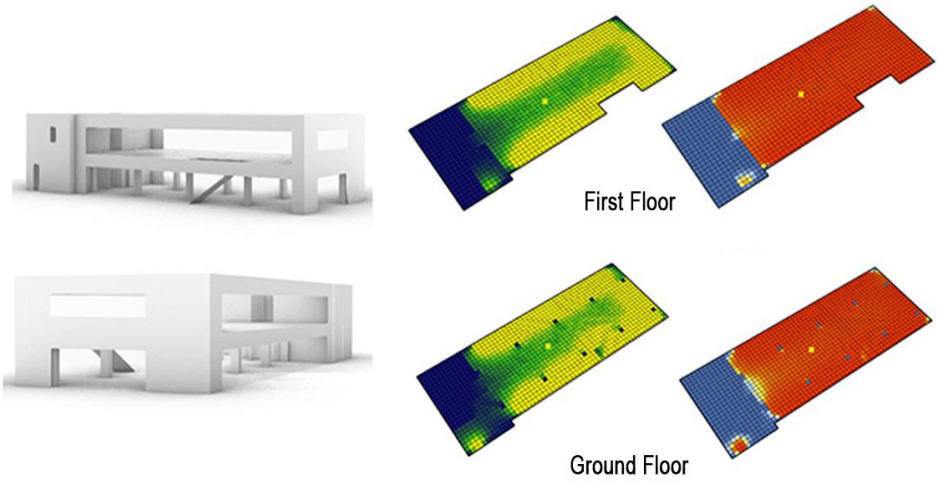

Figure 13: 8th Version

In the 8th version, there is no sun protector. The calculation of the graphic is shown in Figure 13. The results are DF: 6.36%, DA: 80% and DF: 5.36%, DA: 78% for ground and first floor, respectively.

In the 9th version which is demonstrated in Figure 14, there are 45° degree metal sheet sun protectors. The results are DF: 4.2%, DA: 75% and DF: 3.55%, DA 72% for ground and first floor, respectively.

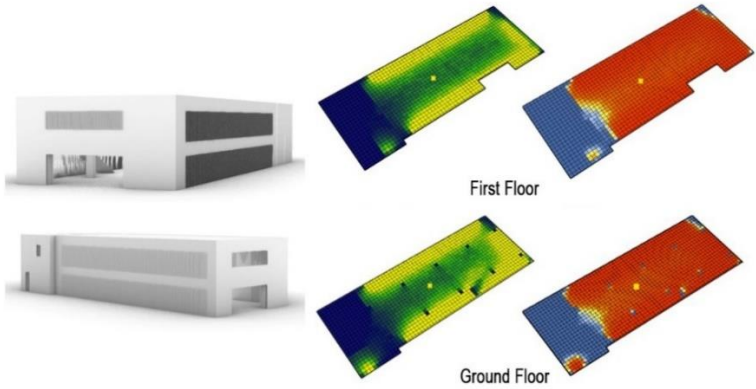

Figure 14: 9th Version

In the 10th version, there is 90° degree metal sheet sun protector façade. The results are DF: 3.55%, DA: 72% and DF: 3.01%, DA: 73% for ground and first floor, respectively. It is demonstrated in Figure 15 In all three versions, the results are valid according to standards.

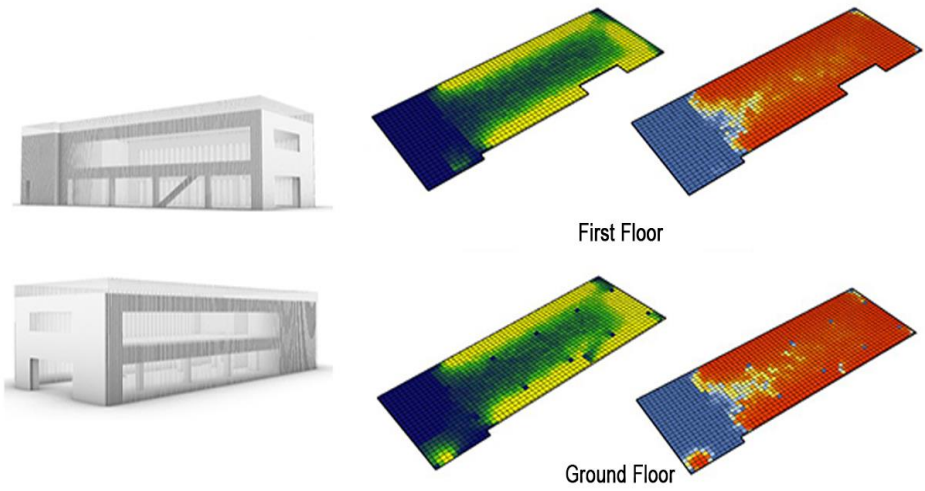

Figure 15: 10th Version

At the end of the simulation process, it is found out that, according to standards, some of the values are valid according to standards IESNA and CISBE but some values are not enough for the use of the building. In table 2 we can see the result of all versions.

As a result of the study, the numeric data were found about DF (daylight factor) that gave a basic explanation about daylight analysis but the important values were DA (daylight autonomy), because of the calculation of DF and DA and considering the calculated values, in the light of the researches that were completed in the last decade.

Table 2: Results of the Simulations

Type of Building	Sun Protector	Size of Window	Glazing Type	Ground Floor		First Floor	
				DF	DA	DF	DA
Actual Building	_	400*210 cm / 400*120cm (A side) 300*210cm / 300*120cm (B side)	Double Glazing Panel LowE-65	3.64%	69%	3.01%	61%
Possibility 1	_	400*210 cm / 400*120cm (A side) 300*210cm / 300*120cm (B side)	Glazing Single Panel 88	5.17%	77%	2.91%	54%
Possibility 2	Metal Sheet Sun Protector Facade (90° degree)	400*210 cm / 400*120cm (A side) 300*210cm / 300*120cm (B side)	Double Glazing Panel LowE-65	2.16%	45%	1.12%	31%
Possibility 3	Metal Sheet Sun Protector Facade (90° degree)	400*210 cm / 400*120cm (A side) 300*210cm / 300*120cm (B side)	Glazing Single Panel 88	2.55%	54%	1.62%	41%
Possibility 4	Metal Sheet Sun Protector Facade (90° degree)	400*210 cm / 400*120cm (A side) 300*210cm / 300*120cm (B side)	Double Glazing Panel Clear 80	2.49 %	50%	1.45%	38%
Possibility 5	Metal Sheet Sun Protector (45° degree)	400*210 cm / 400*120cm (A side) 300*210cm / 300*120cm (B side)	Glazing Single Panel 88	3.64%	69%	2.80%	54%
Possibility 6	Metal Sheet Sun Protector (45° degree)	400*210 cm / 400*120cm (A side) 300*210cm / 300*120cm (B side)	Double Glazing Panel Clear 80	3.23%	63%	2.49%	50%
Possibility 7	Metal Sheet Sun Protector (45° degree)	400*210 cm / 400*120cm (A side) 300*210cm / 300*120cm (B side)	Double Glazing Panel LowE-65	2.55%	54%	1.40%	36%
Possibility 8	_	2100*210 cm / 2100*120cm (A side) 3000*210cm / 3000*120cm (B side)	Double Glazing Panel LowE-65	6,30 %	80%	5.36%	78%
Possibility 9	Metal Sheet Sun Protector (45° degree)	2100*210 cm / 2100*120cm (A side) 3000*210cm / 3000*120cm (B side)	Double Glazing Panel LowE-65	4.20%	75%	3.55%	72%
Possibility 10	Metal Sheet Sun Protector Facade (90° degree)	2100*210 cm / 2100*120cm (A side) 3000*210cm / 3000*120cm (B side)	Double Glazing Panel LowE-65	4.00%	74%	3.01%	61%

Because DA results are more valid than DF results, most of the analyzes were made accordingly. According to accepted DA standards, 7 out of 11 calculated samples receive sufficient daylight. Besides, DF results are valid in these variations. One of them is an example of the actual building. Sun protection and glazing are not suitable in Possibility 2, 3, 4 and 7.

According to the standards, the buildings that are suitable in terms of DF and DA are the actual building, possibility 1, possibility 5, possibility 6, possibility 8, 9th and 10th. These 6 variations were divided into 3 groups according to the changes applied in the simulations. This grouping is shown in Table 3.

Table 3. Simulation Grouping

First Group		Second Group		Third Group		
Actual Building	**1st Possibility**	**5th Possibility**	**6th Possibility**	**8th Possibility**	**9th Possibility**	**10th Possibility**
This group does not have a sunscreen system. Window dimensions have not changed. The glazing of the main building and version 1 are Double Glazing Panel LowE-65 and Glazing Single Panel 88, respectively.		In this group version, 45° sunscreen is used. Window sizes have not been changed. The glazings of 5th possibility and 6th possibility are Glazing Single Panel 88 and Double Glazing Panel Clear 80, respectively.		This group is shaped according to the change in window sizes (A side: 2100 * 210 cm / 2100 * 120cm and B side: 3000 * 210cm / 3000 * 120cm) and the material used as glazing is Double Glazing Panel LowE-65. When, in the 8th variant, sun protector was not applied, in the 9th and 10th variants, sun protector with an angle of 45 ° and 90° were used in simulations, respectively.		

In the first group, the use of Double Glazing Panel LowE-65 or Double Glazing Panel LowE-65 Argon in glazing due to the fact that the western façade of the building is sunlight and some of the main openings are positioned in this part, Glazing Single is used to prevent the disturbing effects of the afternoon sun and radiation. Panel 88 is

more suitable than using. Therefore, Actual Building is more functional than the first variation.

In the second group, the 6th variation is more appropriate in terms of heat insulation. Because the when 5th variation is single-panel glazing, the 6th variation is double-panel glazing. However, Variation 7 considered being inadequate, although not within this group, should also be interpreted as variation 7. Because ground floor DF and DA ratios are calculated according to standards. The only problem is that the first floor does not meet the standards. In version 7, use of artificial light in the toilet part causes low DF and DA. Since there was no opening, this affected all DF and DA ratios. So, the lighting problem of the area where people eat and generally use is not present. Therefore, variation 7 can also be suitable for daylight.

In the 3rd group options, the main openings in the western and eastern facades were considerably widened compared to the actual building. So the 10th option in terms of controlling daylight from the west side which has Sheet 90 ° degree sun protector facade and double glazing panel LowE-65 is more suitable.

CONCLUSION

Although the position of the building is incorrect and the density of the windows on the west side of the building is high, it has been found that 7 samples, including the actual structure, meet the standards as a result of the simulation calculation.

In this respect, the actual building is well suited for receiving daylight. In the interior of the building, daylight is sufficient during the day without the use of artificial light. However, a large number of windows on the west side (A Side of the building) can create an uncomfortable area in the afternoons, especially in the summer. It is stated that the openness rate that should be on the western front should not be more than 2% by the experts (Chiras, 2004). Building H has a 21.3% clearance on the west side. Therefore, to control daylight and reduce radiation intensity, a kinetic sun protector, which angles can be controlled according to daylight, should be applied.

It is important to remember that people spend most of their time in the fast-paced world of today. Particularly people spend most of their time in office spaces or indoors near work areas. The environmental control systems of the space must be well planned for people's time spent in these closed spaces to be both productive and for their physical and mental health. Lighting design and use of daylight are one of these systems. Moreover, it is important to remember that daylight use is more sustainable than artificial lighting.

In order to increase sustainability, it is important to use solar energy adequately on the basis of both temperature control and visual control. The structures to be constructed should be examined in terms of climate type, prevailing wind and sunbathing direction during the planning stage. Building facades and glass systems should be determined according to these properties in order to build sustainable and energy-efficient buildings.

REFERENCES

Alakavuk E. (2018). Structure and Material Usages Concerning Sustainability in Architectural Design Studio, SHS Web of Conferences 48, 01047, ERPA 2018, https://doi.org/10.1051/shsconf/20184801047

Alakavuk, E., Tokuç, A. & Savaşır, K. (2015). Yapı Kabuğu. Sürdürülebilir Yapı Tasarımı Kılavuzu, Mimarlar Odası İzmir Şubesi Yayınları, 22-28.

Ayoub, M. (2019). 100 Years of Daylighting: A Chronological Review of Daylight Prediction and Calculation Methods. Solar Energy, 194, 360-390.

Baş, H., Doğrusoy İ. T. (2019). Analysis of Pedestrian Wind Comfort in Urban Open Spaces:

The Case of İzmir Karşıyaka Shopping District. Megaron, 14 (2), 239-253.

Brotes, L., Wilson M., (2008). The Average Total Daylight. Factor Light & Engineering, 16 (2), 52-57.

Boyce, P., Raynham, P. (2009). SLL Lighting Handbook. CIBSE.

Chiras, D. D. (2004). The New Ecological Home: A Complete Guide to Green Building Options, Chelsea Green Publishing.

Hopkins, R. G. (1963). Architectural Physics: Lighting. London: Her Majesty's Stationary Office. Mardaljevic, J., Andersen, M., Roy, N. & Christoffersen, J. (2011). Daylighting Metrics for Residential Buildings. 27th Session of the CIE, Sun City, South Africa, July 11-15.

Öztürk, M. Z., Çetinkaya, G. & Aydın, S. (2017). Climate Types of Turkey According to Köppen-Geiger Climate Classification. Journal of Geography, 35, 17-27.

Panitz, K., Garcia-Hansen, V. (2013). Daylighting Design and Simulation: Ease of Use Analysis of Digital Tools for Architects. Daylighting design and Simulation: Ease of Use Analysis of Digital Tools for Architects in CIB World Building Congress 2013-Construction and Society, Brisbane Convention & Exhibition Centre.

Ruffles, P. (2017). Lighting Guide 0: Introduction to Light and Lighting. CIBSE.

Reinhart, C. F., Mardaljevic, J., & Rogers, Z. (2006). Dynamic Daylight Performance Metrics for Sustainable Building Design. Leukos, 3(1), 7-31.

Solmaz, A. Ş. (2015) Ecotect. Sürdürülebilir Yapı Tasarımı Kılavuzu, Mimarlar Odası İzmir Şubesi Yayınları, 108-115.

Turan I, Chegut A, Fink D & Reinhart C, (2019). The Value of Daylight in Office Spaces, Building and Environment, doi: https://doi.org/10.1016/j.buildenv. 2019.106503.

CHAPTER 6

ENERGY AND DAYLIGHT PERFORMANCE ANALYSIS OF DOUBLE SKIN FACADE SYSTEMS IN HOT ARID CLIMATE: A CASE STUDY IN KANO, NIGERIA

Assist. Prof. Dr. Ebru ALAKAVUK[1]
Gambo WURMA BARA'U[2]

[1] Assit. Prof. Dr. Yasar University, Architecture Department, İzmir, Turkey.Orcid no: 0000-0001-7482-8116 ebru.alakavuk@yasar.edu.tr

[2] Yaşar University, Graduate School of and Applied Sciences, Architecture Department, barau.gambo@fubk.edu.ng

INTRODUCTION

Typical building facades (DSF) are said to have quite a number of challenges in terms of natural ventilation, thermal comfort, especially in buildings with a high ratio of glass in the facade, in arid and hot climate regions. These problems cherish the architects and other building industry professionals to develop techniques of solving these problems through the utilization of new techniques such as shading devices, color glass among others. The adoption of these techniques has shown a reduction in natural lighting, and the increase in the use of artificial light; which inevitably led to the increase in the interior heat gain. To battle this situation, artificial cooling is used to cool down the heat effect. This increases of energy consumption, which leads to the increase the cost [1].

A double skin facade is mainly used to boost the building's thermal efficiency with great glazing facades formations. DSF is mainly adopted for an architectural reason and its transparency properties because it allows close contact with the surroundings of the building, and the point that it concedes a great amount of daylight to pass into the building deprived of intense glare. Finally, it has an attractive aesthetic value which is much desired by an architects, developers, and owners. Though, there are numerous tasks of using the DFS; one of them is the construction expenditures that is vividly much higher o a conventional glazed-facade. Moreover, the possibility of overheating during days with relatively high temperatures is obvious and consequently, excessive need for cooling the interior spaces may arise

[2].

It is unfortunate that until now, there are still a few buildings that patronize the use of DSF. Thus it is said that it is somehow difficult to find any objective data on the actual performance of buildings with the DSF specifically in a hot arid climate. This research will focus on some of the configuration issues in designing a DSF, where this study aims is to give a broad overview of double skin facade within the earlier specified climate region (hot and dry).

The task anticipated from buildings with DSF is to attain a harmony between the visual aesthetic, acoustics insulation, and the performance in terms of energy efficiency. The elementary structure of DSF consists of the inner skin, an air cavity, and outer skin. The inner skin and the outer skin can be of a single or double pane glass. The DSF can also be combined with shading elements such as louvers to moderate solar gains and consequently the cooling mandate of the building is reduced. Nevertheless, heat is ensnared in the air cavity of the DSF when the weather is hot, due to solar gains and thermal transfer of the exterior skin. Depending on the design, the gap of the DSF is commonly ventilated naturally or mechanically to drive out the excess of heat gained [3].

Key innovation in GF skills has equipped the architects and experts a chance to integrate the Components of the building envelope within sustainability philosophies but preserving a great level of capability. That is the reason why GF construction systems and materials must be

planned and fixed appropriately to deliver an exciting living environment, while maintaining a sustainable system for the environment and the society **[4].**

Since the late 1970s, reliance on artificial cooling systems in buildings has been growing, continuously which in consequence increases the maintenance cost of these buildings. The formations of some commercial building facades in hot and dry regions have an excessive impact on dwindling/growing the building's maintenance demand. In hot arid climates, about 45% of the cooling loads emanate from the facade's configuration **[5].**

1. DEFINITION AND CONCEPTS OF DSF SYSTEMS

1.1. Definition of DSF

The most exhaustive meaning of DSF was given by [6]. Based on the explanations he gave, a double skin façade is a facade composed of multi layers, which has an interior and exterior layer that consists of a buffer zone applied as a shield against solar and ventilation control.

"Double-skin facades are multi-layer skins construction with an interior skin, an intermediate cavity, and an exterior skin [7]. These skins could be of either single or double pane glass made of special qualities and characteristics. Shading devices are usually placed at the intermediate cavity for thermal comfort in the manner that these devices can be adjusted. The constructions DSF process could widely be grouped under, Shaft-box facade, Box Window façade, Multi-story façade and Corridor facade".

1.2. Concepts of double skin facade

The BBRI, (2002) portrayed DSF in the sequence below:

- Exterior Skin: Usually it is a toughed single glazing and may be solely glazed.
- Interior Skin: Detached double glazing unit (double and single pane clear, Low e argon among other glasses can be used). Most often this layer is not glazed wholly.
- The cavity amid the two skins: Its ventilation could be exclusively natural or artificial. The cavity width may vary as a function of the applied concept between the range of 200mm to 2m or even more. This width influence upkeep of the façade.

The DSF concept as "a duo of glass skins distinguished by an air gap with a depth ranging from 20 cm to several meters" According to him "the air space is attached with the outdoor atmospheres so that the windows of the inner façade can be operable, even in the high-rise buildings pending to wind pressures; this system permits cooling at night time and natural ventilation of the building [8].

When solar radiation is high, the air space has to be efficiently ventilated, to surpass overheating. In this regard, the basic criteria are the cavity depth and the size of the openings in the outer skin. Depending on the wind pressure and the prevailing climatic conditions, the air change within the cavity of the building façade [9].

1.3. Classification of DSF according to airflow/ ventilation mode

Double Skin Facades composition may be categorized in diverse directions. It can be classified based on construction mode, target and method of air flow within the intermediate space, among others.

1.3.1 Buffer DSF System:

The insulating glass adopted in this method is to domain natural daylight into buildings as well as upgrading its thermal insulation. Two layers of single glazing are used at an interval ranging from 250mm to 900mm or more, enclosed and permitting uninterrupted air into the building thru openings that can be opened. The figure below shows an example of a buffer DSF system.

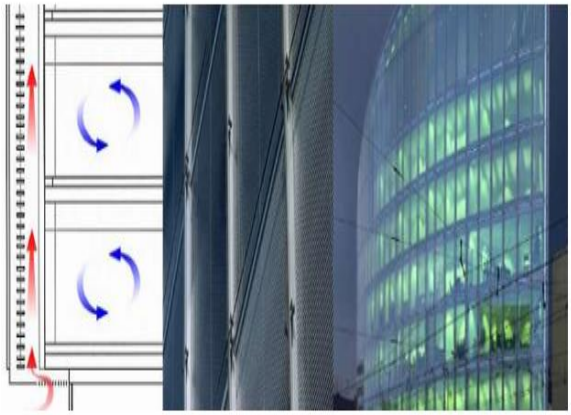

Figure 1*:* Buffer DSF: Business promotion centre Germany. (Source: www.fosterandpartner.com)

1.3.2 Extract Air DSF System:

This involved of an extra glazing layer positioned on the interior of a core façade of double glazing which makes the intermediate air space to partake in cooling the building. The unwanted used air is extracted through the intermediate space using mechanical means (fans), which moderates the interior glazed skin while the exterior skin of insulating glass decreases thermal transmission. Solar shading elements are also placed within the air cavity with depth ranging between 150mm-900mm [10]. This synthesis is often used in regions where natural ventilation is precluded or places with acoustic discomfort, aggressive wind loads, among others. (See figure: 2 below):

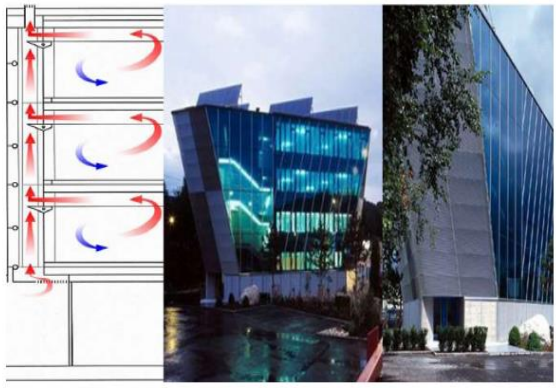

Figure 2*:* Extract Air DSF (Bürogebäude Felbermayr, Salzburg, Austria. Source: www.architecten.at

1.3.3 Twin Face DSF System:

This is composed of ordinary curtain wall system within a single glazed building skin. The exterior skin may be made with specially treated glass to blend with the intended function. Sun shading elements may be incorporated. This synthesis should have an

intermediate air space of at least 500mm-600mm to allow for cleansing. Natural ventilation is allowed in the twin faced DSF due to the presence of an opening which distinct it from the buffer and extract air DSF system. The internal skin gıves insulation for minimizing loss of heat from the interior, whereas the external skin functions as a guard to the air cavity contents (shading elements).

Figure 3: Twin Face DSF Daimler Benz (Debis) Building, Berlin.

Source: www.coltinfo.net

1.3.4 Hybrid DSF System:

This system of DSF is the association of any two of the above mentioned DSF systems used in a situation where any among the systems prior mentioned does not accommodate to the building system involved. The buildings may use a unit of any material or screens on either of the sides of the basic environmental barrier. Best example of hybrid DSF system to be cited is **t**he Renzo Piano's designed structure "Jiao center" located in New Caledonia, (figure 4).

Figure 4: New York Times Building and Detail of ceramic shading elements
Source: www.brianrose.com & architecture.co

1.4. Classification of DSF according to cavity partition

Most comparable DSF typologies are portrayed in the following sequence [11], [12], (figure 5):

- **Box window type**: In this case horizontal and vertical partitioning divide the façade in smaller and independent boxes.
- **Shaft box type**: In this situation, a set of box window elements are mounted on the skin. These elements are mounted alongside the vertical shafts situated in the façade to ensure efficıency in stack effect.
- **Corridor façade**: This system shows horizontal demarcation for fire prevention, ventilation and acoustic reasons.
- **Multi storey Double Skin Façade**: In this situation, there is no division vertically or horizontally within the air gap. The large openings within the building provide ventilation within the air cavity.

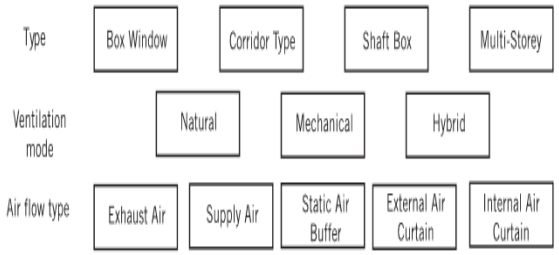

Figure 5: Classification of DSFGrphical

1.5 Advantages of double skin facade

- Acoustic Insulations:

Based on some authors' perception, the acoustic insulation can be one of the highly important rationales to use a Double Skin Façade. Degree of the interior nuisance can be minimizing inside an office building decreasing both the room to room sound transmission (interior nuisance) and the transmission from exterior sources (external nuisance). The acoustic insulation concerning the internal and the external nuisance can be attained by adopting this Double Skin Façade especially if incorporated with the quantity of openings which can be indeed very vital.

- Energy Savings:

Fundamentally, Double-Skin Façades can save energy when efficiently designed. Habitually, energy savings that can be achieved due to the additional facade may seem inspiring when the conventional insulation of the exterior wall is reduced. "Where DSF

constitute window ventilation possible, energy savings can be largely attained or where the period in which natural ventilation can be achieved was substantially extended. By avoiding a mechanical air supply, costs for electricity can be reduced. This will greatly exceed the savings mentioned before" [13].

- Thermal Comfort:

Compared to the outdoor air temperature, the air within the DSF cavity is warmer during the winter period; the internal ration of the façade can upholds heats that are more close to the levels of thermal comfort. Likewise, during the summer it is really crucial that the system is well planned so as the temperatures within the intermediate space will not increase excessively. Appropriate composition of DSF configuration and type, size of openings, type as well as the location of sun shading elements and pane types can assure enhanced results for all climatic regions and all types of building, (table 1).

Table 1: Advantages of DSF

Advantages mentioned by author	Oesterle et al., (2001)	Compagno, (2002)	Claessens et al.	Lee et al., (2002)	B.B.R.I., (2002)	Arons, (2000)	Faist, (1998)	Krogh, (2000)	Jager, (2003)
Lower construction cost (comparing to electrochromic, thermochromic photo-chromic panes)	√								
Acoustic insulation	√			√		√	√	√	√
Thermal insulation during the winter	√	√		√	√		√	√	
Thermal insulation during the summer	√	√		√			√	√	
Night time ventilation	√	√	√	√		√			
Energy savings and reduced environmental impacts						√			
Better protection of the shading or lighting devices	√	√		√					√
Reduction of the wind pressure effects	√	√	√						√
Transparency – Architectural design				√	√	√		√	
Natural ventilation	√	√		√		√	√		√
Thermal comfort – temperatures of the internal wall	√	√		√	√	√	√	√	
Fire escape	√								
Low U-Value and g-value		√				√		√	

Source: Harris Poirazis (2006) "*Double Skin Facades*"

1.6 Disadvantages of double skin façade

- Higher Construction Cost:

In comparison to a conventional façade, "there is no any dispute in saying that double skin facades are more costly than single skin forms: the process of construction of the external skin and the intermediate space between the two skins forms the former type more sophisticated*"* [13].

- Supplementary Maintenance Cost:

Equating the Double Skin to the Single Skin type of façade, one can easily see that the Double Skin type much costly in terms of construction, operating, and maintenance expenses [14], highlighted method of estimating the costs and expenses and described it extensively, (table 2).

Table 2: Disadvantages of DSF

Disadvantages mentioned by author	Oesterle et al. (2001)	Compagno (2002)	Claessens et al.	Lee et al. (2002)	B.B.R.I. (2002)	Arons (2000)	Faist (1998)	Kragh, (2000)	Jager (2003)
Higher construction costs	√				√	√			√
Fire protection	√				√				√
Reduction of rentable office space	√								√
Additional maintenance and operational costs	√		√		√				√
Overheating problem	√	√			√		√		√
Increased air flow speed					√				
Increased weight of the structure			√						√
Daylight	√								
Acoustic insulation	√				√				√

Source: Harris Poirazis (2006) "Double Skin Facades"

1.7 Examples of DSF in hot arid climate

Heat prevention is of prime concern in warm climates as a means to moderate energy usage and deliver comfort to dwellers.

1.7.1 Arcapita Bank headquarters, Manama, Bahrain

The Arcapita Bank headquarters, Manama, Bahrain designed by SOM Associates uses a double façade system to simultaneously provide an exterior system and shading. In this occasion, the building offers dwellers with the impress of a wholly glass façade building without the extreme heat gain.

In the upper part of this building accommodates some offices covering the area of 18,500 square meters with intense glazing that provide pleasant view to the outdoor activities. Benefit can be derived from this solution for its easiness in installation and consequently inferior maintenance costs. The louvres are placed between double-skin air gaps to help in mitigating solar heat gain, (Figure 6).

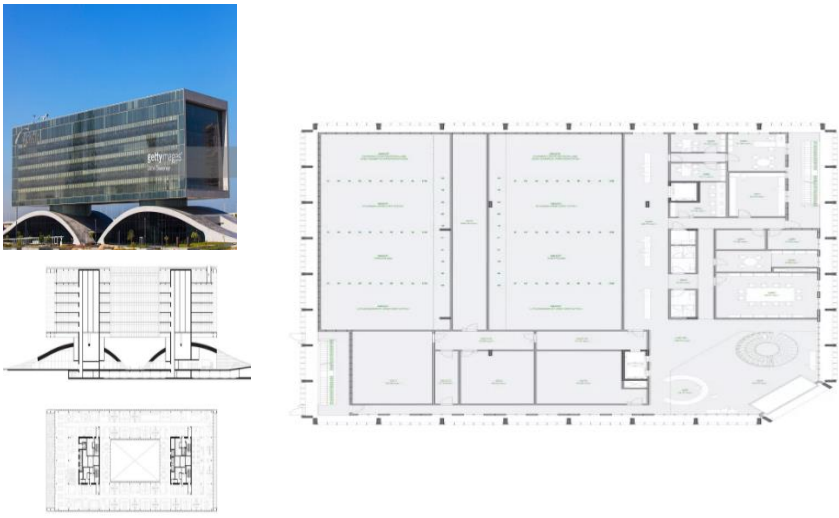

Figure 6: The Perspective view of the building and the bank layout, and the longitudinal section at the top of the floor plan. Source: (SOM Associates.)

1.7.2 Tel-aviv University Nanoscience Centre

Tel-aviv University Nanoscience Centre is a compressed building of cubic form, similar to a diamond and revolved at 45°. A cost-effective land mark structure well-assimilated into the predominant green environment and the confined urban context. Sitting on a crucial spot, a cross point at the main pedestrian axes, and a reference for the East gate to balance the whole area together with the Natural History Museum. A building that will function as a firsthand place for Nanoscience and Nanotechnology that will involve inspire and inspire diverse spectators and re-define the model of the laboratory building by crafting flexible and modular laboratories enhanced by a substantial space for communication and cooperation.

The Façade was a glazed envelope sheltered and enclosed by a second white external skin, comprising of an effective grid of vertical and horizontal constituents intermingling utilizing the core configuration of the building, (figure 7).

Figure 7: Tel-aviv University- Nanoscience Centre. OAB-FERRATER & ASSOCIADOS (2012)

1.7.3 Sowwah Square, Abu Dhabi, UAE

Goettsch Partners has designed a 529,360 m^2 development with climate response strategies for the envelope. The building utilizes a double skin façade system with cavity mechanically ventilated to create a shield zone to provide guard from the severe outdoor environment in Abu-Dhabi. At Sowwah Square (Figure 9) the double skin façade type is a multi-story starting from the fourth floor to the top of the building. An active solar shading system is integrated on the exterior surface of the cavity and can track the sun to optimize the shading. The shading system helped to prevent the intermediate space from overheating because it has minimized the projected solar energy on the intermediate space. “Utilizing an outboard lite with a very high shading coefficient, the design team was able to effectively block 76 percent of the solar energy from ever entering the air cavity”, [15].

Taking the exhaust air from office spaces and injecting it back to the cavity to flush out the warm air was used to achieve getting the intermediate buffer zone, (figure 8). “Through these efforts, the design team expects the double-skin cavity to be an average temperature of 89º F (31 ºC) when the exterior temperature extents 115º F (46 ºC), (figure 9)This will permit the great U-value of the shielded internal glazing to more simply block the air cavity’s radiating energy [16].

Figure 8: Sowwah Square Building, Abu Dhabi UAE. Source: [16].

Figure 9: Sowwah Square Building, Abu Dhabi UAE. Source: [16].

2. METHODOLOGY

2.1 Design Strategies in Hot And Arid Climate

Climatic factors greatly influence on the building performance specifically daylight as well as its energy consumption. Decreasing energy consumption, via natural resources and producing healthier, comfortable, and sustainable living functions are the aims of a climatic- responsive sustainable building design (Hui 2000). Viable design and construction approaches are of pronounced importance these days. One may say that sustainability was previously a motivating potency, revealing its rationality thru the various forms and procedures used. Consequently, from those days till today, there are

no sufficient transformation in difficulties and necessities encountered in design and construction environment; however several developments have been realized in terms innovative technologies and modernization of materials. Consequently, all-inclusive deliberation on building process should be ensured. Moreover, climatic- responsive design, choice of materials and building performances need to be assessed together and the final product should accomplish well during its lifespan.

2.2 Data Acquisition

Data acquisition was based on the following categorization of the research design [17]:

- Exploratory (user perception)
- Descriptive (case studies)
- Experimental (simulation)

Personal interview practiced and questionnaires were administered as basic source of data to determine the indoor conditions within the selected building under study. Data in relation to building location, materials configuration were gathered through the earlier mentioned mechanism. To achieve the targeted results, the workflow indicated in figure below should be adhered to while conducting the simulation experiment, (figure 10).

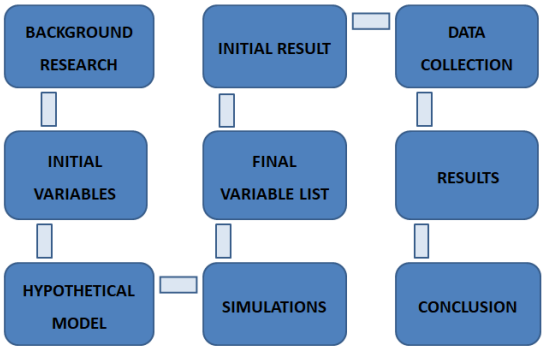

Figure 10: Methodology Workflow

2.3 Instrument for data collection

These instruments include:

- Physical Survey
- Drawings
- Interview / Survey Questions
- Computational tools (Simulations)

2.3.1 Questionnaire design process

The figure 12 below shows how survey questions are logically and sequentially developed, (figure 11).

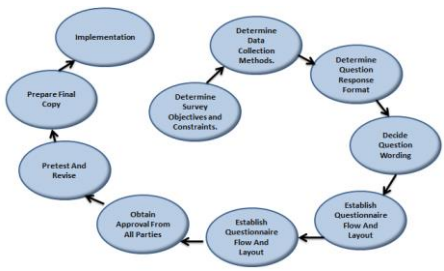

Figure 11: Questionnaire design process

2.3.2 Survey questions administration process

Based on the final stage of the above mentioned Figure, one hundred and fourteen (114) Questionnaires were administered to both the Staff and Customers using the building under study. These Survey questions were successfully shared by the Researcher with the aid of one other person who happens to be a staff within the building under study. After reasonable period of time, responds were obtained from various respondents only twelve (12) out of one hundred and fourteen (114) questionnaires were not received yet bringing the total number of questionnaires returned to one hundred and two (102).

Some challenges encountered in the course of administering the survey questions include the difficulty of some respondents especially the customers' side to respond to the survey questions, although the survey questionnaire was designed in such an interesting way that can easily be answered and be filled logically. Some of the respondents were not willing to accept the survey questions and to some extent some of the staff also refused to welcome the survey. Moreover, in the course of this survey some of the respondents exhibit some degree of misunderstanding the aim of the survey but notwithstanding, they responded to the questions as much as possible though there were some of them who required interpretation of some questions before they were able to respond to them.

2.4 Ladybug + Honeybee Simulation tools

The method to be adopted for evaluating the energy performance and natural daylight within the office building under study is Honeybee and Ladybug which also would allow for the visualization of Energy and daylight Simulations results as well as some visual information about the study location in terms of Temperature, Sun paths Relative humidity among others [18].

2.4.1 Energy Simulations

The workflow established in this research began with the generation of 3D model of the office building by means of a three dimensional parametric modeler tool called “Grasshopper”, which is plug-in for Rhinoceros. Other environmental analysis plugins adopted are Ladybug + Honeybee. Ladybug Apparatuses is an association of free computer applications that upkeep environmental design and application of all existing environmental design software parcels. Ladybug tools help in connecting 3D Computer-Aided Design (CAD) interfaces to the prior stated simulation engines. Ladybug Tools uses weather data analysis to aid the parametric workflow of innovative simulation process and is very vital in analyzing the energy performance of a building.

2.4.2 Daylight Simulations

Ladybug and Honeybee are important design tools that permit designers to have answers to very significant environmental questions in the initial phases of a project when there is the greatest design

flexibility and potential impact. Via these tools permits the design teams to demonstrate composite environmental features and visualize how our designs react to those factors. This iterative parametric procedure is crucial to meet each project's distinctive performance goals where form follows performance and is used to determine daylight performance of a building [19].

2.4.3 Diagrammatic flowchart of genetic algorithm

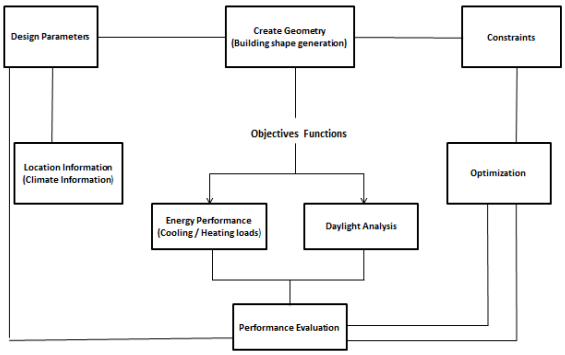

Figure 12: Ladybug + Honeybee Energy/Daylight Genetic Algorithm flowchart

2.4.4 Description of parametric model and decision variables

The Parametric model developed for an office building comprised Double-skin glazed facades with aluminium mullions with an air cavity between them. The parametric model allows for changing the glazing configuration (glazing type and ratio), and the change of different time that produce different values based on the predominant weather. All the decision variables are changeable using some intervals and were fixed with minimum and maximum values limits as indicated in the (Table 3) below.

Table 3: Parametric decision variables and extent of their values

Variables	*Minimum Values*	*Maximum Values*
Glazing Type	1	3
Cavity Depth	500 cm	2M
Month	January	December
Day	Day 1	Last Day of the Month
Time	8:00 AM	6:00 PM

2.4.5 Honeybee

The connection between Grasshopper as the graphical user interface design environment and the validated simulation engines was made possible via Honeybee. These Simulation appliances as mentioned earlier include; EnergyPlus, OpenStudio, Radiance, and Daysim which assess the energy consumption of the building, daylighting and thermal comfort. Honeybee also facilitated connectivity between these validated (Daysim, Radiance, EnergyPlus and OpenStudio) simulation engines and, Grasshopper graphical programming interface, (figure 13, figure 14).

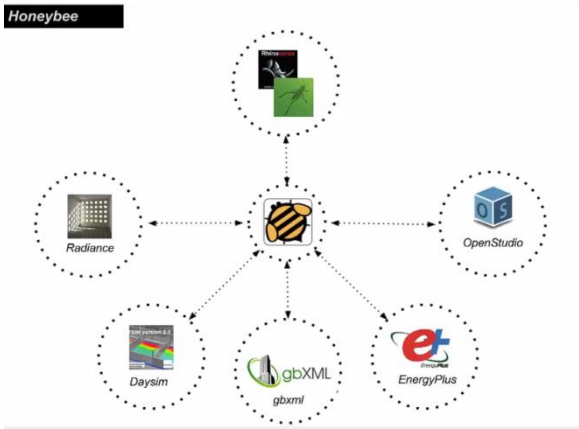

Figure 13: Ladybug + Honeybee connectivity to Energy and Daylight Simulation Engines. Source: www.mebd-penndesign.info/honey.

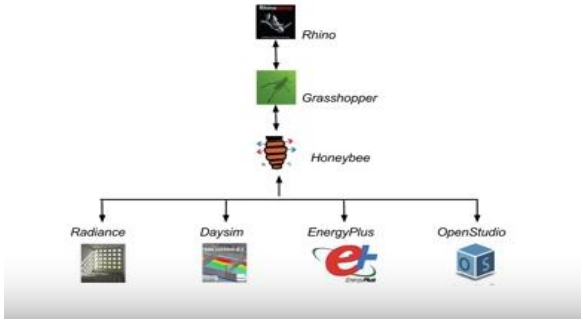

Figure 14: Ladybug + Honeybee connectivity to Energy and Daylight Simulation Engines. Source: www.mebd-penndesign.info/honey.

2.5 Ladybug (Visualization)

This is an open and free basis environmental-friendly plugin for Grasshopper3D. Grasshopper3D, is a "graphical algorithm editor" (grasshopper3d.com) plugin for Rhino, a 3D modeling apparatus which is increasingly becoming a desired modeling instrument for architects, designers, and students. Ladybug profits the parametric strategy of Grasshopper to permit the designer to discover the direct

relationship amongst environmental data and the generation of the design thru graphical data outputs that are extremely assimilated with the building geometry.

Ladybug supports the download and the importation of standard EnergyPlus Weather files (EPW) into Grasshopper. It offers a diversity of 3D communicative climate graphics that back the decision-making progression during the initial stages of design. Thru solar radiation studies, sunlight-hours modeling view analyses, Ladybug play a crucial role at the early design stage, it also aid in data and results visualization. It is integrated with visual programming environment that allows instantaneous feedback on design modifications and a high degree of customization, (figure 15).

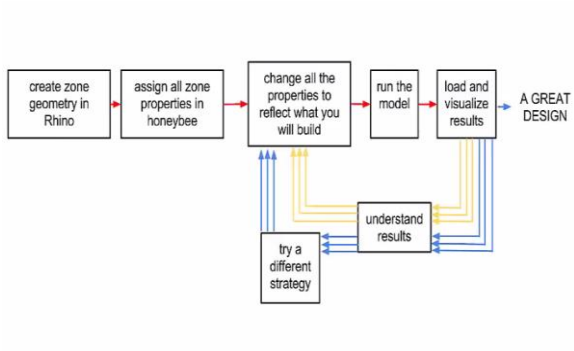

Figure 15: Ladybug + Honeybee Diagrammatic Flowchart Source: www.mebd-penndesign.info/honey.

3. CASE STUDY: ZENITH BANK KANO, NIGERIA

3.1 Nigerian Climate

The fundamental operate of all buildings is to fit to the predominant climate and furnish with an internal and external environment that is comfortable and conducive to the dwellers. Nevertheless, in this era of global warming and drastic climate change, comfort provision for the occupants of a building is quite challenging and very fundamental. This is in consequence of growing series of challenges confronting professionals presently to produce buildings that will be fit and comfortable for the 21st century. This chapter presents climatic condition of hot arid climate within the study area, as well as its effect on the building facades. This study looks into the climate condition of Nigeria in relation with climatic zones for architectural design. Nigeria's climate, as it is in most West African countries, is identified by strong latitudinal zones, becoming drastically drier as one moves north from the coast.

The wet season customarily starts in February or March as humid Atlantic air, famous as the southwest monsoon, occupies the country in the coastal and southeastern portions of Nigeria. The commencement of the rains is often manifested by the prevalence of high winds and dense but scattered squalls. The dispersed quality of this rainstorm is exclusively manifest in the northern regions, though there may be plentiful rain in some minor regions while some other places remain dry. Toward the end of April to the first week of May in most occasions, the raining season begins through the southern part of

the Niger and Benue river basins. Habitually in far north of Nigeria, it is mostly toward May end or early June when rains indeed commence. The uttermost of the rainy period befalls over utmost of northern part of Nigeria in August, as soon as air from the Atlantic shields the whole country. In southern districts, this era indicates the August dip in rainfall. Even though hardly absolutely dry, this dip in precipitation, which is particularly marked in the southwest, can be beneficial agriculturally, for it allows a momentary dry period for grain harvesting, (figure 16).

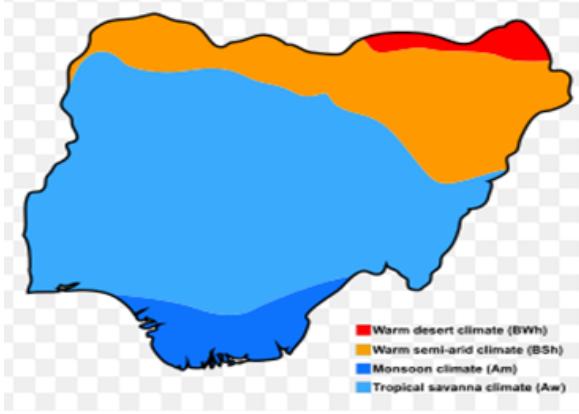

Figure 16: Nigeria Climatic Zones.

In Nigeria, temperatures all through are mostly high; daily variations are more definite than periodic ones. Maximum temperatures befall thru the dry season; rains adequately afternoon highs thru the wet season. Middling lows and highs for Kano are 27° C and 33° C respectively in January and 33° C and 28° C in June respectively, (figure 17, figure 18). Even though average temperatures differ

slightly from coastal to inland regions, inland regions, specifically in the northeast, have larger excesses. There, temperatures extent as high as 44° C afore the onset of the rainfalls or descent as low as 6° C during an invasion of cool air from the northern part from December to February.

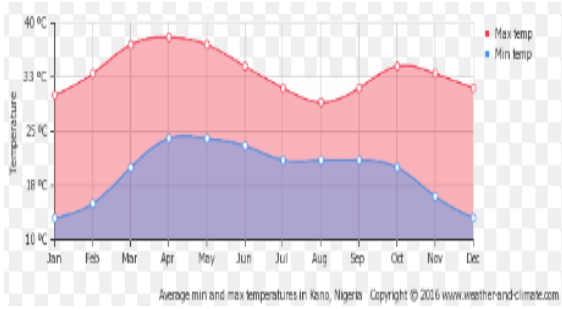

Figure 17*:* Average temperature of Kano, Nigeria.

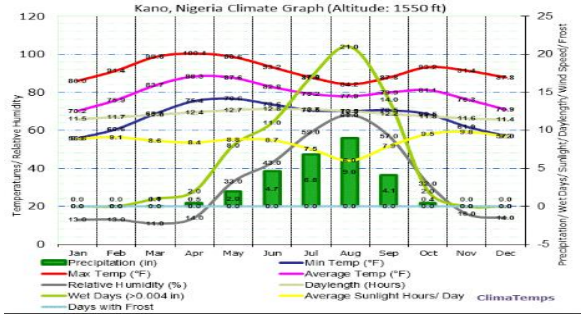

Figure 18: Climate Graph of Kano, Nigeria.

3.2 Survey Analysis

According to the survey, the total respondents were ninety two for both of the two categories, where the males constituted 67.65% and the females constituted the remaining 32.35% with their ages ranging

from eighteen years upward. Information in this survey were obtained from one hundred and two (102) respondents stratified into two groups of sixty (60) Customers and forty two (42) staff completed returned questionnaires. Most of these respondents were between the ages of eighteen (18) to seventy (70) years in the customer's category and between twenty one to sixty (21-60) years in the staff category. From these age distributions, 3% were from the age of 18 to 20 years, while 24.5% were from the age of 21 to 30 years, and 37.25% were from the age of 31 to 40 years, and 22.5% were from the range of 41 to 50 years, then 9.8% were from the age group of 51 to 60 years, then 2.95% were from the age group of 61 to 70 years.

The information obtained from this field work was gathered by the means of properly planned and designed questionnaires constituted of ten (10) items for the customers and eleven (11) items for the staff in general composed of twelve (12) items. Most of which were multiple choice, rating scales and bipartite scales questions. It should be understood that the first part of the survey question which consist of item 1, 2 and 3 was aimed at identifying the group sample item 5 was aimed at assessing respondents view about the building in terms of level of comfort within its interior. The survey question also try to find the respondents feelings in terms of their thermal sensitivity as this could pave way in rating the building based on its thermal performance in both summer periods. In fact this survey also raised an awareness about the importance of adopting double skin façade in our buildings in hot and arid climates without interrupting the ample supply of natural daylight as well as maintaining the thermal comfort

in one hand and conforming to the features of contemporary Architecture that suggest the use of massive glazing for the facades.

For the purpose of this research, Bar and Pie charts were used as a graphical medium for the representation and for visual analysis through observation and comparison of the information obtained from the survey (questionnaires).

3.2.1 Survey results

The graphical representation of the survey above is presented in the sequence below with some highlights about each outcome.

1.) What is your age?, (figure 19)

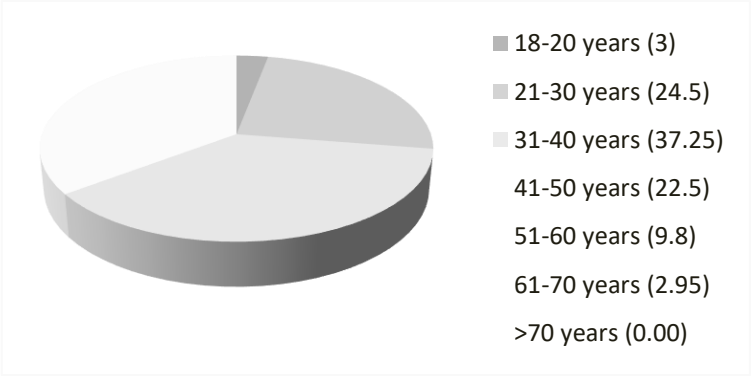

Figure 19: Age distribution of the respondents (%)

2.) What is your gender?, (Figure 20)

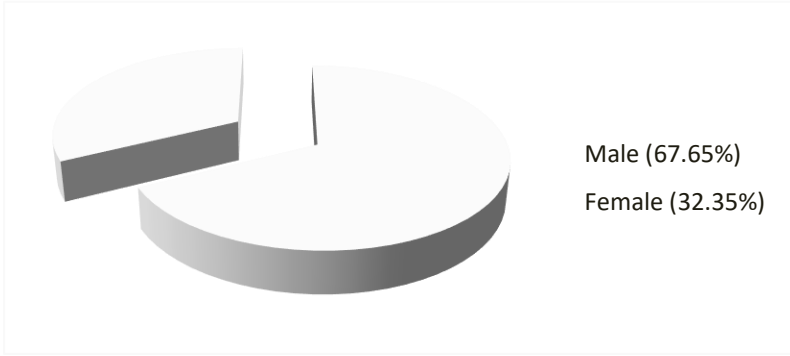

Figure 20: Gender status of the Respondents

3.) What is your highest educational qualification?, (Figure 21)

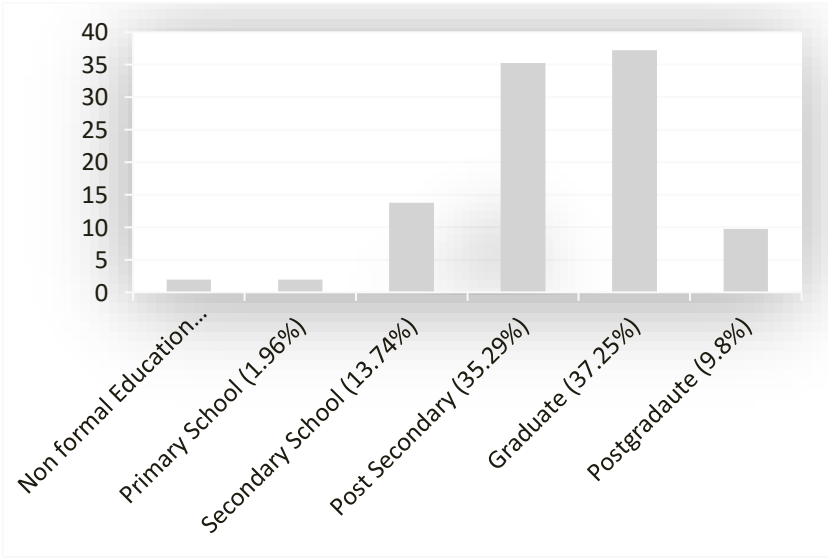

Figure 21: Educational status of respondents

According to the above survey results, the results indicated that about 37% of the respondents with the highest percentage were graduates and the lowest percentage of 1.96% fell into those who had Non-formal and primary certificates.

4.) What is your Occupation? (Figure 22)

Figure 22: Occupational status of the respondents

5.) How would you rate this building in terms of comfortability? *(*Figure 23*)*

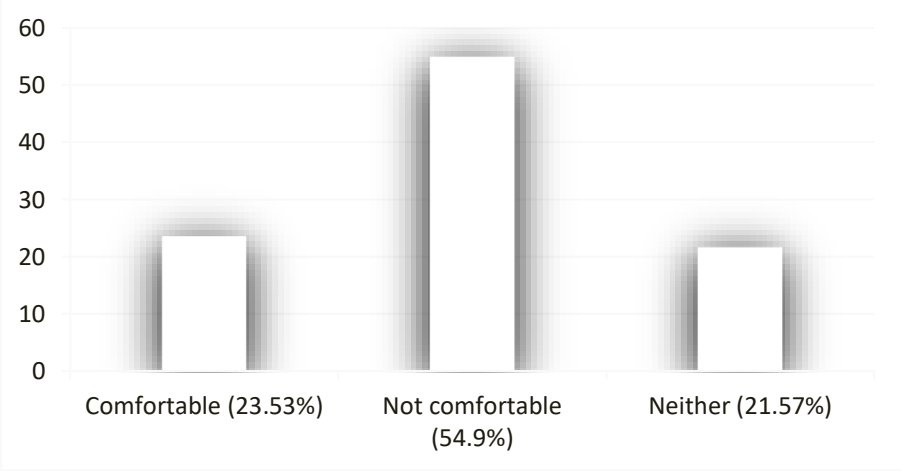

Figure 23: Comfort level rating

Figure above shows the general overview of the building under study by the users in terms of comfortability. Their response indicates that most of them were not comfortable.

6.) How would you rate your thermal sensitivity? *(*Figure 2*4)*

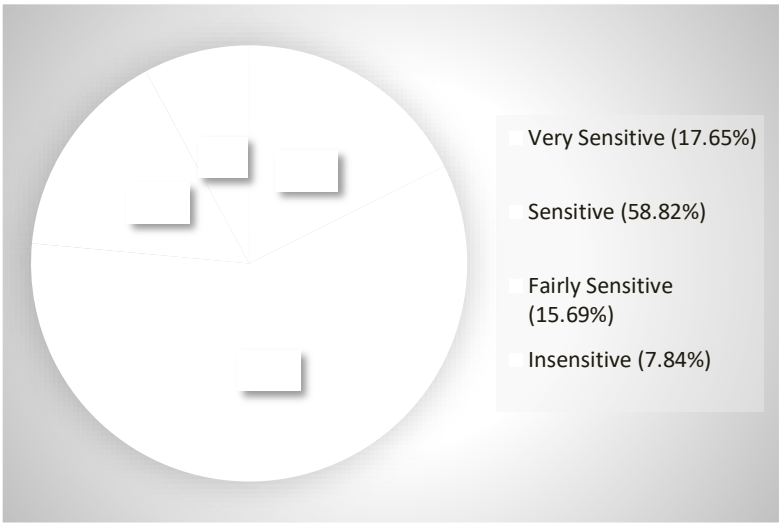

Figure 24: General rating of the respondents' thermal sensitivity.

According to the figure above, the survey shows that about 60% are sensitive to thermal with about 18% who are very sensitive to thermal as such proper consideration should be adhered to during the pre-design stage to ensure adequate thermal insulation materials were used as well as taking measures in designing the air cavity and other shading materials.

7.) How would you rate double skin façade as an important aspect to this environment? *(*Figure 2*5)*

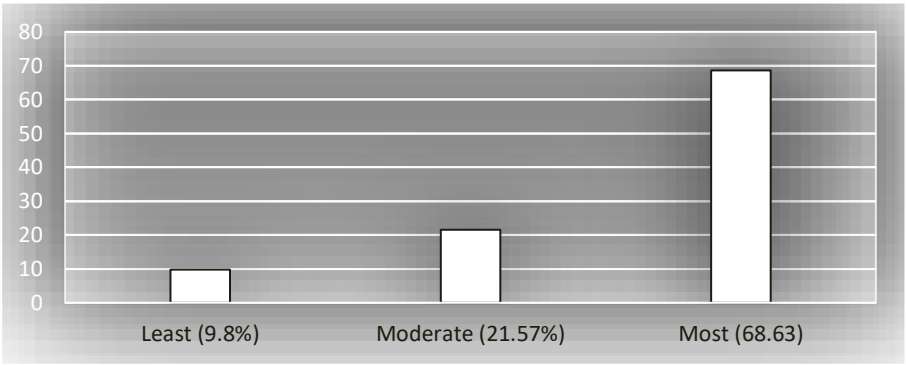

Figure 25*:* General rating of the Double Skin Façade in terms of its importance.

The figure above indicates that about 69% of the respondents perceive double skin façade as an important aspect of the environment based on their experience of both buildings with single and double skin with glazed façade. Only 9.8% of the respondents view it (DSF) as least important, leaving 21.57% with intermediate opinion about the importance of the double skin façade application in buildings.

8.) Generally, how would you the level of natural daylight in this environment? *(*Figure 2*6)*

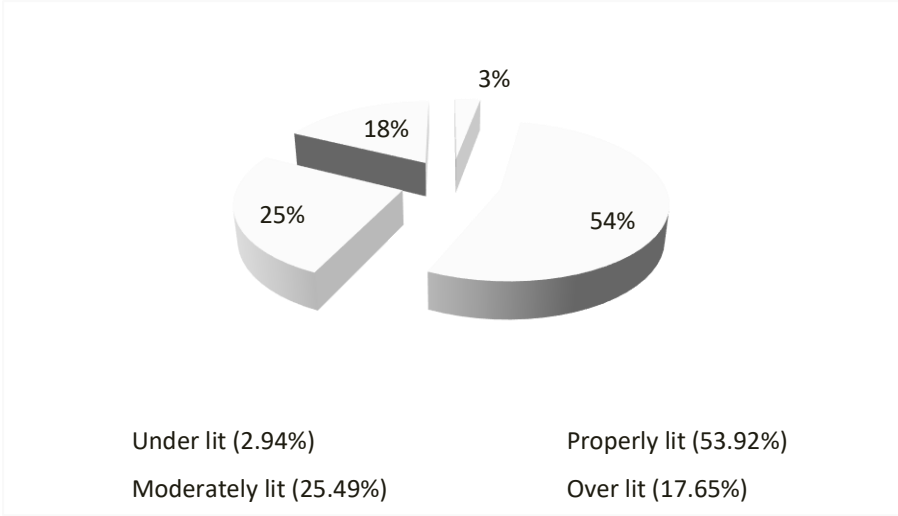

Figure 26*:* General rating of the environment in respect to daylight

Natural daylight delivery to the inner spaces of the building is of supreme importance. Nevertheless, due to some improved curiosity in the use of daylight in the strategy of low-energy, viable buildings are leading numerous architects and engineers to reflect inventive ways of developing the profits of daylight. It is very vital that the positive benefits of daylight were not compromised and do not become flummoxed with the negative impacts related to the intense solar radiation, thereby adopting the use of contemporary architecture building materials (glazing) and properly configuring them through the concept double skin façade that that can efficiently provide the required interior illumination and can relatively reduce the thermal transmission (U-Value) as well as solar heat gain (G-Value).

9.) How would rate the level of heat during summer in this environment? *(*Figure 2*7)*

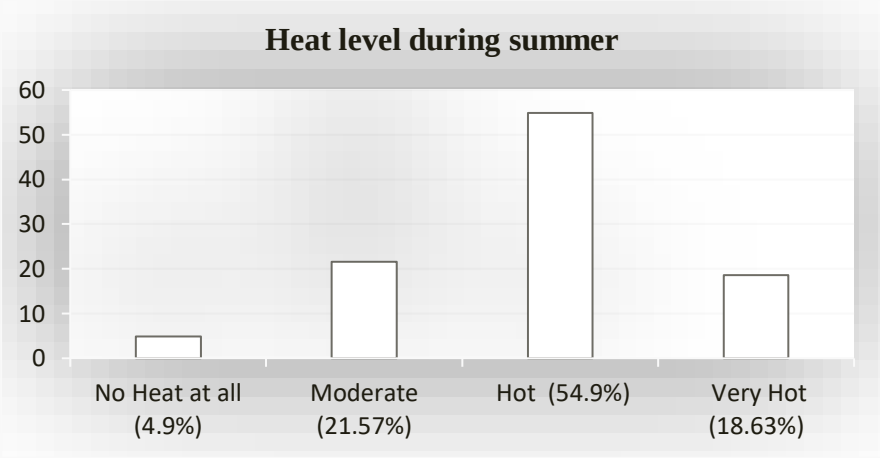

Figure 27*:* General rating of heat level during summer

The above figure indicated that about 55% of the respondents consider the building as hot environment, and about 21% consider it as moderate in terms of hotness during summer, and only about 5% consider it as efficient in terms of heat and about 19% consider it as very hot environment and consequently cooling load may be high hence, energy consumption will be relatively high. In view of that, there is need to evaluate the performance of the façade configuration so as to find the best or suitable façade formation so as to minimize the cooling load and consequently decrease the energy consumption.

10.) How would rate the level of cold during winter in this environment? *(Figure 28)*

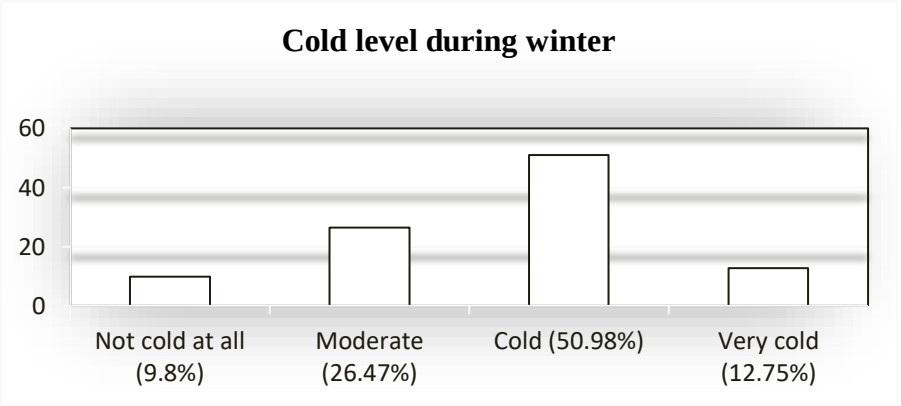

Figure 28: General rating of level of cold during winter

According to the responses obtained as represented in figure xx and Figure xx above, majority of the occupants are not comfortable both during summer and winter, therefore this research will try to find the genesis behind it and suggest some possible solutions using computer energy and daylight simulation tools precisely Ladybug + Honeybee.

3.3 Case Study Building

Zenith bank Nigeria plc was founded in May, 1999 and begins its operations in July the same year but then as a commercial institution. On June 17, 2004 the bank became a public limited company and was counted on October 21, 2004 on the Nigerian Stock Exchange (NSE) In consequence of the vastly prosperous Initial Public Offering (IPO).

The building is a prototype to all Zenith bank branches across the nation. Zenith bank is headquarter is located in Lagos, Nigeria; Zenith Bank has more than 500 branches and financial offices nationwide, it exists in all state capitals including Abuja (FCT). United Kingdom Financial Service Authority befitted Zenith bank as the first Nigerian

bank to be certified by the (FSA) In April 2007, resulting to Zenith Bank (United Kingdom) Limited. The building is located Along Maiduguri Road, Kano State within Kano city as a financial institution which many people patronize and visit daily during the five working days (Mondays to Fridays, 7 ‘o clock in the morning to 6 ‘o clock in the evening. *(*Figure 2*9)*

Figure 29: Showing the study area location.

The figure above illustrates the location of the case study building which is located in Kano city, Kano state in the north-west part of Nigeria bordering Jigawa, Katsina, Zamfara and Kaduna states.

3.3.1 Case Study Building Layout

The selected building is a two-storey building, with a double skin glazed facade. Each floor area is 672 m^2 excluding the cavity depth. The cavity depth is 500mm. It has a length of 28 m and a width of 24 m and 11 m storey height, *(*Figure 3*0)* .

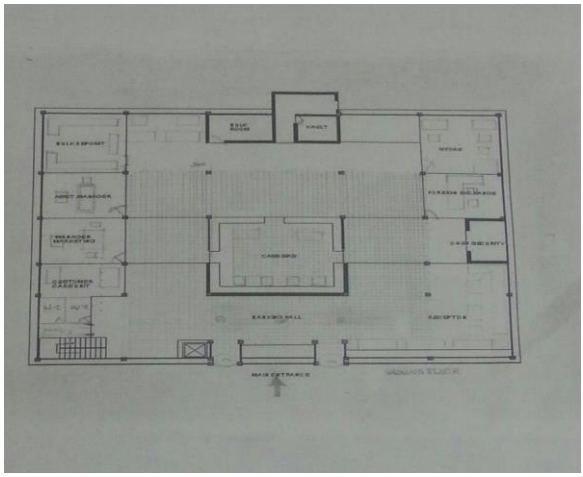

Figure 30*:* Floor Plan of the Building under study (Ground floor)

The floor plan above shows the layout and the interior arrangement of functions within the building. The building has double skins with double entrances which serve also as exits and are automatically operated to control the people's movement in and out for ensuring proper security. The banking hall is situated in the ground floor, as well as some auxiliary functions like; the customer care unit, the cashiers, foreign exchange, the vault, assistant manager, bulk room, storage among other functions. The building has an ample circulation space that allows free movement from one point to another with restriction to vault, bulk room and storage areas, *(*Figure 31*)* .

Figure 11*:* Approach View of Zenith Bank Nigeria Plc. Maiduguri Road, Kano, Nigeria.

The hypothetical building is intended to resemble the typical size and construction type of commercial buildings in Nigeria specifically in Kano city. The building adopt the norm of "**Cubism**" which was defined as concept developed in the early twentieth century, distinguished mainly by an emphasis on formal structure rather than their natural forms by transforming them to their geometrical peers, and unifying the planes of the signified objects independently of representational necessities [20].

3.3.2 Base Case Model

As earlier mentioned, the selected building is a two-storey building, with a double skin glazed facade. Each floor area is 672 m^2 excluding the cavity depth. The cavity depth is 500mm. It has a length of 28 m and a width of 24 m and 11 m storey height, *(*Figure 32*)* .

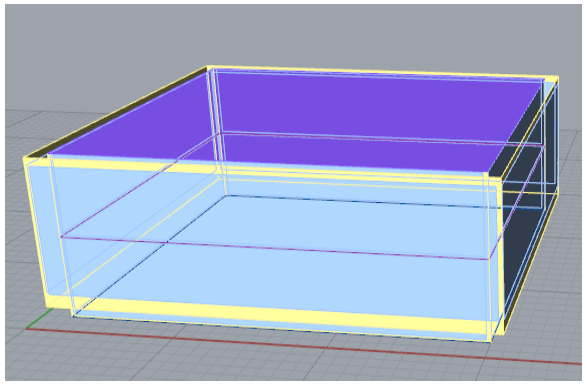

Figure 32*:* Base case model

3.4 Ladybug + Honeybee Simulation Tools

The objective function of the process is aimed at utilizing parametric workflows to achieve optimum energy saving and natural daylight within the office building under study. Ladybug permits in showing different outcome for Energy and daylight Simulations as well as some visual information about the study location in terms of Temperature, Sun paths Relative humidity among others.

3.4.1 Honeybee Energy Simulations

Table 4 below shows some energy simulation values for Cooling and Heating loads as well as the artificial lighting requirements of the selected hypothetical model with different glazing configurations at different times. The depth of the air cavity between the interior and exterior skin also serves as a decision variable, (table 4).

Table 4: Energy Simulation Results

S/NO.	INNER GLAZIN	DEPTH (Centimeters	INNER GLAZING	U-VALUE BTU/h.ft².°F	SHGC W/m²	VT (W/m²)	THICKNESS (cm)	MONTH	COOLING LOADS Kwh/m²	LOADS Kwh/m²	LIGHTING Lumen/watt
1	Single_Pane	50 cm	Double_Pane	0.85/ 0.83	0.73/0.65	0.69 / 0.63	0.25	January	107.04	16.28	448.59
2	Single_Pane	50 cm	Double_Pane	0.85/ 0.83	0.73/0.65	0.69 / 0.63	0.25	February	196.98	22.88	843.25
3	Single_Pane	50 cm	Double_Pane	0.85/ 0.83	0.73/0.65	0.69 / 0.63	0.25	March	325.77	26.16	129.19
4	Single_Pane	50 cm	Double_Pane	0.85/ 0.83	0.73/0.65	0.69 / 0.63	0.25	April	1949.21	26.22	169.53
5	Single_Pane	50 cm	Double_Pane	0.85/ 0.83	0.73/0.65	0.69 / 0.63	0.25	May	1741.98	26.25	214.39
6	Single_Pane	50 cm	Double_Pane	0.85/ 0.83	0.73/0.65	0.69 / 0.63	0.25	June	1494.79	26.25	257.45
7	Single_Pane	50 cm	Double_Pane	0.85/ 0.83	0.73/0.65	0.69 / 0.63	0.25	July	1081.19	46.25	299.59
8	Single_Pane	50 cm	Double_Pane	0.85/ 0.83	0.73/0.65	0.69 / 0.63	0.25	August	473.72	27.11	344.45
9	Single_Pane	50 cm	Double_Pane	0.85/ 0.83	0.73/0.65	0.69 / 0.63	0.25	September	890.76	46.25	386.39
10	Single_Pane	50 cm	Double_Pane	0.85/ 0.83	0.73/0.65	0.69 / 0.63	0.25	October	894.96	46.25	429.65
11	Single_Pane	50 cm	Double_Pane	0.85/ 0.83	0.73/0.65	0.69 / 0.63	0.25	November	973.75	46.25	472.71
12	Single_Pane	50 cm	Double_Pane	0.85/ 0.83	0.73/0.65	0.69 / 0.63	0.25	December	819.19	26.25	514.85
13	Low_E_Argon	50cm	Double_Pane	0.64/ 0.83	0.38/0.65	0.56 / 0.63	0.25	April	1350.82	33.11	169.53
14	Low_E_Argon	50cm	Double_Pane	0.64/ 0.83	0.38/0.65	0.56 / 0.63	0.25	May	1205.03	32.58	214.39
15	Low_E_Argon	50 cm	Double_Pane	0.64/ 0.83	0.38/0.65	0.56 / 0.63	0.25	August	269.44	33.29	344.45
16	Low_E_Argon	50 cm	Double_Pane	0.64/ 0.83	0.38/0.65	0.56 / 0.63	0.25	September	820.98	32.58	386.39
17	Low_E_Argon	50 cm	Double_Pane	0.64/ 0.83	0.38/0.65	0.56 / 0.63	0.25	November	850.32	32.58	472.71
18	Low_E_Argon	50 cm	Double_Pane	0.64/ 0.83	0.38/0.65	0.56 / 0.63	0.25	December	605.71	32.58	514.85
19	Single_Pane	100 cm	Double_Pane	0.85 / 0.83	0.73 /0.65	0.69 /0.63	0.25	April	1734.36	30.34	132.67
20	Single_Pane	100 cm	Double_Pane	0.85 / 0.83	0.73 /0.65	0.69 /0.63	0.25	May	1237.38	28.15	193.25
21	Single_Pane	150 cm	Double_Pane	0.85 / 0.83	0.73 /0.65	0.69 /0.63	0.25	August	400.34	29.71	323.68
22	Single_Pane	150 cm	Double_Pane	0.85 / 0.83	0.73 /0.65	0.69 /0.63	0.25	September	534.22	54.79	295.79
23	Single_Pane	200 cm	Double_Pane	0.85 / 0.83	0.73 /0.65	0.69 /0.63	0.25	December	624.81	34.38	457.81

In the Table 4 above, about 23 scenarios were analyzed thereby assigning various configurations of the glazing type: (Single Pane, Double Pane and Low E Argon) in the interior and exterior façade, Cavity depth: (50 cm, 100 cm, 150 cm and 200 cm) at different time throughout the year. Base case was analyzed based on each month of the year (January to December) having the same glazing configuration and the cavity depth and the results were obtained and recorded as in the table above. The results revealed that glazing configuration has a greater influence in the energy consumption of the building as well as the depth of the cavity. It is also observed that due lack of shading

elements within the cavity increases the cooling loads of the building, therefore some shading elements should be mounted amidst the air cavity.

The analysis also revealed that wider the cavity the less cooling load is required; therefore one should be cautioned enough in designing the air cavity. Hottest and coolest period is also very vital in the provision of the shading elements that may be adjustable or removable when required. Comparatively, from the above table, three different configurations were compared to evaluate the best formation in terms of energy performance at the same time (August) and the best formation was found to be; Low E Argon in the interior skin, double pane in the exterior skin with an air cavity of 50 cm. The second best option was that with Single pane in the inner skin, double pane in the outer skin with an air cavity of 150 cm. Then the third one was that with façade configuration of single and double pane in the inner and outer skins respectively and the air cavity of 50 cm.

3.4.2 Honeybee Daylight Simulations

In the Table 5 below, about 22 scenarios were analyzed thereby assigning various configurations of the glazing type: (Single Pane, Double Pane and Low E Argon) in the interior and exterior façade, Cavity depth: (50 cm, 100 cm, 150 cm and 200 cm) at different time throughout the year. Base case was analyzed based on each month of the year (January to December) at different day and a specific time, having the same glazing configuration and the cavity depth and the results were obtained and recorded as in the table below.

Comparatively, from the table below, two different configurations were compared to evaluate the best formation in terms of daylight performance at the same time (August) and the best formation was found to be; single pane in the interior skin, double pane in the exterior skin with an air cavity of 150 cm compared to the second option which was Single pane in the inner skin, double pane in the outer skin with an air cavity of 50 cm, (table5).

Table 5: Daylight Simulation Results (Lux)

S/NO	Glazing Type Inner Skin	Cavity Depth Cm	Glazing Type Outer Skin	Visual Transmittence W/m²	Month	Day	Time	Illuminance value (lux)
1	Single_Pane	50 cm	Double_Pane	0.69/0.63	January	12	10:00 AM	878.44
2	Single_Pane	50cm	Double_Pane	0.69/0.63	February	12	9:00 AM	518.77
3	Single_Pane	50 cm	Double_Pane	0.69/0.63	March	15	3:00 PM	1108.23
4	Single_Pane	50 cm	Double_Pane	0.69/0.63	April	28	6:00PM	1239.49
5	Single_Pane	50 cm	Double_Pane	0.69/0.63	May	12	8:00 AM	915.37
6	Single_Pane	50 cm	Double_Pane	0.69/0.63	June	9	12:30 PM	1447.87
7	Single_Pane	50 cm	Double_Pane	0.69/0.63	July	15	1:00 PM	1221.08
8	Single_Pane	50 cm	Double_Pane	0.69/0.63	August	5	9:00 AM	579.52
9	Single_Pane	50 cm	Double_Pane	0.69/0.63	September	20	4:00 PM	673.45
10	Single_Pane	50 cm	Double_Pane	0.69/0.63	October	17	1:45	1008.76
11	Single_Pane	50 cm	Double_Pane	0.69/0.63	November	10	5:00 PM	603.34
12	Single_Pane	50 cm	Double_Pane	0.69/0.63	December	12	6:00 PM	573.08
13	Low_E_Argon	50 cm	Double_Pane	0.56/0.63	October	1	1:00 PM	1252.39
14	Double_Pane	50 cm	Single_Pane	0.63/0.69	May	12	8:00	1541.33
15	Double_Pane	50 cm	Single_Pane	0.63/0.69	January	28	11:00 AM	936.88
16	Double_Pane	50 cm	Single_Pane	0.63/0.69	January	1	6:00 PM	962.26
17	Tripple_Pane	50 cm	Single_Pane	0.37/0.69	March	11	2:00 PM	1101.37
18	Double_Pane	50 cm	Double_Pane	0.63/0.63	September	11	9:00 AM	539.51
19	Single_Pane	100 cm	Double_Pane	0.69/0.63	April	25	5:00 PM	1344.67
20	Single_Pane	100 cm	Double_Pane	0.69/0.63	May	11	9:00 AM	1008.78
21	Single_Pane	150 cm	Double_Pane	0.69/0.63	August	12	9:00 AM	784.28
22	Single_Pane	200 cm	Double_Pane	0.69/0.63	December	13	6:00 PM	821.04

The results revealed that glazing configuration has a greater influence in efficient provision of Daylighting to the building as well as the depth of the cavity and the period of time. It is also observed that due lack of shading elements within the cavity influences the illumination of the building interior thereby causing intense glare and consequently causing discomfort to the occupants of the building, therefore some

shading elements should be mounted amidst the air cavity.

3.5 Ladybug Data Visualization

As stated in the previous chapter, Ladybug offers a diversity of 3D communicative climate graphics that back the decision-making progression during the initial design stages. Ladybug was used for the visualization of some basic climatic data which very vital in ascertaining the energy consumption of a building as well as the daylighting. The figures below visualize different climate-based information including the Sun path, Relative humidity, Outdoor temperature, cooling and heating loads among others, *(*Figure 33*)*.

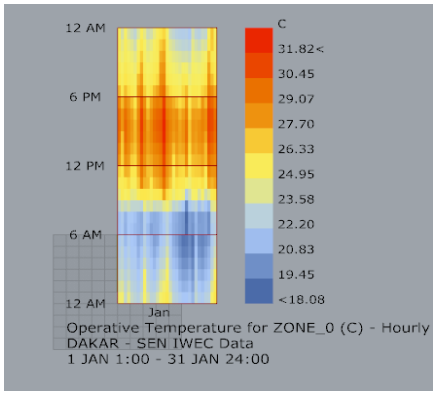

Figure 33: Showing operative temperature for zone_0

It is stated earlier that Ladybug allows for the visualization of data about the prevailing weather with the aid of some components like the import epw weather component, 3D colour chart, legend par, analysis period among other components. The figure 46 above illustrates the operative temperature from the first day of January to the last day of

the month. From the map, we can observe that the temperature begin to rise from around 10:30 in the morning up to 6:00 in the evening. The highest temperature is 31^0C and the lowest at 18^0C and this can help tremendously in evaluating the façade suitable configuration, *(*Figure 34*)*.

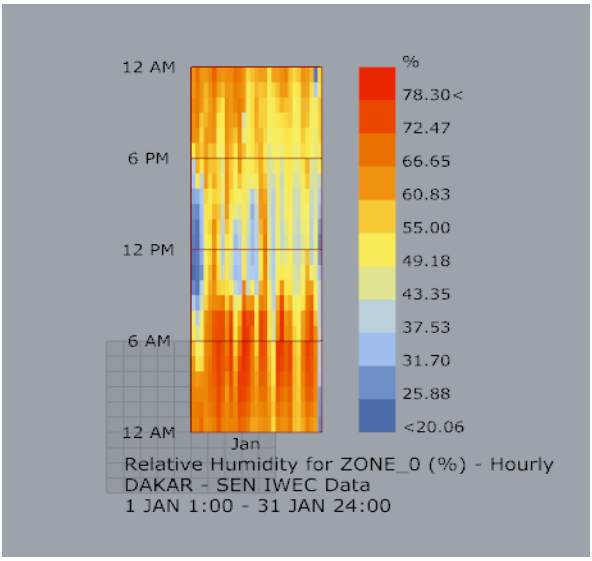

Figure 34: Showing relative humidity for zone_0

The figure 47 above illustrates the percentage of the relative humidity within the building and based on this we can evaluate some comfort level within the interior of the building. According to some review of literatures, the relative indoor humidity should be within the range of 40 to 60% for health and comfort, (Figure 35).

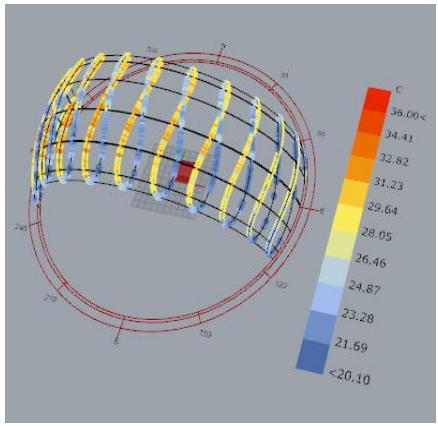

Figure 35: Showing the Sun Path in relation to Temperature as well as Relative Humidity respectively.

The figure 48 above illustrates the sun path, it shows the position of the sun as it rose and move along the meridian at different time of the year and its relationship to the building, how it affect the building in terms of solar radiation and from there, we can evaluate the suitable shading elements and its best position on the façade *(*Figure 36*)*.

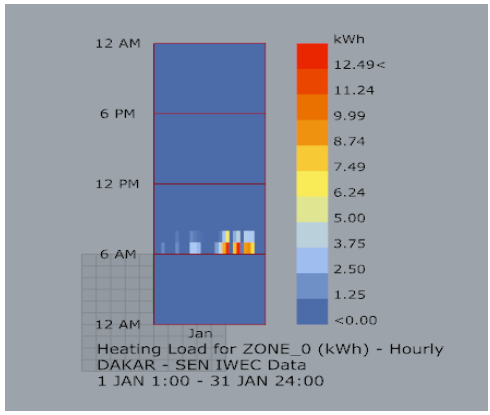

Figure 36: Showing the Heating Loads for Zone_0

The figure 50 above illustrates the energy required for the heating of the interior of the building under study in January to maintain the indoor temperature in an acceptable range. And from the figure it is observed that the heating load is manageable since it is relatively low. The heating is just required from around 6:00 up to 10:00 in the morning in the month of January, (Figure 37).

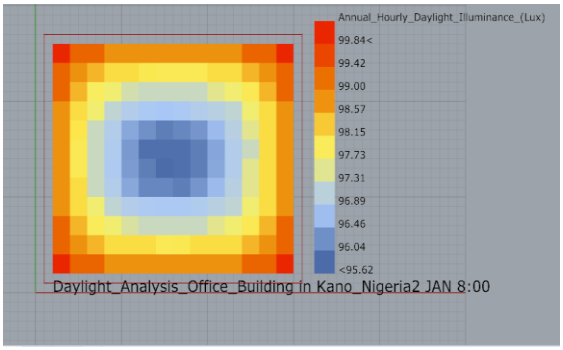

Figure 37: Annual Hourly Daylight Illuminance Map (2/ Jan. at 8:00 Am).

Figure 51 above illustrates the illuminance map within the building. According to the legend, the blue portion indicates the area that lack sufficient illumination and the darker the blue colour become; the darker the portion is in terms of lighting. And the Reddish part represents the highly lit portion, and then the brownish portion is less illuminated compared to the reddish portion then followed by the yellowish portion.

CONCLUSION

The current research initially introduced the aim to predict the energy consumption and daylighting performance of an office building in Kano, Nigeria. These goals were achieved by investigating on the energy consumption and daylight performance of the building by consideration of different sets of parameters. These variables established as the main responsive aspect for the energy use intensity. Adopting the parametric model, several simulations were conducted computationally. In these tests, we calculated different solutions with altered values of independent variables under study. The computer parametric approach performed most of the process in an automated fashion. The investigation of the energy performance for the office building is remaining constant between 8 to 18 hours of the five working days (Mondays to Fridays).

Attentive to energy use in buildings necessitates substantial amounts of data opinions. These data are needed to evaluate the possible effects of energy efficiency and daylight improvements. Much less detailed information is available on energy consumption in office buildings, which includes different types of working hours and variants of activity within buildings. Buildings want energy space for heating, water heating, lighting, refrigeration, ventilation and auxiliary facilities. These uses collectively with restrained utilizations and office equipment, interpretation for about half of total request for energy and a comparable ratio of all energy related CO_2 releases.

Enhancements to the effectiveness with which energy is used in buildings could offer substantial chances for reducing emissions.

It can be seen clearly that the change in value by certain degrees and alteration of some parameters has a change in the effect of energy as well as the illuminance values. Within the scope of the research, it is examined that around 22 different options having different glazing types and cavity depth. However, further research can easily apply the method to all several other options especially by incorporating the air cavity with some suitable shading elements. In this way, the energy performance of the building and efficient daylighting can effectively be achieved. It is very vital to study further but deeply about the best and suitable shading devices that can efficiently be incorporated in the double-skin facade air cavity especially those that can be movable or changeable according to the prevailing weather.

Moreover, the best formation in terms of energy performance in the month of August was found to be; Low E Argon in the interior skin, double pane in the exterior skin with an air cavity of 50 cm. Hence, the best formation in terms of daylight performance in the month of August was found to be; single pane in the interior skin, double pane in the exterior skin with an air cavity of 150 cm.

REFERENCES

Shameri M.A. et al, (2011) Shameri, M.A. et al "*Perspectives of double skin façade systems in buildings and energy saving"* renewing Sustain. Energy Rev., vol. 15, no. 3, pp. 1468–1475, Apr. 2011

Faggembauuu, D., et al, Numerical analysis of the thermal behavior of glazed ventilated facades in Mediterranean climates, Solar Energy 75 (2003) 229–239

Elizabeth G., et al (2004) Energy Information Administration EIA, 2011. https://www.eia.gov

Winxie, (2007). Performance Assessment Strategies: A computational framework for conceptual design of tall structure. Architecture and the Built Environment, 1 (1-40).

Elkadi, H. et al, (1999). Daylighting Design Tools, "The Bimonthly News Letter of Daylighting Collaborative, 2(1)"

Oesterle et al., "*Double skin facades Integrated planning*," Prestel Verlag Munich, Germany, 2001.

Kim et al. "*Determining photosensor conditions of a daylight dimming control system using different double-skin envelope configurations*," Indoor Built Environ., vol. 16, no. 5, pp. 411–425, Oct. 2007

B. Blocken, et al., Optimization of the energy performance of multiple-skin facades, in: Ninth International IBPSA Conference, Montreal, Canada, and August 15–18, 2005.

Impact of Building Shape on Thermal Performance of Office Buildings in Kuwait. Energy Conversion and Management, 50, 822–828.

Saelens' (2002)*"High Performance Commercial Building Facades"*

Lee, E. et al. (2002) "*Sustainable energy in office buildings"*

Soberg, (2008) "Renewable and sustainable energy"

Charron, R., et al., Optimization of the performance of double-facades with integrated photovoltaic panels and motorized blinds, Solar Energy 80 (2006) 482–491.

European Standard EN 832, Thermal performance of buildings – Calculation of energy use for heating – residential buildings, 1998

Loveday, D.L. and Taki, A.H., Convective heat transfer coefficients at a plane surface on a full scale building fac ¸ade, Int. J. Heat Mass Transfer 39 (1996) 1729–1742.

Gliner, Morgan & Leech, (2000) "Building envelope shape design in early stages of the design process: Integrating architectural design systems and energy simulation." Automation in Construction 32, 196-209.

Van Paassen, D., Defining the performance of the double skin facade with the use of the simulation model, in: Eighth International IBPSA Conference, Eindhoven, Netherlands, August 11–14, 2003.

Zimmermann, M., Low Energy Cooling–Case Studies Buildings, EMPA ZEN, Switzerland, 1998.

Random House, Inc. (2018) Dictionary.com Unabridged Based on the Random House Dictionary, ©

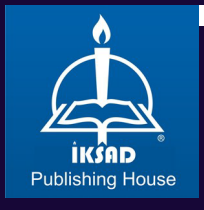

ISBN: 978-625-7139-55-7